The thesis committee for Bernardo Tomas Perez
Certifies that this is the approved version of the following thesis:

Structural Evaluation and Testing of Damaged

Reinforced Concrete Bent Caps

APPROVED BY
SUPERVISING COMMITTEE:

Trevor Hrynyk, Supervisor

Oguzhan Bayrak

Structural Evaluation and Testing of Damaged Reinforced Concrete Bent Caps

by

Bernardo Tomas Perez

Thesis

Presented to the Faculty of the Graduate School of

The University of Texas at Austin

in Partial Fulfillment

of the Requirements

for the Degree of

Master of Science in Engineering

The University of Texas at Austin

May 2019

Dedication

To my beloved father, whose guidance and support

have always helped me move forward

Acknowledgements

First, I would like to thank my family, especially my brother, Santiago Perez, and my father, Bernardo Perez; their drive and support have encouraged me to continuously grow. To my mother, Nancy Ortega, thanks for your unconditional love.

I am privileged to have worked with Dr. Trevor Hrynyk. His wisdom and experience guided this research project. Under his supervision, I was able to reaffirm my passion for structural engineering. It has been an honor working with him. Thank you for your valuable advice and commitment to this project.

I am deeply grateful with the technical and administrative staff of the Ferguson Structural Engineering Laboratory. In particular, I want to extend my deepest gratitude to Michael D. Brown who helped me with the planning and execution of most activities I performed in the laboratory.

To Jarrod Zaborac, Xiaomeng Ge, and Xiaoyi Chen, fellow colleagues and friends: thanks for your help with this project. My appreciation goes to all the other students I met during my time in FSEL. I am glad to call many of you my friends.

I want to acknowledge Zachary Kates, one of the best structural engineers I have met. His professional guidance encouraged me to study in the University of Texas and to get involved with academic research.

Finally, I would like to thank the Texas Department of Transportation (TxDOT) for providing financial support for this research, Fyfe Co. LLC for their guidance with the CFRP materials, and the Phil M. Ferguson Endowed Presidential Graduate Scholarship for the additional financial support.

Abstract

Structural Evaluation and Testing of

Reinforced Concrete Bent Caps

Bernardo Tomas Perez, M.S.E

The University of Texas at Austin, 2019

Supervisor: Trevor Hrynyk

The structural assessment of aged and existing reinforced concrete infrastructure represents a major challenge faced by the structural engineering community. The growing inventory of degrading civil infrastructure throughout the world advocates addressing a number of real-world needs: evaluating the implications of now-deficient design details comprising existing structures, assessing causes of visual distress observed in reinforced concrete infrastructure and its impact on structural performance, and verifying the feasibility of structural retrofit strategies to maintain adequate levels of safety and extend service life.

This thesis presents findings obtained from an experimental research program involving the field-extraction and subsequent laboratory testing of two reinforced concrete bent caps removed from a pair of 60-year old bridges. The bridges forming the subject of this investigation were scheduled for replacement as a result of several structural performance-related issues, including extensive shear cracking observed in the bent caps comprising both bridges. Bent cap cracking damage was documented prior to removal from the field and was used as a means of benchmarking in-service load levels. The bent caps

were subsequently tested in the laboratory in a manner that simulated service dead loads and extreme lane loading scenarios.

The first bent cap was tested as-built, while the second bent cap was retrofitted using a carbon fiber-reinforced polymer wrap to investigate the suitability of such retrofits for enhancing the shear resisting performance of damaged reinforced concrete bent caps. Results from the testing of the first shear-damaged bent cap showed that, while the cap had developed severe diagonal cracking under service and was constructed with very light shear reinforcement levels that would not satisfy modern design standards, it possessed significant post-cracking shear strength. The second, retrofitted bent cap achieved meaningful shear resistance enhancements when compared to the non-retrofitted bent cap, and was ultimately governed by the flexural failure modes. In summary, both reinforced concrete bent caps possessed significant residual post-cracking shear strengths despite having developed large-widths shear cracks while in service and having been constructed with only light shear reinforcement volumes and shear reinforcement placement details that do not conform with modern design provisions.

Table of Contents

List of Tables

List of Figures

CHAPTER 1 INTRODUCTION

1.1 Research Significance

The structural assessment and management of built reinforced concrete infrastructure represents a major challenge faced by the structural engineering community. With the inventory of ageing and degrading civil infrastructure continuing to grow throughout much of the world, work aimed toward addressing this challenge is motivated by a number of real-world needs: evaluating the implications of now-deficient design details comprising existing structures, assessing causes of visual distress observed in reinforced concrete infrastructure and its impact on structural performance, and verifying the feasibility of structural retrofit strategies to maintain adequate levels of safety and extend service life.

This thesis presents findings obtained from an experimental research program involving the field-extraction and subsequent laboratory testing of reinforced concrete (RC) bent caps removed from a pair of 60-year old bridges located at Interstate Highway 20 and Service Highway 351, in Abilene, Texas.

1.2 Research Objectives

This project aims, through large-scale experimentation, to determine the structural adequacy and residual shear strength of two RC bent caps that were extracted from service due to, in part, large diagonal cracking developed in the bent cap webs. The viability of using a CFRP wrap to improve the shear resisting performances of the damaged bent caps is investigated and comparisons to traditional code provisions are provided.

1.3 Scope

To determine the extent of the cracking damage and the ultimate shear strength of the RC bent caps, the following primary tasks were performed:

1. Visual inspections of the RC bent caps noting crack patterns, locations and widths.
   - *Site inspections* were conducted prior to the removal of the bridge superstructures.
   - *Laboratory inspections* were conducted after the extraction and delivery of bent caps to the laboratory, to determine the as-received state of damage of the specimens.
2. Pre-test characterization of concrete mechanical properties.
   - Concrete cores from the exterior faces of the bent caps were extracted and tested.
3. Retrofitting of the RC column stubs to permit structural testing.
4. Carbon fiber reinforced polymer (CFRP) retrofit of the interior damaged spans of BC2.
5. Conduct ultimate load testing of both the unretrofitted and the CFRP-retrofitted decommissioned RC bent caps.
6. Post-test characterization of bent cap concrete and steel reinforcing bars.
   - Concrete cores were extracted from the interior of the bent caps and tested.
   - Steel reinforcing bar samples were extracted from each bent cap and tested.
7. Structural assessment of the decommissioned bent caps using AASHTO LRFD Bridge Design Specifications, 8th Edition and ACI 440.2R-17.

1.4 Thesis Organization

This thesis is divided into five chapters. Chapter 2 presents the design an overview of the bent cap design; and the results obtained from the site and laboratory inspections of

the two RC bent caps. The procedure to obtain crack patterns, widths, and locations is detailed along with the measured data, and the as-built layout of the steel reinforcement is shown.

Prior to the structural testing of the bent caps, the three column stubs comprising each cap were retrofitted to ensure that they would perform adequately over the course of testing the bent cap specimens. The procedure used to retrofit the RC column stubs is described Chapter 3. Further, the damaged interior span regions of Bent Cap 2 were also retrofitted using a unidirectional CFRP wrap. The design of the CFRP retrofit are also provided in the chapter. Furthermore, Chapter 3 describes the test setup, data collection instrumentation, and procedure used to carry-out the ultimate load testing of the decommissioned bent caps. Test results are presented individually, on a test-by-test basis, and compared and discussed at the end of the chapter.

Based on the experimental results obtained, Chapter 3 provides an assessment of the RC bent caps' structural performance. The AASHTO LRFD Bridge Design, 8th Edition provisions were used as comparative measures for the assessment of the RC bent caps.

The final chapter, Chapter 4, summarizes the key findings and conclusions obtained from each task of the experimental program.

Appendix A presents the test results of Bent Cap 1 not presented in the body of the thesis, and the inspections drawings. Appendix B presents the test results of Bent Cap 2 not presented in the body of the thesis, and the inspections drawings.

CHAPTER 2 THE STUDY BENT CAPS

2.1 Background

RC bent caps (BC) are bridge substructure components supported by columns and used to carry the bridge superstructure and its associated loads (AASHTO 2017). These primary structural elements are commonly employed in bridge structures comprising roads and highways throughout North America. In this project, two RC bent caps that were extracted from two nominally identical bridges comprised the investigation. The bridge superstructures consisted of continuous steel girders that were supported by three, three-column, RC bent caps and two end abutments.

An aerial image of the bridge site prior to demolition and showing the approximate locations of the two RC bent caps forming the subject of this investigation is presented in Figure 2.1. Further, the photographs presented in Figure 2.2a and 2.2b provide visual overview of the two bent caps while in service, named Bent Cap 1 (BC1) and Bent Cap 2 (BC2).

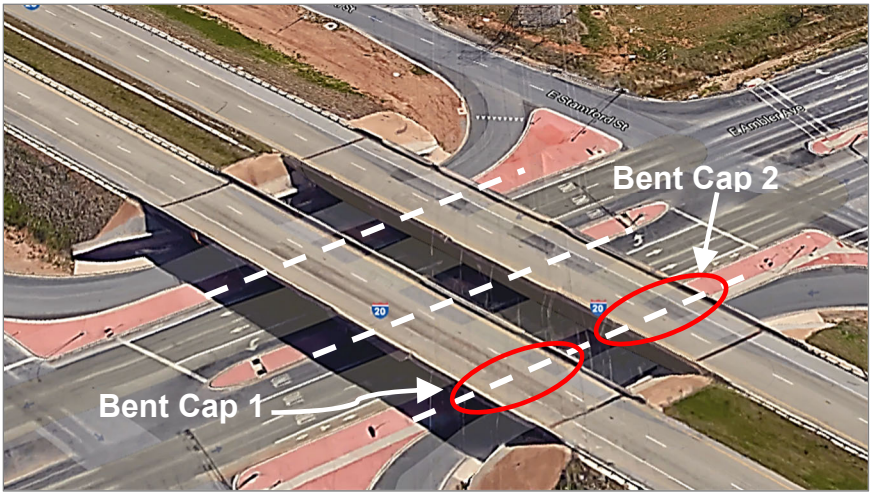

Figure 2.1. Aerial view of bridges at IH 20 and SH 351 (Google 2013)

(a) BC1 (west face)

(b) BC2 (west face)

Figure 2.2. Bent caps while in service

The RC bent caps were symmetric about their centerlines and supported by columns that were regularly spaced at 15 ft. on center. The bent caps were loaded at five points along their lengths, by way of the steel girders comprising the bridge superstructure and the girder lines (GL) were regularly spaced at 9 ft. and 2-1/2 in. on center. Refer to Figure 2.3 for bent cap elevation view with GL locations and column spacing dimensions.

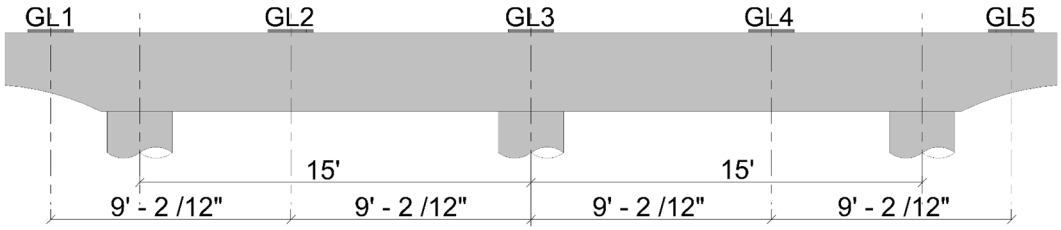

Figure 2.3. Bent cap girder lines (GL) and support spacing dimensions

In nearly all of the bent caps comprising the two bridges, large-width diagonal cracks were observed within the interior spans of the bent caps, immediately adjacent to the exterior columns. Figure 2.4 presents examples of the wide shear cracks that had developed while the bridges were in service. The largest diagonal cracks observed in the bent caps generally comprised the cap regions located between the exterior column and the adjacent interior GL.

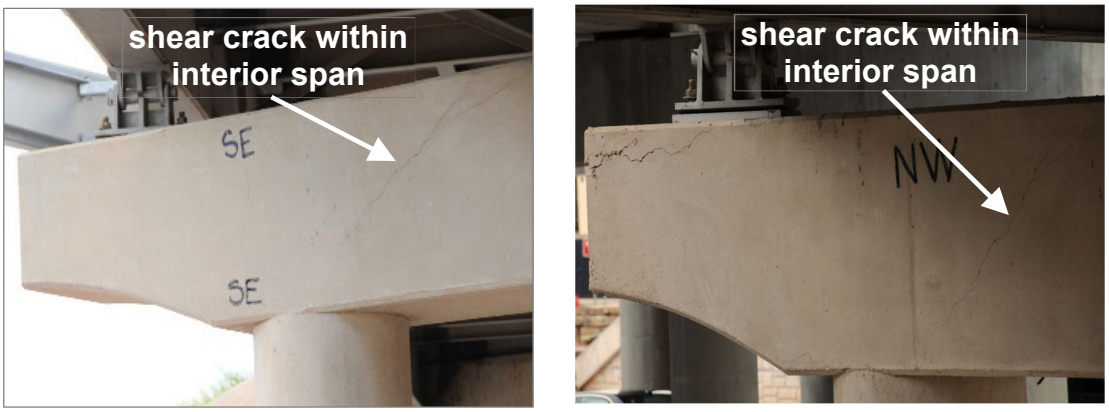

Figure 2.4. Interior span shear cracks

2.1.1 BENT CAP DESIGN DETAILS

The original design of the bent caps comprising the bridges was done in accordance with the AASHO 1957 design provisions and, from available design documents was based on an allowable reinforcement service stress of approximately 20 ksi and considering Class 'A' concrete which is to have a nominal strength of about 3.0 ksi. It should be noted that structures constructed in North America prior to 1963 typically used intermediate grade steel reinforcement with yield stress capacities on the order of 40 ksi (CRSI 2001).

The bent caps were approximately 40 ft. long and were constructed with square cross sections that were 36 in. deep, 30 in. wide, and had geometries that tapered over the end cantilever regions such that the section height was reduced to 24 in. (refer to Figure 2.3). The flexural reinforcement was varied along the lengths of the bent caps with reinforcement ratios as large as 0.70 % being provided in the negative bending regions and 0.40 % in the positive bending regions. Note that, at several locations along the lengths of the bent caps, the longitudinal reinforcement was curtailed. Relevant to the bent cap cross section shown in Section A-A of Figure 2.5, (2) of the No. 11 bars and the single (i.e., (1)) No. 10 bar comprising the flexural tension reinforcement are curtailed beneath the girder lines comprising the interior spans of the bent cap (refer to Figure 2.5).

Transverse steel reinforcement consisted of closed stirrups that were regularly spaced at 5-1/8 in. within the overhangs, providing a reinforcement ratio of 0.40 %. In the interior spans of the bent caps, the transverse steel reinforcement was spaced at 18 in., which pertained to a spacing of h/2, and resulted in a transverse reinforcement ratio of 0.11 %. It is worth noting that while the transverse reinforcement spacing exceeds the requirements permitted by most modern standards and guidelines, for the concrete employed in the design of these bent caps, the transverse reinforcement ratio provided in the interior spans of the bent caps would satisfy many modern minimum shear reinforcement requirements if stirrups with yield stresses of 50 ksi or greater were employed (AASHTO 2017; fib MC 2010).

The placement of the steel reinforcement used in the construction of the RC bent caps was verified with the use of a ground penetrating radar (GPR). Additional details regarding the inspection of the reinforcement placement are provided later in this chapter.

2.1.1.1 Available Design Documents

Design drawings of the bridge structures which comprised the bent caps were made available to the FSEL research team. Because of the age of the structures (i.e., these caps were approximately 60 years old at the time of extraction), the quality and information provided on the construction documents was limited. For example, information that is directly-relevant to the structural assessment of a bridge component, such as the required yield stress or grade of the steel reinforcement was not specified in the original design documents. It is worth noting that, for the evaluation of existing infrastructure, the absence of these details is a likely scenario and, unfortunately, increases the uncertainty associated with related structural assessments and examinations of these types of structures. The design documents are attached in Appendix D.

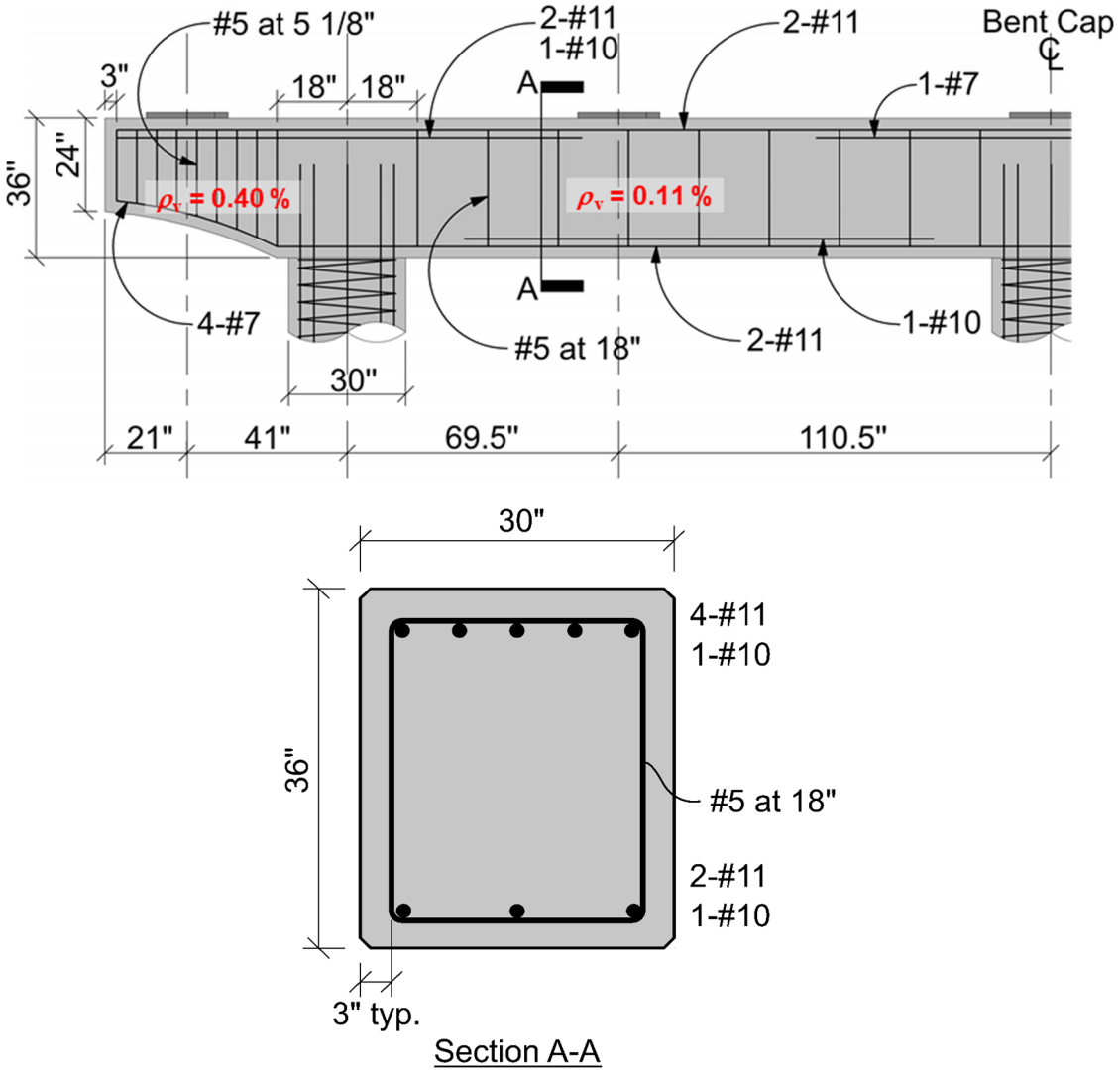

Figure 2.5. Bent cap design details

2.2 Bent Cap Inspections

Both bent caps were inspected in the field prior to extraction from service and under dead load loading conditions (bridge weight only). Further, the two bent caps were also inspected at the Ferguson Structural Engineering Laboratory (FSEL) immediately after extraction from the bridge and shipment to the laboratory. Each visual inspection consisted of the following activities:

- Documenting concrete cracking patterns, with particular attention paid to crack locations, lengths, and orientations;
- Measuring concrete crack widths at several locations for each of the observed diagonal cracks and at a limited number of locations for vertically-oriented cracks (note that all on-site crack width measurements were done using crack comparators with a crack width resolution of 0.002 in. (0.05 mm));
- Taking high-resolution photographs to document the visually-observed cracking damage identified for the two RC bent caps that were inspected, the general state of the bridges immediately prior to demolition, and the surrounding bridge site.

Note that the identified larger-width, "primary," shear diagonal cracks (see Figure 2.6), extend from the outside columns to the loads stemming from the first interior girder line on both sides of the bridge (i.e., GL2 and GL4 for the 5-girder bridges).

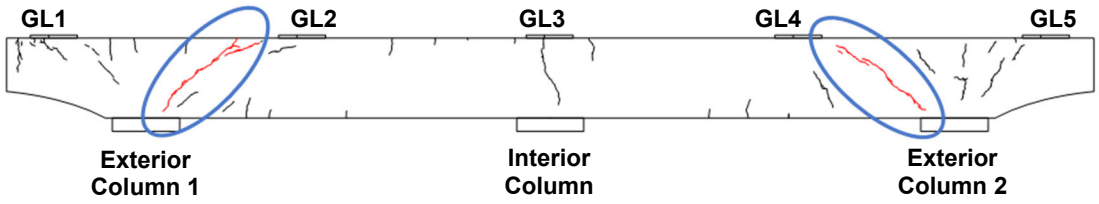

Figure 2.6. Larger-width, "primary," shear diagonal cracks

2.2.1 FIELD INSPECTIONS

The site inspections were carried-out by three members of FSEL and required approximately one-half day on-site. The dates corresponding to the bent cap site inspections were 4/27/17 and 8/24/17 for Bent Caps 1 and 2, respectively. Again, it is important to note that the superstructure of the bridge was still in-place during the in-service inspections of the caps.

Multiple crack width measurements were taken over the length of the widest and most pronounced cracks to document crack width variations. However, in small-width cracks, or for cracks with limited width variations established from the crack measurements, only one crack width measurement was recorded. Visible bent cap cracking damage was further documented using a high-resolution camera. Photographs focused on capturing cracks feature details as well as overall bridge and site conditions were taken. A small sample set of these photographs is presented in Figure 2.7.

Digital drawings that document the measured concrete cracking patterns, crack widths, and also the placement of the as-designed steel reinforcing bars comprising the RC bent caps are shown in Appendix A and B. In general, the most severe cracking damage was primarily located within the first interior shear spans, that is, between the two outermost girder lines on each side of the bent cap. Moderate flexural cracking was observed in the two interior spans of the bent caps, in both the positive and negative moment regions. Some concrete spalling and chipping was also observed on the outermost faces of the bent caps and on the corners along the length.

(a) dominant shear crack (southwest face of BC1)

(b) dominant shear crack (northwest face of BC1)

Figure 2.7. Dominant shear cracks of BC1 and BC2

(c) dominant shear crack (southeast face of BC1)

(d) close-up of dominant shear crack (northeast face of BC1)

(e) dominant shear crack (southwest face of BC2)

(f) dominant shear crack (northwest face of BC2)

(g) end region cracking, chipping, and spalling (north end of BC2)

(h) bridge in service prior to removal

Figure 2.7. Dominant cracks of BC1 and BC2

Most of the concrete cracks documented in the field inspections of the two bent caps were found to have widths on the order of approximately 0.008 to 0.012 in. (0.20 to 0.30 mm). However, larger-width, “primary,” shear cracks in the form of diagonal cracks

were found to extend from the outside columns to the application of forces stemming from the first interior girder lines on both sides of the bridge (i.e., GL2 and GL4 for the 5-girder bridges). These eight cracks had maximum measured crack widths that ranged from 0.028 to 0.059 in. (0.70 to 1.50 mm) and an average crack width of approximately 0.024 in. (0.60 mm). Note that this maximum crack width is nearly three times the average measured crack width obtained from the rest of the cracks on the bent caps (~0.008 in. [0.22 mm]).

2.2.2 LABORATORY INSPECTIONS

The two RC bent caps forming the basis of this project were received at FSEL on different dates. Bent Cap 1 was received on 06/09/17 and Bent Cap 2 was received on 08/30/17. The two caps were transported from the site of the bridges to FSEL on flatbed trucks and unloaded using a pair of cranes servicing the laboratory. For inspection purposes, the bent caps were temporarily positioned in their upright orientations and vertically supported at reaction points located immediately adjacent to the column stubs (i.e., at three locations along the lengths of the caps). Figure 2.8 shows the unloading and temporary placement of the two RC bent caps within FSEL.

Figure 2.8. Receipt and unloading of Bent Cap 2 at FSEL (08/30/2017)

Crack measurements were taken over the length of the widest and most pronounced cracks using increments of approximately 6” of separation between measurement locations. However, in the case of relatively minor / small-width cracks, or for cracks with limited width variations established from the crack measurements, a single crack width measurement was recorded and presented in the digital crack maps created to document the crack data. Visible bent cap cracking damage was further documented using a high-resolution camera. Note that the documented inspection data have been included in an Appendix A attached at the end of this memorandum, which present a series of digital drawings that have been developed for the purpose of documenting measured concrete cracking patterns, crack widths, and the as-built placement of the steel reinforcement bars comprising the RC bent caps. Primary shear cracks comprising the two RC bent caps are presented in Figure 2.9.

Significant damage was located within the first interior shear spans, between the two outermost girder lines on each side of the bent cap. Flexural cracking was also found

at positive and negative moment regions in the two interior spans of the bent caps. In contrast with the in-field observations, additional moderate flexural cracking was observed in the two interior spans of the bent caps, in both the positive and negative moment regions. Further, additional diagonal/shear cracking was observed at the first interior shear spans.

The eight primary cracks were found to have maximum measured crack widths that ranged from 0.022 to 0.039 in. (0.55 to 1.00 mm) and an average crack width on the order of 0.016 in. (0.41 mm). However, it should be noted that the majority of all the documented cracks (i.e., considering both shear and flexural cracks) had width measurements on the order of approximately 0.003 to 0.012 in. (0.10 to 0.30 mm).

Superficial damage occurred during the transportation of the bent caps from the bridge site to FSEL. This damage was generally localized to locations where the bent caps were secured with chains to the shipping trailer. Further, some additional concrete spalling/chipping was noted to occur in the corner regions of the bent caps; but, in all cases, this subsequent damage was located in secondary regions that did not influence the primary cracking damage observed during the field inspections (i.e., outside of the regions of diagonal shear cracking).rack measurements were taken over the length of the widest and most pronounced cracks using increments of approximately 6” of separation between measurement locations. However, in the case of relatively minor / small-width cracks, or for cracks with limited width variations established from the crack measurements, a single crack width measurement was recorded and presented in the digital crack maps created to document the crack data. Visible bent cap cracking damage was further documented using a high-resolution camera. Note that the documented inspection data have been included in Appendix A (BC1) and Appendix B (BC2) attached at the end of this memorandum, which present a series of digital drawings that have been developed for the purpose of

documenting measured concrete cracking patterns, crack widths, and the as-built placement of the steel reinforcement bars comprising the RC bent caps.

Significant damage was located within the first interior shear spans, between the two outermost girder lines on each side of the bent cap. Flexural cracking was also found at positive and negative moment regions in the two interior spans of the bent caps. In contrast with the in-field observations, additional moderate flexural cracking was observed in the two interior spans of the bent caps, in both the positive and negative moment regions. Further, additional diagonal/shear cracking was observed at the first interior shear spans.

The eight primary cracks were found to have maximum measured crack widths that ranged from 0.022 to 0.039 in. (0.55 to 1.00 mm) and an average crack width on the order of 0.016 in. (0.41 mm). However, it should be noted that the majority of all the documented cracks (i.e., considering both shear and flexural cracks) had width measurements on the order of approximately 0.003 to 0.012 in. (0.10 to 0.30 mm).

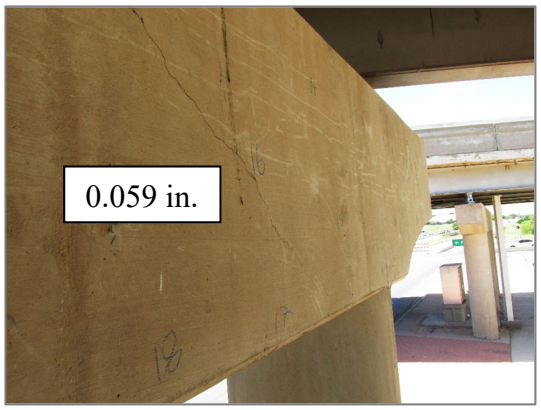

(a) In-field largest width primary crack on SW face of BC1

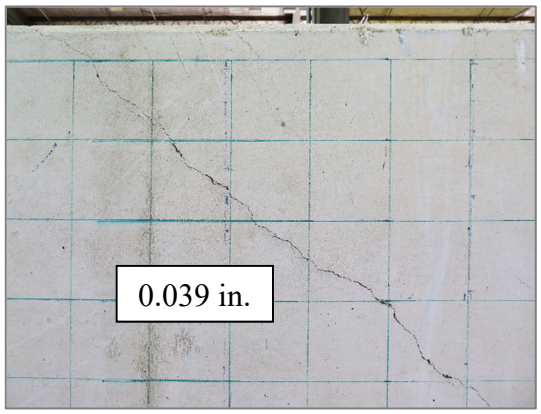

(b) In-lab largest width primary crack on SW face of BC1

(c) In-field largest width primary crack on SE face of BC2

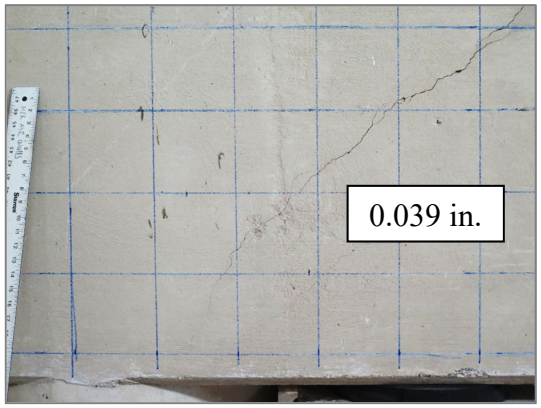

(d) In-lab largest width primary crack on SE face of BC2

(e) In-field largest width crack on NW face of BC2

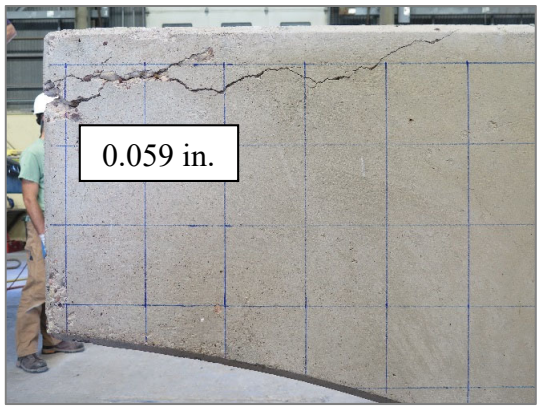

(f) In-lab largest width crack on NW of BC2

Figure 2.9. Largest width cracks of BC1 and BC2

2.2.2.1 As-Built Design: Steel Reinforcement Localization

The steel reinforcement provided in the bent caps was located with the use of a ground penetrating radar (GPR). The as-built steel reinforcement can be observed in Figure 2.10, in which its location is compared with the design-specified reinforcing bar placement provided on the design drawings. From this it can be seen that the majority of the stirrups comprising the tapered cantilever portions of the caps were placed with significant and varying levels of stirrup inclination. The stirrups comprising the interior spans of the bent caps were generally consistent with the design documents. However, it should be noted that the first stirrup placed in the interior spans, adjacent to the exterior column stubs, are located 3 in. away from the face of the columns. Thus, for the specified stirrup spacing of h/2 (18 in. for these bent caps) this results in the very next stirrup comprising the interior spans being placed approximately 18 in. from the face of the column. As a result of this large stirrup spacing, it can be seen that in many cases, the largest shear cracks almost entirely spanned between the locations of the stirrups. Similar results were obtained for the west face of BC1 and for the two faces of BC2. Figures summarizing the reinforcement positioning and the measured cracking damage are presented in Appendix A for BC1, and Appendix B for BC2.

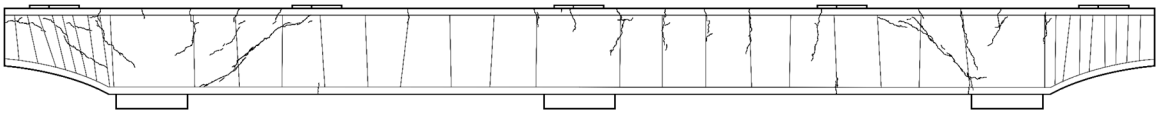

Figure 2.10. GPR-located steel reinforcement and crack map of BC1 (east face)

2.2.3 BENT CAPS INSPECTIONS SUMMARY

The primary shear cracks had a maximum measured width of 0.039 in. (1.00 mm) after extraction from the bridges and receipt at the laboratory. However, while inspected in the field, prior to removal, the maximum primary crack width comprising the two bent caps

was measured to be 0.059 in. (1.50 mm). Considering only the primary shear cracks (refer to Figure 2.6), the cracks measured in the laboratory had an average width of 0.016 in. (0.41 mm) while the widths of the same diagonal cracks measured in the field had average value of 0.024 in. (0.60 mm).

Table 2.1 summarizes the maximum and average crack widths measured in the laboratory upon receipt of the caps, and in the field prior to extraction from the bridges.

Table 2.1. Maximum and average crack widths measured in-field and in-lab

	BC1		BC2	
	In-Field Measurement	In-Lab Measurement	In-Field Measurement	In-Lab Measurement
Max. Crack Width (in.)	0.059	0.039	0.118	0.059
Avg. Crack Width (in.)	0.015	0.009	0.011	0.008

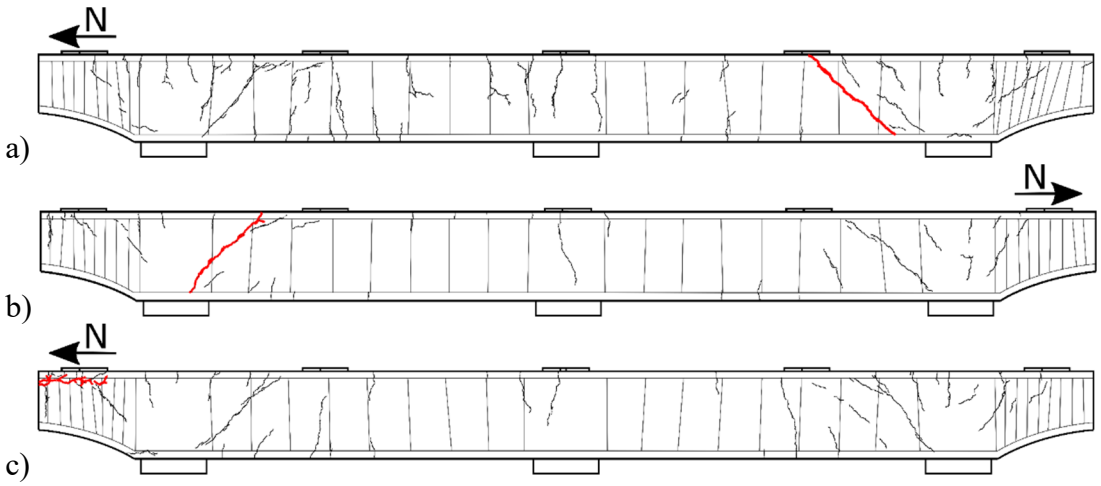

Figure 2.11. Largest crack width locations (represented in red); a) west face of BC1, b) east face of BC2, c) west face of BC2

Note that, in the case of BC2, the maximum crack width was found to be located on the northwest face of the bent cap, beneath the outermost girder line bearing plate where some localized concrete damage was observed (refer to Figurer 2.9a and 2.9f). The

maximum width primary shear crack measured for BC2 was 0.059 in. (1.50 mm) in the field and 0.039 in. (1.00 mm) in the laboratory. Recall that Figure 2.9 presents photographs showing the primary crack locations and widths. Figure 2.11 shows the location of the largest width cracks for each bent cap and the stirrups GPR locations.

2.3 Material Properties Characterization

Material property characterization was subdivided into two phases of work: *pre-test* characterization and *post-test* characterization. For organizational purposes, all the material property testing is presented in this chapter. Prior to the testing of the RC bent caps, 4-in. diameter concrete cores were extracted from the exterior vertical faces of the bent caps for the purpose of evaluating the compressive strength of the concrete comprising the caps. The cores were extracted from visually-undamaged locations, in regions that were unlikely to influence the structural performances of the caps during load testing. Further, after testing of the bent caps was completed and the caps were cut into sections, additional core samples were extracted from the interiors of the cap cross sections. Pre-test and post-test extracted concrete cores were found to have similar compressive mechanical properties. One core from each bent cap was retained for petrographic examination, the results from which are also discussed in this chapter.

The average concrete compressive strength, which was based on the testing of several core samples, was found to be on the order of 2.4 ksi for BC1 and 2.3 ksi for BC2. This concrete strength was significantly lower than the nominally-specified value of 3.0 ksi. Thus, the poor quality of the concrete was evident per the results of the core testing and was also apparent from lack of bond between the steel reinforcement and the concrete that was observed during the post-test steel reinforcing bar extraction.

Numerous reinforcing bars were extracted from each bent cap to determine the steel material properties. It is worth noting that the reinforcing bars were extracted after the testing of the bent caps and thus, are part of the post-test material characterization efforts. The results from the steel coupon testing showed that the longitudinal bar yield strengths typically ranged from 30 to 40 ksi, and the stirrup yield strengths were on the order of about 60 ksi (ranging from 56 to 75 ksi). Recall that the design service stress was noted as 20 ksi on the original design drawings.

Lastly, the mechanical properties of the CFRP employed to retrofit the interior spans of BC2 were also evaluated experimentally. In summary, the results from the CFRP coupon tests provided very similar properties to the specified values reported by the manufacturer.

2.3.1 CONCRETE

This subsection presents results from the extraction and testing of concrete cores and a petrography examination of the bent cap concrete.

2.3.1.1 Coring Samples

A series of concrete cores were taken from both of the bent caps for the purpose of evaluating the mechanical properties of the concretes comprising the RC caps. A total of sixteen 4-in. diameter cores were extracted from each bent cap: 12 from the outer faces (extracted prior to bent cap testing) and 4 from within the core of each bent cap (extracted after the ultimate strength testing of the bent caps was completed). For both caps, 15 of the concrete core specimens were tested for the purpose of evaluating mechanical properties and, in each case, one core was retained for the purpose of performing petrographic analyses.

The concrete cores were extracted from visually-undamaged locations of the bent caps (typically in the flexural compressive regions of the caps), outside of GRP-documented steel reinforcement locations. The interior concrete cores were extracted from the center of the cross-section of the bent caps. The concrete core locations are presented in Figure 2.12a and 2.12b for BC1, and Figure 2.12c and 2.12d for BC2. The exterior concrete cores were drilled from the vertical finished faces of the bent caps, and the interior cores were taken parallel to the longitudinal axes of the bent caps. Note that the concrete cores denoted with a letter 'I' were extracted from the interior core of the bent caps, while the cores denoted with the letter 'E' were extracted from the exterior face of the bent caps.

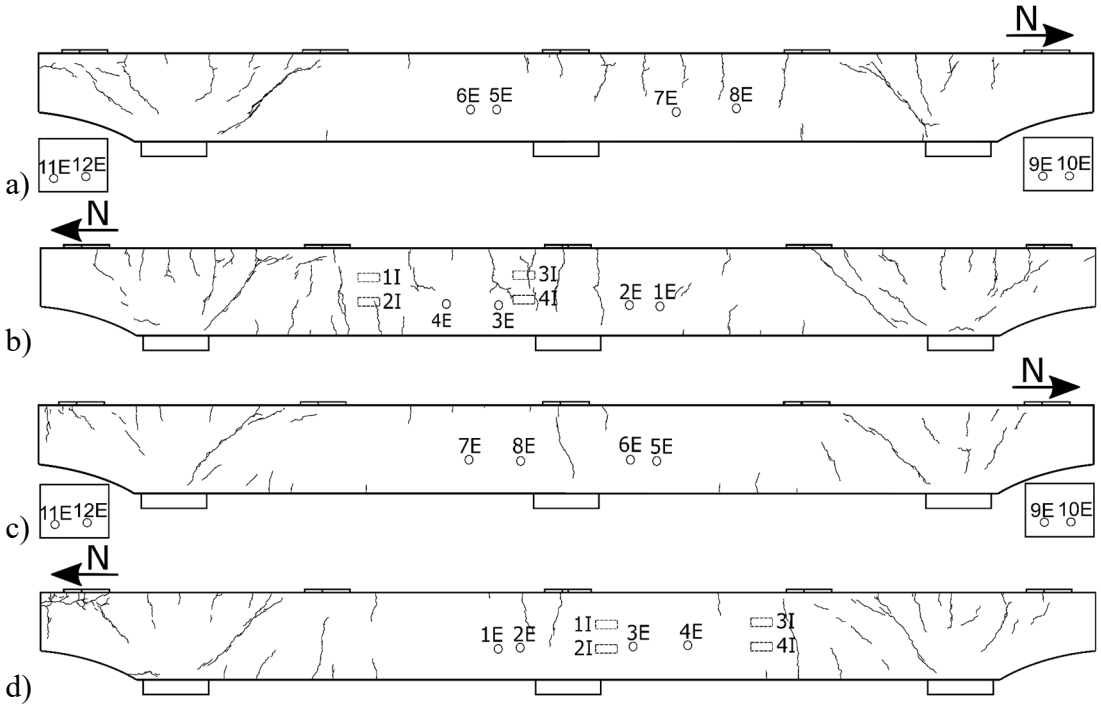

Figure 2.12. Concrete core locations; a) BC1 east face, b) BC1 west face, c) BC2 east face, d) BC2 west face

The concrete cores were tested using a a MTS universal testing machine with a calibrated resolution of 0.01 kip, which coincides with an approximate resolution of 0.80 psi for the 4-in. concrete cores extracted from the bent caps. The compression tests were

performed using a machine displacement rate between 0.060-0.0150 in./min. A compressometer employing two high resolution strain transducers was mounted to the concrete core for the purpose of measuring axial strains over the course of compression testing. Figure 2.13 shows the concrete core test setup.

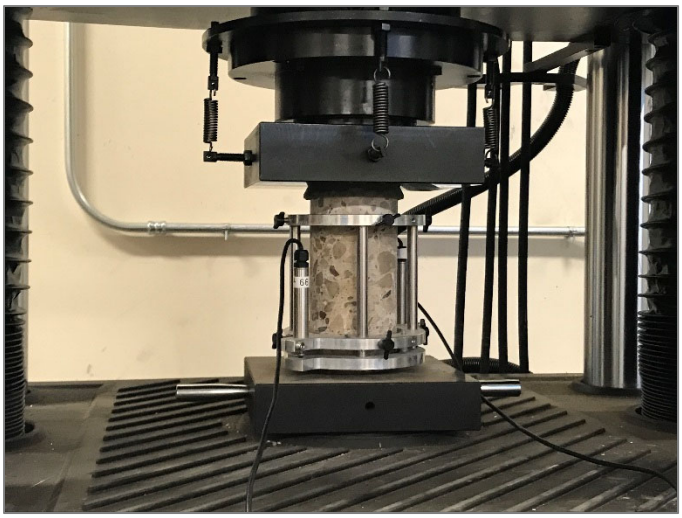

Figure 2.13. Compression test setup on the MTS universal testing machine

From the data obtained from the core compression testing, the full stress-strain response of each core was developed. Further, the data from the tests were also used to evaluate key concrete mechanical properties: the tested compressive strength of the concrete (f'c Test), the factored compressive strength of the concrete cores per ASTM C42/C42M (f'c ASTM) which approximately accounts for damage done to the concrete during the core drilling/extraction process, compressive strain coinciding with the maximum stress (ε'c), and the modulus of elasticity (Ec). Note that the concrete modulus of elasticity was evaluated using test data coinciding with prescribed stress and strain levels set forth by ASTM C39/C39M.

BC1 mechanical properties and characteristics are summarized in Table 2.2 and Figure 2.14a presents the experimental stress-strain response for each concrete core obtained during the compression test. The stress was normalized by dividing the

compressive stress at certain load by the maximum compressive stress, which was plotted with its respective normalized strain on Figure 2.14b. Two cores (4E and 11E) broke prematurely during extraction from the bent cap; as such, instrumentation for collecting strain data was unable to be used and only strength results were obtained.

Table 2.2. Summary of BC1 concrete core results

Name	Loc.	Test Rate (in./min)	D (in.)	L/D	A (in.^{2})	f'c Test (psi)	f'c ASTM (psi)	ε'c (me)	Ec (ksi)
1I	IN	0.0135	4.005	2.02	12.60	2200	2330	0.944	3450
2I	IN	0.0135	4.003	1.99	12.58	2150	2270	2.001	1570
3I	IN	0.0135	4.008	1.67	12.62	2050	2080	1.592	1860
4I	IN	0.0135	4.004	2.02	12.59	1880	2000	2.314	1800
1E	SW	0.0060	4.003	1.99	12.58	2230	2360	1.813	2120
2E	SW	0.0060	4.004	2.02	12.59	2050	2170	0.906	4120
3E	NW	0.0135	4.005	2.02	12.60	2030	2150	1.966	1980
4E	NW	0.0135	4.008	1.67	12.62	2540	2580	N/A	N/A
5E	SE	0.0060	4.005	1.85	12.60	2210	2310	1.914	2480
6E	SE	0.0135	4.006	2.02	12.61	1370	1460	1.496	2300
7E	NE	0.0120	4.007	2.03	12.61	2380	2520	1.928	2320
8E	NE	0.0135	4.017	2.02	12.67	2150	2280	1.688	2200
9E	N	0.0150	4.004	2.00	12.59	3240	3430	1.867	2120
10E	N	0.0135	4.007	2.05	12.61	3410	3620	2.457	2290
11E	S	0.0135	4.005	1.52	12.60	2720	2690	N/A	N/A
					Average:	**2310**	**2420**	**1.781**	**2350**
					Coefficient of Variation (%):	**22**	**22**	**26**	**29**

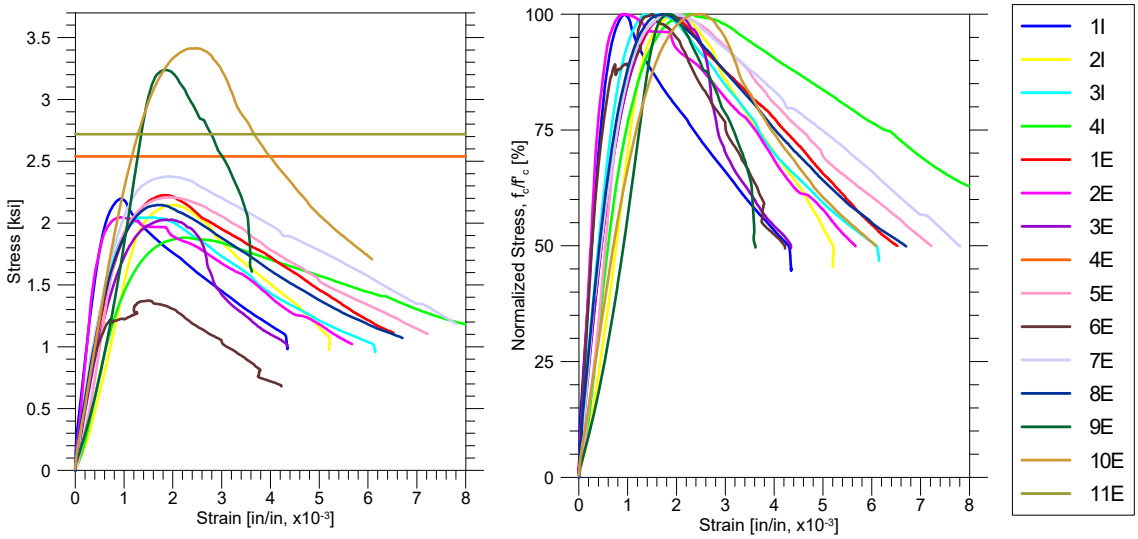

(a) measured stress-strain response

(b) normalized stress-strain responses

Figure 2.14. Concrete cores results of BC1

BC2 mechanical properties and characteristics obtained from the core testing are summarized in Table 2.3 and Figure 2.15a presents the experimental stress-strain responses obtained for each concrete core obtained during the compression test. The stress was normalized by dividing the compressive stress at certain load by the maximum compressive stress, which was plotted with its respective normalized strain on Figure 2.15b.

The specified minimum concrete strength from the original construction drawings was established as 3.0 ksi, based on the noted concrete classification 'A' in reference to the AASHO 1957 design provisions. As shown in the preceding tables, the average compressive strengths of the concrete cores were significantly lower than that specified (with an average on the order of about 2.3 ksi for BC1 and 2.4 ksi for BC2). This is likely due, in part, to preexisting damage caused by the coring process; but the results obtained from the concrete material testing also suggests that there may be quality concerns related to the concrete. Given the variability of some of the cores (minimum of approximately 1.3

ksi and a maximum of approximately 3.5 ksi), the concrete strength clearly varies over the depth and length of the caps.

It is worth noting that the coefficient of variation for the calculated maximum compressive strength values was of 22% for BC1 and of 28% for BC2. Such variability indicates a large dispersion of compressive strength values with respect the mean; however, this level of variation is arguably reasonable given the age of the existing bent caps. Nevertheless, the majority of the extracted cores for both bent caps had a compressive strength of approximately 2.0 ksi.

Table 2.3. Summary of BC2 concrete core test results

Name	Loc.	Test Rate (in./min)	D (in.)	L/D	A ($in.^2$)	f'c Test (psi)	f'c ASTM (psi)	ε'c (me)	Ec (ksi)
1I	IN	0.0135	3.994	1.98	12.53	1660	1750	1.539	2000
2I	IN	0.0135	4.002	1.99	12.58	1950	2070	1.472	2080
3I	IN	0.0135	4.003	1.98	12.59	1790	1890	1.076	3570
4I	IN	0.0135	4.004	1.98	12.59	1690	1790	1.852	1500
2E	NW	0.0135	4.016	2.08	12.67	1750	1850	2.538	1430
3E	NW	0.0135	3.976	2.13	12.42	1760	1860	2.273	1660
4E	SW	0.0135	3.976	1.95	12.42	1880	1990	2.710	1730
5E	NE	0.0135	4.003	2.15	12.58	2420	2550	1.544	2650
6E	NE	0.0135	3.976	2.15	12.42	2620	2770	2.355	2120
7E	SE	0.0135	3.990	2.11	12.50	1960	2080	2.973	1320
8E	SE	0.0135	3.990	2.12	12.50	1940	2050	2.440	2290
9E	N	0.0135	3.976	2.10	12.42	1910	2020	2.358	1730
10E	N	0.0135	3.976	2.12	12.42	2030	2150	2.509	1970
11E	S	0.0135	4.003	2.13	12.58	3530	3740	1.487	3650
12E	S	0.0135	3.990	2.12	12.50	3510	3720	2.053	2530
					Average:	**2160**	**2290**	**2.079**	**2150**
					Coefficient of Variation (%):	**28**	**28**	**27**	**33**

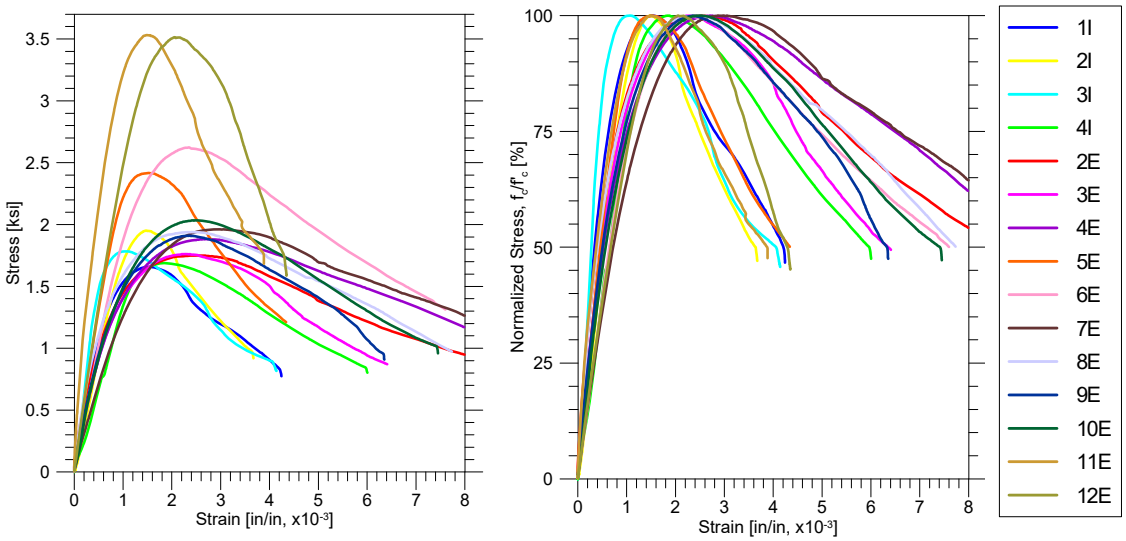

(a) measured stress-strain response (b) normalized stress-strain responses

Figure 2.15. Concrete cores results of BC2

Two cores from each bent cap presented significantly larger compressive strength than the average (9E and 10E of BC1; 12E and 11E of BC2). In both bent caps, these cores were extracted from the outermost vertical faces (i.e., the end faces) of the specimens. Note that, if such cores are unaccounted to determine the mechanical properties of the concrete, the compressive strengths of BC1 and BC2 would be of 2.2 ksi (CoV = 20%) and 2.1 ksi (CoV = 14%) respectively.

2.3.1.2 Petrography

One core from each bent cap was selected for petrographic examination. The results of the petrographic examination showed that both cores had similar components and component proportioning. Numerous hairline cracks and microcracking was observed in the two cores, but no evidence of alkali-silica reaction (ASR) was observed. Approximately 2-in. deep carbonation from the finished surfaced was observed, which may have been caused by the abundance of cracks and microcracks. The petrographic report is attached in Appendix F. A summary of key findings from the petrographic report is provided below:

- The paste was composed of hydrated Portland cement with no fly ash, slag cement, or other supplemental cementitious materials
- Both cores were comprised of natural gravel coarse aggregate with a nominal top size of 1 in. and consisted of primarily limestone with small portions of chert and quartzite. The fine aggregate was a natural sand which consisted mainly of quartzite and chert, with minor limestone
- Despite chert and quartzite being susceptible to ASR, no evidence of such reaction was observed.
- The cores presented numerous hairline crack sand microcracks, particularly in the outer 3/4 in. of the core. The cracks are not typical of drying shrinkage and are not from an internal expansion mechanism
- Carbonation was found 2 in. deep from the finished face of the cores, which is most likely to be a function of the abundant cracking and microcracking of the cores

2.3.2 STEEL REINFORCEMENT

Steel reinforcing bars were extracted from the bent caps after ultimate load testing of the two RC bent caps was completed. The steel reinforcement comprising the two caps were evaluated by way of uniaxial tensile testing of standard reinforcing bar coupons. A minimum of three longitudinal bars, for each type/size longitudinal bar, and three stirrups were tested to determine the properties of the steel reinforcement comprising each cap. Figure 2.16 presents a summary of the locations associated with the extracted steel bars.

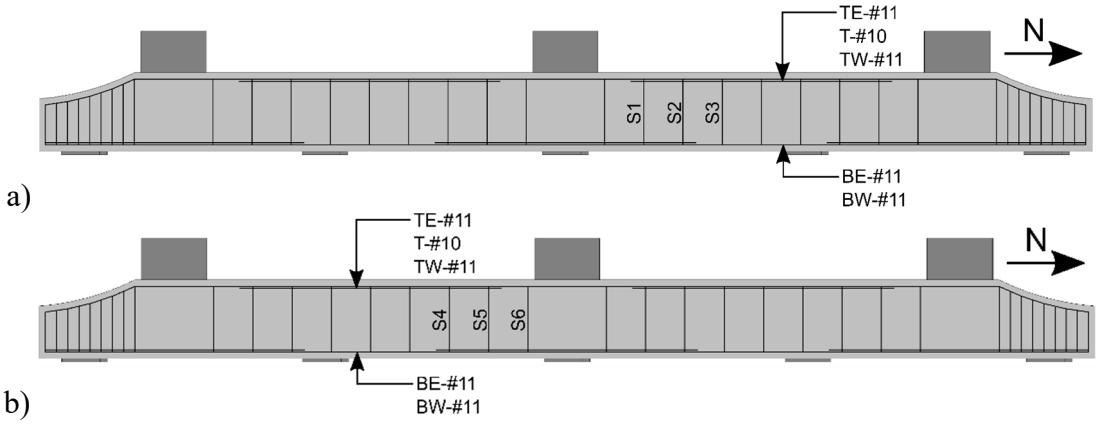

Figure 2.16. Extracted steel reinforcement location; a) Bent Cap 1, b) Bent Cap 2

The steel reinforcement was extracted by cutting the concrete around the steel bars using a circular saw. After cutting, bent cap prisms containing the rebar were removed from the bent cap. With the use of a small hammer, the extracted concrete was removed from the rebar, as illustrated in Figure 2.17. It is worth noting that the cement adhesion to the rebar was minimal; in most cases, the concrete essentially 'fell-off' of the steel rebar with only limited impact from the hammer. No other treatment was necessary to remove cement particles off the steel reinforcement.

(a) extracted concrete encased rebar

(b) concrete encased rebar after sledgehammer impact (stirrup)

(c) concrete removal from longitudinal rebar

Figure 2.17. Rebar extraction

2.3.2.1 Steel Reinforcement Deformation Patterns

Two different types of bar deformation patterns were identified for the steel bars comprising the damaged RC bent caps: a herringbone deformation pattern and a spiral pattern. The herringbone shape consists of lugs oriented perpendicular to the longitudinal axis of the rebar while the spiral pattern has lugs positioned in a diagonal orientation with respect the longitudinal axis of the rebar. Figure 2.18 shows a comparison of the deformed bars extracted from the bent caps.

The mechanical properties of the steel reinforcement had significant variability because of the different types of bars used for construction, even for bars of the same size. It was noted that the herringbone patterned bars had larger variability than the spiral patterned bars.

(a) spiral deformation pattern

(b) herringbone deformation pattern

Figure 2.18. Lug deformation patterns identified for extracted steel reinforcing bars

2.3.2.2 Mechanical Properties Characterization

To characterize the mechanical properties of the steel reinforcement, coupons were tested under uniaxial tension loading, until bar rupture was achieved. A high-precision extensometer was used to measure the change of length of the bar over the course of testing for the purpose of developing bar strain measurements. It should be noted that the extensometer was removed at each test when its elongation reached a value of

approximately 0.80 in. which, in all cases, corresponded to strains exceeding the onset of rebar yielding. After the removal of the extensometer, the cross-head displacement of the testing frame was used to estimate the strain of the coupons throughout the post-yield response range. Table 2.4 and Table 2.5 summarize the extraction location, size, type, and number of coupons tested for each bar extracted from the two RC bent caps (BC1 and BC2).

Table 2.4. Summary of extracted bars from BC1

Bar Name	Location	US Bar No.	Bar Type	Corrugation	# of samples
TE-#11	Top east	#11	Longitudinal	Herringbone	3
TW-#11	Top west	#11	Longitudinal	Spiral	3
BE-#11	Bot east	#11	Longitudinal	Herringbone	3
BW-#11	Bot west	#11	Longitudinal	Herringbone	3
T-#10	Top middle	#10	Longitudinal	Herringbone	3
S1	See Figure 2.16	#5	Transverse	Herringbone	2
S2	See Figure 2.16	#5	Transverse	Herringbone	2
S3	See Figure 2.16	#5	Transverse	Herringbone	2

Table 2.5. Summary of extracted bars from BC2

Bar Name	Location	US Bar No.	Bar Type	Corrugation	# of samples
TE-#11	Top east	#11	Longitudinal	Spiral	3
TW-#11	Top west	#11	Longitudinal	Spiral	3
BE-#11	Bot east	#11	Longitudinal	Spiral	3
BW-#11	Bot west	#11	Longitudinal	Spiral	3
T-#10	Top middle	#10	Longitudinal	Herringbone	1
S4	See Figure 2.16	#5	Transverse	Herringbone	2
S5	See Figure 2.16	#5	Transverse	Herringbone	2
S6	See Figure 2.16	#5	Transverse	Herringbone	2

The data obtained from the coupons of the same bar was averaged to find its mechanical properties. The average stress-strain response of each bar are plotted in Figures 2.19 through 2.22.

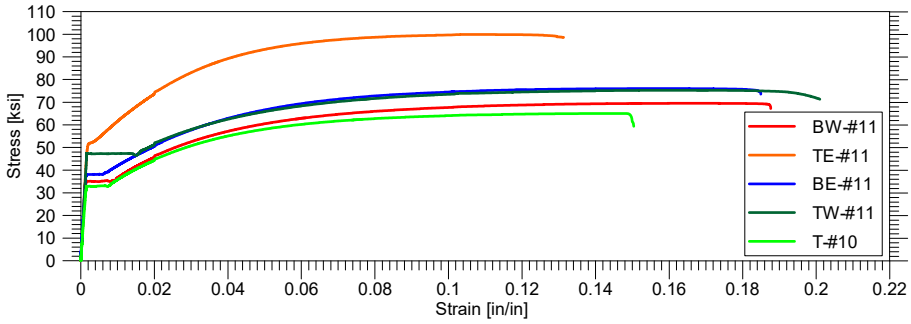

(a) No. 11 longitudinal bars

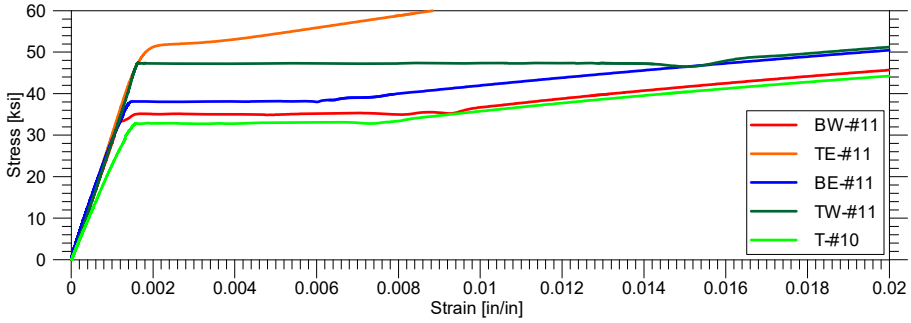

(b) yield plateau zoom-in

Figure 2.19. BC1 No. 11 longitudinal bar stress-strain curves

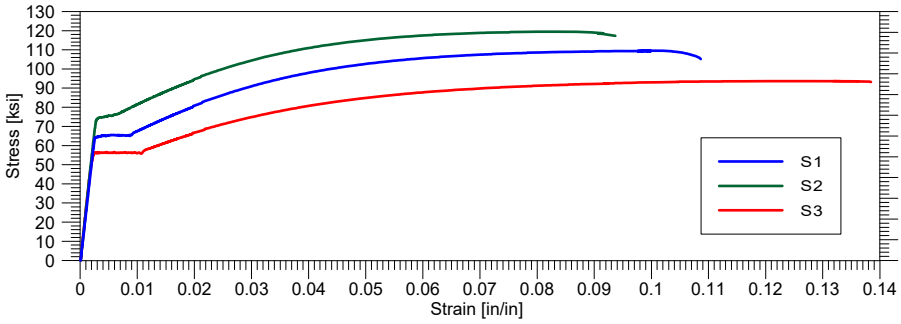

(a) No. 5 stirrups

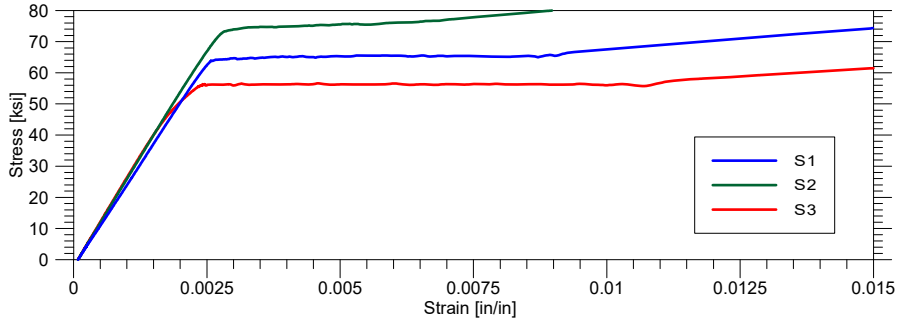

(b) yield plateau zoom-in

Figure 2.20. BC1 No. 5 stirrup stress-strain curves

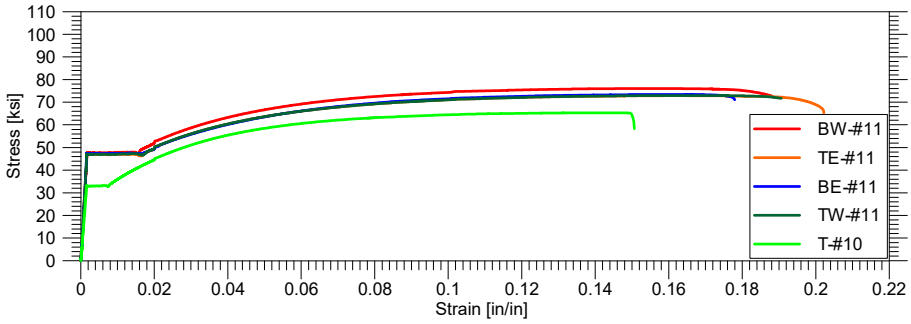

(a) No. 11 longitudinal bars

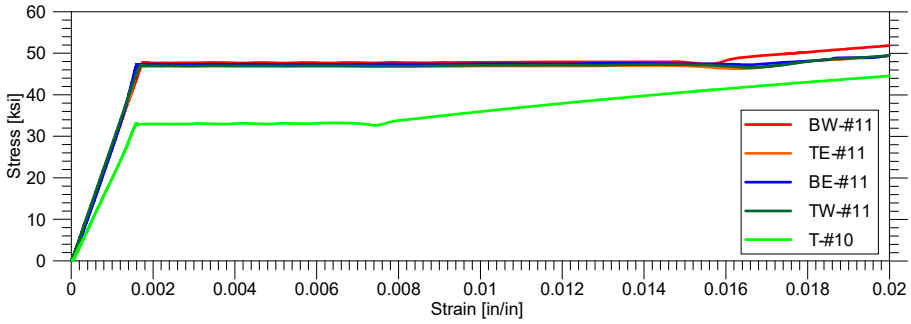

(b) yield plateau zoom-in

Figure 2.21. BC2 No. 11 longitudinal bar stress-strain curves

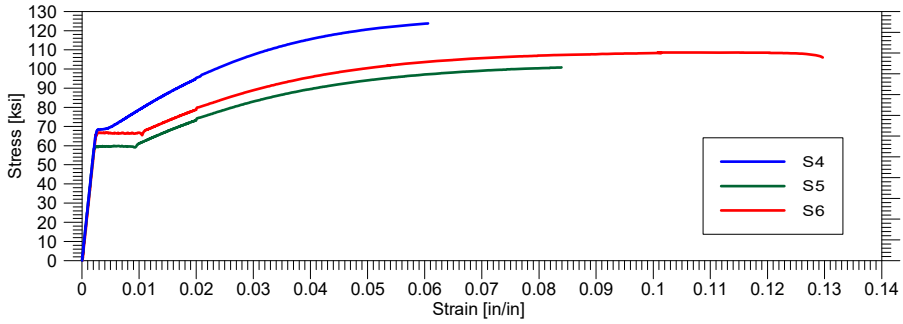

(a) No. 5 stirrups

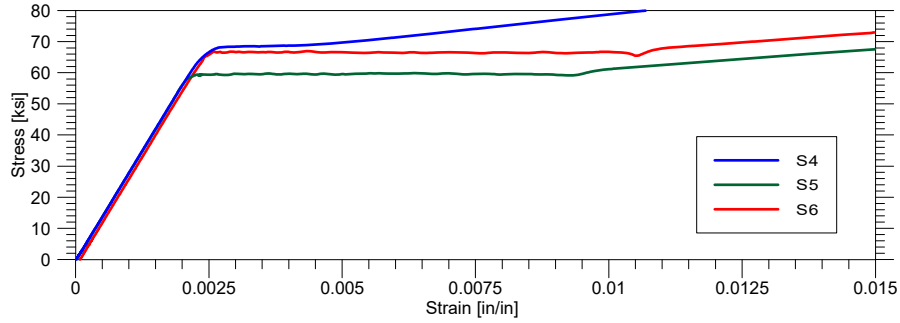

(b) yield plateau zoom-in

Figure 2.22. BC2 No. 5 stirrup stress-strain curves

Figure 2.23 is intended to serve as a key and illustrates the properties and associated notations used in reporting the evaluated mechanical property data for each steel bar. Tables 2.4 and 2.5 summarize the mechanical properties of the steel reinforcement extracted from the bent caps.

On the basis of the findings of the steel reinforcement extraction and testing, the following was concluded:

- The yield stress for the steel reinforcement comprising bent cap 1 was in the order of 43 ksi for #11 bars (i.e., longitudinal reinf.) and 65 ksi for #5 bars (i.e., transverse reinf.).
- The steel reinforcement comprising bent cap 2 had a yield stress of 47 ksi for #11 bars and 64 ksi for #5 bars.
- It was noted that the highest variability in terms of mechanical properties was presented on the herringbone patterned steel reinforcement. For this type of bars, the yield stresses varied from 35 to 52 ksi for #11 bars, while all the #11 spiral patterned bars had a yield stress in the order of 47 ksi. In addition, all the stirrups presented the herringbone pattern, which had yield stresses that varied from 56 to 75 ksi.

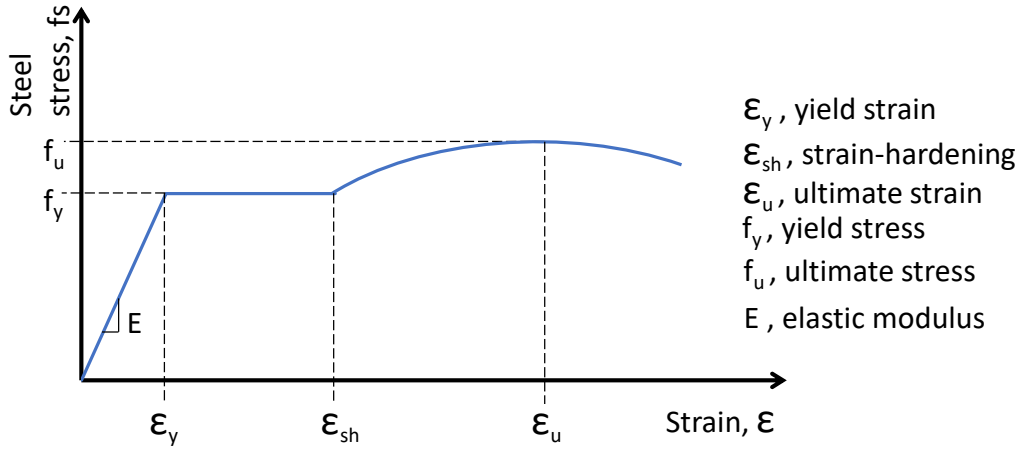

Figure 2.23. Typical steel reinforcement stress-strain curve showing reported data

Table 2.6. BC1 steel reinforcement mechanical properties

Bar Name	ε_y (x10^{-3})	ε_{sh} (x10^{-3})	ε_u (x10^{-3})	f_y (ksi)	f_u (ksi)	E (ksi)
TE-#11	2.1	3.7	107.9	52	100	30840
TW-#11	1.6	15.7	165.4	47	75	29640
BE-#11	1.4	6.1	157.4	38	76	26860
BW-#11	1.4	9.7	169.1	35	70	28640
T-#10	1.6	7.4	145.6	33	65	21650
S1	2.6	9.2	100.6	65	110	26330
S2	2.8	6.6	82.0	75	120	27910
S3	2.3	10.9	125.7	56	94	27430
#11 avg	1.6	8.8	150.0	43	80	28990
#10 avg	1.6	7.4	145.6	33	65	21650
#5 avg	2.6	8.9	102.8	65	108	27220

Table 2.7. BC2 steel reinforcement mechanical properties

Bar Name	ε_y (x10^{-3})	ε_{sh} (x10^{-3})	ε_u (x10^{-3})	f_y (ksi)	f_u (ksi)	E (ksi)
TE-#11	1.7	17.1	162.0	47	73	28140
TW-#11	1.7	17.3	161.9	47	73	28460
BE-#11	1.6	17.0	160.7	47	73	29540
BW-#11	1.7	15.9	154.4	48	76	28340
T-#10	1.6	7.6	136.7	33	65	21100
S4	2.6	4.7	60.6	69	124	28200
S5	2.2	9.4	83.9	60	101	28070
S6	2.5	106.7	103.2	67	109	28160
#11 avg	3.5	16.8	159.8	47	74	28620
#10 avg	1.6	7.6	136.7	33	65	21100
#5 avg	2.4	58.1	93.6	64	105	28110

2.3.3 CARBON FIBER REINFORCED POLYMER

A unidirectional carbon fiber-reinforced polymer (CFRP) retrofit system (i.e., CFRP wrap combined with a compatible epoxy resin) was used to strengthen the interior spans of Bent Cap 2 in order to increase the shear-capacity to a level that was approximately equal to the estimated flexural capacity of the member. This section of the thesis presents

the mechanical properties of the Tyfo SCH-41 Composite that was used to carry-out the CFRP-retrofit of Bent Cap 2. Note that, for reference and comparative purposes, the reported manufacturer's properties for the CFRP retrofit system are included in Appendix G of this thesis.

A total of 21 randomly selected CFRP-resin coupons were tested. However, coupons that were observed to fail in the regions of the fixture grips were deemed invalid and were discarded. Of the 21 coupons that were tested, only 10 coupon test specimens were observed to fail within the mid-height gauge length regions. Thus, the CFRP coupon results presented in this thesis are based on the results of these 10 coupons. The coupons were extracted from 2 different laminates named laminate 1 (L1) and laminate 2 (L2).

The uniaxial tensile testing of the CFRP coupons was done using a MTS universal testing machine. Over the course of the experiments, the strain and axial load were recorded at a rate of 5 Hz. The experiments were performed in a displacement-controlled manner at a rate of 0.03 in./min. A 2 in. gauge length extensometer was attached to the coupons using rubber bands, and was used to measure coupon extension and, in turn, compute the tensile strain development within the gauged regions of the loaded specimens. Gage 16 (0.063 in.) aluminum tabs were provided in the gripped regions of the coupons in an effort to alleviate stress concentrations between the machine grips and the CFRP test specimens. Figure 2.24 shows the test setup used to carry-out the CFRP coupon testing.

Figure 2.24. CFRP coupon test setup

As-fabricated coupon dimensions and the tests results obtained are reported in Table 2.6 and compared with the manufacturer's reported values. In addition, the stress-strain responses of each coupon are plotted in Figure 2.25. It is worth noting that the manufacturers values are based on a uniform coupon thickness of 0.04 in. (i.e., a thinner CFRP-resin matrix than the average thickness value of the fabricated coupons). Typically, the amount of resin employed in the coupon preparation impacts the strength and stiffness of the CFRP-resin matrix, in which oversaturated coupons perform poorly in comparison with mildly saturated coupons. Therefore, the larger CFRP-resin matrix thickness of the fabricated coupons with respect the manufacturer's coupons resulted in a slightly lower strength and stiffness to that of the manufacturer's test values. The coupon preparation and testing may also be different than the one employed by the manufacturer, which may be a reason of the property's differences.

Table 2.8. CFRP coupons testing results

Coupon Name	Width (in.)	Thick. (in.)	Area (in^2)	Ultimate Stress (ksi)	Elastic Modulus (ksi)	Ultimate Strain ($x10^{-3}$)
L1-1	1.199	0.045	0.054	136	11820	11.0
L1-2	1.215	0.042	0.051	131	12120	10.8
L1-3	1.218	0.045	0.055	133	11130	11.1
L1-4	1.153	0.042	0.049	145	13210	11.0
L1-5	1.180	0.042	0.050	140	11600	12.0
L2-1	1.165	0.046	0.053	131	11200	11.2
L2-2	1.165	0.044	0.052	146	11630	10.5
L2-3	1.192	0.040	0.048	136	12460	10.7
L2-4	1.177	0.042	0.049	148	11950	11.9
L2-5	1.202	0.038	0.046	134	12000	10.5
Average:	**1.187**	**0.043**	**0.051**	**138**	**11910**	**11.1**
Manufacturer Typ. Test Value	-	0.040*	-	143	13900	10.0
Percentage of manufacturers values	-	107%	-	97%	86%	111%

* Manufacturer's values based on 0.04 in. coupon thickness which leads to discrepancy between fabricated coupons and the manufacturer's typical test values

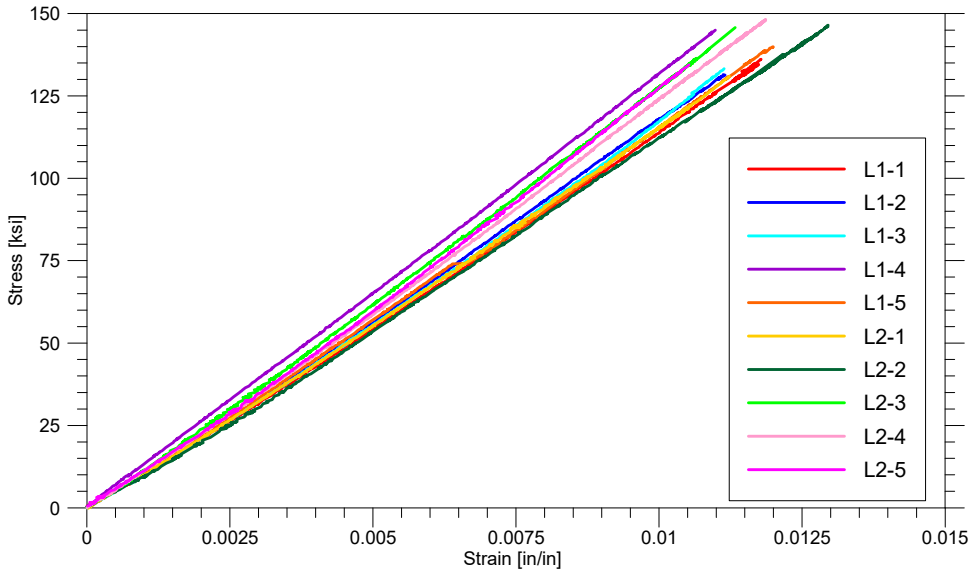

Figure 2.25. CFRP coupon stress-strain responses

2.6.3 CHAPTER SUMMARY AND CONCLUSIONS

The concrete and steel reinforcement mechanical properties of the decommissioned bent caps were established by way of experimental testing. Further, the mechanical properties of the CFRP retrofit system were determined and compared with the manufacturer's reported values. Key findings obtained from the aforementioned mechanical property testing activities are as follows:

- The mean and factored compressive strengths of the concretes comprising BC1 and BC2 were of 2.4 ksi and 2.3 ksi, respectively. In both cases, these values were significantly lower than the design-specified strength value of 3.0 ksi for Class A (1957 AASHO) concrete. Note that the factored compressive strengths being referred to include the strength enhancement factor specified by ASTM C42/C42M to approximately account for concrete damage that likely occurred during the core drilling and extraction process.
- The poor adhesion of the cement to the steel reinforcement extracted from the bent caps raises further questions regarding the quality of concrete used in the construction of the bent caps.
- The results of the petrographic examination showed that both cores had similar components and component proportioning. Numerous hairline cracks and microcracking was observed in the two cores, but no evidence ASR was observed. Approximately 2-in. deep carbonation from the finished surfaced was observed, which may have been caused by the abundance of cracks and microcracks
- Generally, the steel reinforcement mechanical properties were in-line with the construction drawings. The results from the coupon testing showed that the longitudinal bar yield strengths typically ranged from 30 to 40 ksi, and the stirrup yield strengths were on the order of about 60 ksi (ranging from 56 to 75 ksi). With

the exception of the No. 10 longitudinal bars, all of the steel reinforcement would arguably be deemed as satisfying the 20 ksi reinforcement service stress requirement specified in the original design drawings.

- The CFRP retrofit system used for the shear strengthening of Bent Cap 2 was tested and found to be in-line with manufacturer's specifications. Minor discrepancies between the manufacturer's values and tested values can be attributed to the coupon preparation techniques (i.e., the resulting coupon thickness) used.

CHAPTER 3 EXPERIMENTAL PROGRAM

The interior, previously damaged, span regions of both bent caps were loaded to failure to determine their ultimate capacity; and the overhangs of Bent Cap 1 were also tested to failure. Bent Cap 1 was tested as-built, while the interior spans of Bent Cap 2 were retrofitted using a CFRP wrap. In addition, the column stubs of the bent caps were strengthened using a steel jacket with high-performance non-shrink grout. This chapter describes the retrofitting of the bent caps and discusses the testing procedure, instrumentation, and results.

3.1 Bent Cap Retrofits

This section summarizes the major retrofits performed on the RC bent caps. The column stubs of both bent caps were strengthened to ensure that they would be capable of carrying required support reaction forces developed during the structural testing of the RC bent caps. Additionally, the interior spans of Bent Cap 2 were retrofitted using a CFRP wrap in an effort to increase its shear capacity.

3.1.1 COLUMN STUB RETROFIT

The column stubs comprising the two RC bent caps were retrofitted in an effort to strengthen them for the purpose of permitting subsequent structural testing. Steel tubes of ¼-in. thickness, 31-in. inside diameter, and 18-in. height were used to reinforce and encase, by way of high-performance non-shrink grout, the existing column stubs comprising the bent caps. Refer to Appendix D for detailed procedure of the column stub retrofit.

The concrete cover of the column stubs was chipped off from the side surfaces of the stubs until the column spiral reinforcement was exposed along the perimeter, over the height of the stub. At the base of the column stubs, an approximate 2-3 in. of concrete cover

was left intact to ensure that the column stub-bent cap connection geometries of the specimens remained unaltered from that provided in-service. Loose debris was removed from the chipped off surface to guarantee proper adhesion between the grout and the roughened surface. Figure 3.1 shows the concrete cover removal, the placement of the steel jacket enclosing the column stub, and the finished column stub rtetrofit.

Steel tubes were placed on top of a 3/4 in. fibreboard that enclosed the perimeter of the column stub and provided separation of the stubs retrofit from the surfaces of the bent cap. Such separations ensured the unaltered as-in-service geometry. Finally, the high-performance grout was mixed, poured in the steel jacket, and the top surface of the grout was smoothed to guarantee a flat surface, as shown in Figure 3.1d.

A total of 9 grout cubes (3 cubes per column stub) of 2 x 2 x 2 in. were cast during the column stub retrofit operations for each bent cap. The grout cubes were tested 28 days after casting to evaluate the compressive strength of the high-performance grout. The average compressive strengths of the grouts comprising each of the column stub retrofits cast for both bent caps are shown in Table 3.1. Recall that the average concrete compressive strength of the concrete comprising the bent caps was on the order of about 2.4 ksi. Thus, the grout strengths obtained for the stub retrofits far exceeded the existing material strengths comprising the caps.

(a) Concrete cover removal

(b) Column stub with perimeter-enclosing fibreboard and removed concrete cover

(c) Steel jacket enclosing column stub

(d) Finished column stub with finished top surface

Figure 3.1. Column stub retrofit procedure

Table 3.1. Column stub retrofit grout compressive strength

	Grout Average Compressive Strength (ksi)			
	North Support	Middle Support	South Support	Average
Bent Cap 1	10.1	6.6	9.2	8.6
Bent Cap 2	8.1	8.6	8.4	8.4

3.1.2 Carbon Fiber Reinforced Polymer Interior Span Retrofit

The shear-cracked interior spans of Bent Cap 2 were retrofitted using a unidirectional carbon fiber-reinforced polymer (CFRP) wrap to investigate its effectiveness in increasing the strength and stiffness of the shear-cracked bent cap. The location of the completed interior span retrofit, and a photograph of one of the completed

retrofits, is presented in Figure 3.2. Note that the retrofit of BC2 was designed and completed after the testing of the interior spans of BC1.

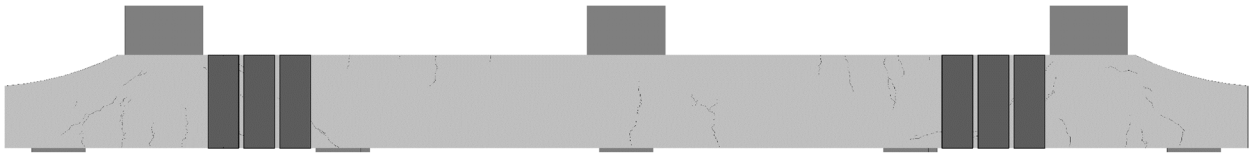

(a) Bent Cap 2 CFRP retrofit locations

(b) Interior span 1 prior to retrofit

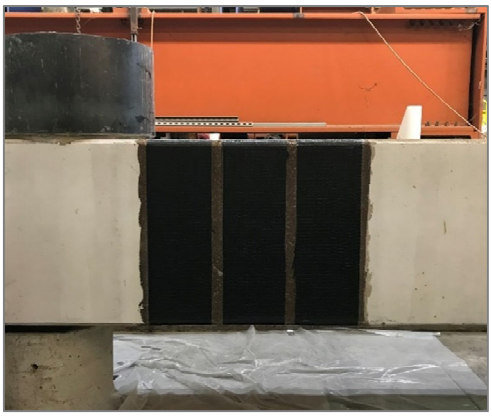

(c) Interior span 1 with CFRP retrofit

Figure 3.2. Retrofitted Bent Cap 2

The objective of the proposed CFRP retrofit design was to increase the shear capacity of the shear-cracked interior span to a level that was approximately equal to the flexural capacity. The retrofit design was developed on the basis of ACI 440.2R-17 and with consideration of a full-wrap CFRP configuration (i.e., without the use of anchors or supplemental bonding/fastening elements). The CFRP used for the design and retrofit was Tyfo SCH-41 Composite. Refer to Appendix D for the detailed procedure employed to install de CFRP wraps.

Figure 3.3 presents a summary of the developed CFRP retrofit. The RC bent cap was estimated to fail in flexure when the shear demand at the critical section (i.e., the interior span) develops a shear force demand of approximately Vu = 280 kip. Thus, the retrofit was designed such that the shear resistance of the strengthened section (i.e., Vn =

Vc + Vs + Vf) exceeded 280 kip. Employing the provisions of ACI 440.2, providing 12-in. wide CFRP strips @ 14 in. on-center is estimated to yield a nominal sectional shear strength of Vn = 296 kip. Note that Vn was calculated without any safety factor. Refer to Appendix C for details regarding the design calculations pertaining to the retrofitted span.

The installation process for the CFRP material and the proposed CFRP retrofit design were developed in coordination with Fyfe Co. LLC. They provided feedback on the proposed retrofit design, gave guidance about the surface preparation and installation procedure of the CFRP, and also provided documentation regarding the CFRP installation procedures.

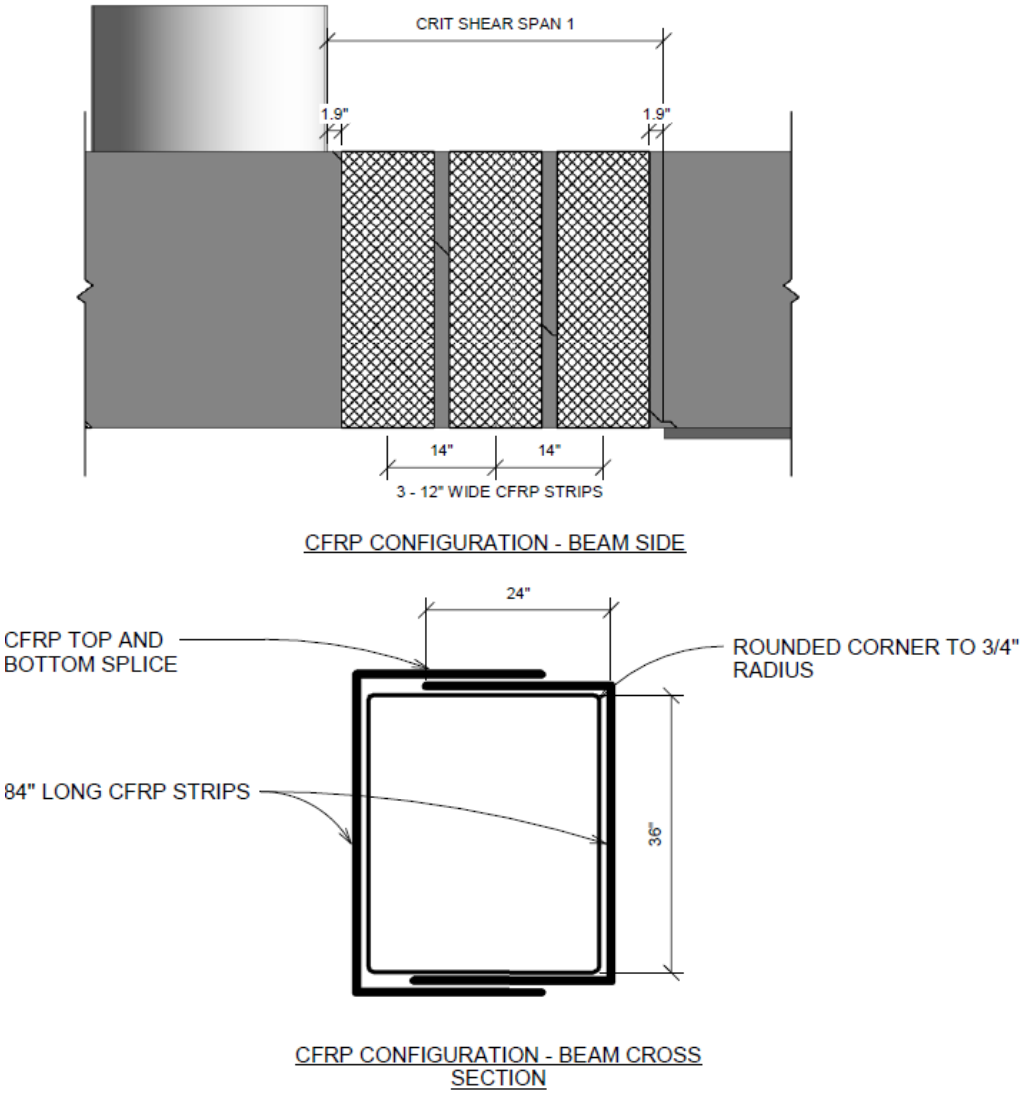

Figure 3.3. CFRP design details

3.2 Bent Cap Ultimate Load Tests

The primary objective of the ultimate load testing was to evaluate the structural performance of the shear-cracked interior span regions of the bent caps. Additionally, the overhangs comprising one of the bent caps were also tested in an effort to evaluate their load resisting performance.

The interior spans were initially loaded in a manner that approximately simulated uniform service dead load loading conditions and corresponded to the load level that caused the existing diagonal cracks to exhibit crack widths that were comparable to those measured during the in-field inspections of the bent caps. The interior spans were subsequently loaded to failure under simulated lane loading conditions. Bent Cap 2 interior spans were retrofitted, prior to testing, using a unidirectional carbon fiber-reinforced polymer (CFRP). The load resisting performance of CFRP-wrapped spans comprising BC2 were compared with the results obtained from the interior span tests performed on BC1. A total of six tests were performed on the two damaged bent caps. The test regions considered in each of the ultimate load tests and the cap regions employing CFRP retrofits are illustrated in Figure 3.4. Note that for brevity, only the test results from tests BC1-1, BC2-1, and BC1-3 are presented in this section. Appendix A (BC1) and Appendix B (BC2) show the results of the remainder of the experiments.

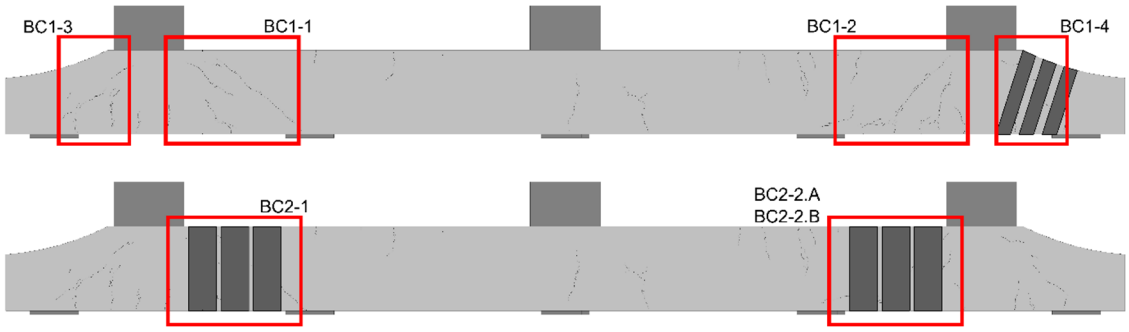

Figure 3.4. Mapping of performed tests, (top) BC1 tests, (bottom) BC2 tests

3.2.1 INTERIOR SPAN TESTS

3.2.1.1 Test Setup

To ensure that uniform support and loading conditions were provided during the testing of the continuous bent cap members, the bent caps were tested in an 'upside-down' configuration (i.e., girder lines corresponding to the bottom surface of bent cap and the

supporting columns were physically located on the top surface of the bent cap). The top reaction beams shown in Figure 3.5 (i.e., the red, green, and yellow members) were designed with variable lengths to accommodate the geometry of strong floor serving as the primary reaction structure. In consideration of these variable lengths, the reaction beams were fabricated with different depths in an effort to provide approximately equal flexural stiffnesses for each column reaction assembly, resulting in near-uniform column reaction stiffnesses.

Hydraulic rams were provided at the location of each of the girder lines to simulate the applied loading from the superstructure to the bent cap. Load cells were placed at each column reaction point and at each hydraulic ram to measure the applied loads and reactions along the length of the bent cap. Additionally, strain gauges were installed on the steel rods supporting the reaction beams and were used as a means of verifying the load cell measurements comprising the column reaction assemblies. Linear potentiometers were provided along the length of the bent cap to monitor bent cap deflections. Finally, digital image correlation (DIC) systems were used to monitor the concrete strain and deformation behavior within the test regions.

3.2.1.1.1 Loading Procedure

The test frame was designed to approximately simulate the loading conditions experienced by the bent cap while in service. Preliminary modeling of the superstructure was used to estimate the loads transferred from the superstructure to the bent cap as a result of the superstructure dead load. The magnitudes of the dead loads transferred from the superstructure to the bent cap at each of the GLs were approximately equal and estimated to be on the order of 70 to 75 kip. Therefore, the first phase of loading consisted of simulating service dead load by applying equal magnitude point loads at the location of

each of the five GLs. During this phase of loading, it was found that in order to develop crack widths within the existing shear cracks that were approximately similar to those measured during the in-field inspection of the bent cap, an initial girder load of 80 kip was required at each GL.

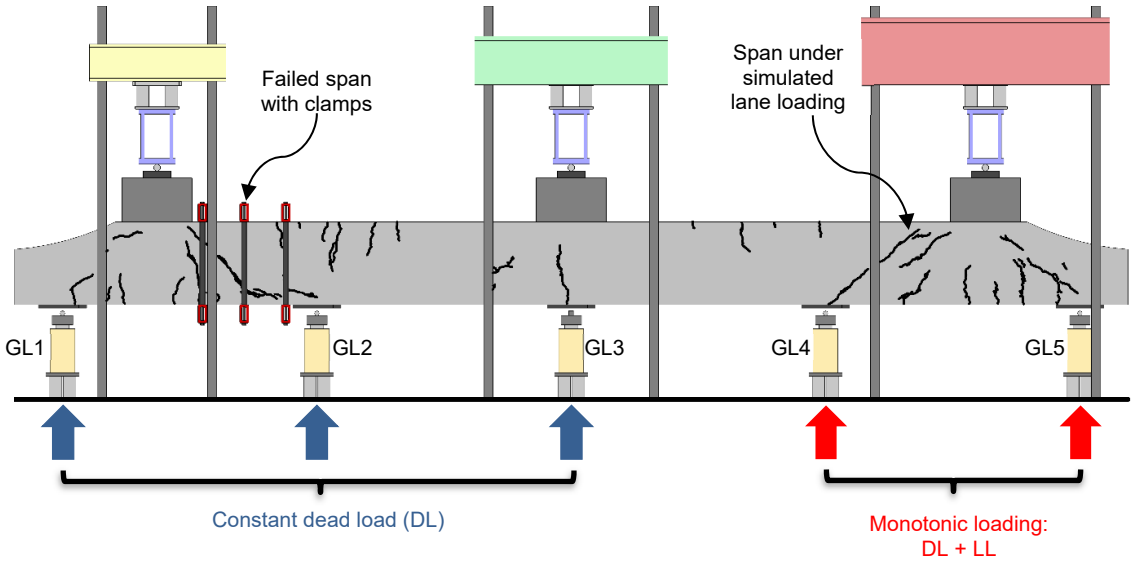

Figure 3.5. Typical interior span test loading conditions and GL locations (east face)

The second phase of loading consisted of applying isolated lane load to the two outermost GLs (i.e., GL1 and GL2 for BC1-1; GL4 and GL5 for BC1-2). These loads were applied using a series of predefined load stages, over which the loading was intermittently paused to permit the inspection of the bent cap and the measurement of crack widths. After failure of one interior span was achieved, the failed span was strengthened using external clamps and the full test procedure was repeated; however, with isolated lane loading applied to the interior span located at the opposite end of the bent cap. The loading configuration used for the second interior span test of BC1-2 is presented in Figure 3.5.

3.2.1.1.2 Instrumentation

The data collected over the course of testing included the applied loads and reactions, the bent cap vertical deflections, and the strain and deformation behavior within the interior span region.

Load cells of 500 kip capacity were placed at each column reaction point and at each hydraulic ram to measure the applied loads and reactions along the length of the bent cap. Three load cells were used at each of the hydraulic rams and four load cells were used at the top reaction beams (i.e. above the column stubs). Additionally, strain gauges were installed on the steel rods supporting the reaction beams and were used as a means of verifying the load cell measurements comprising the column reaction assemblies. The pressure in the hydraulic rams was also monitored at different load stages of the experiment to verify the applied loads.

Linear potentiometers were provided along the length of the bent cap to monitor vertical deflections. Aluminum angles supported at the points of zero deflection (i.e., at the centerlines of the column stubs) functioned as the reference line for the linear potentiometers to measure the bent cap deflection. The potentiometers were strategically aligned with each hydraulic ram to directly measure deflections at the applied load locations. In addition, linear potentiometers were also placed at the points of zero deflection to verify that no displacement occurred at

Finally, digital image correlation (DIC) systems were used to monitor the strain and deformation behavior within the interior spans test regions (i.e. the strain of the concrete for the unretrofitted case, and the strain of the CFRP for the retrofitted case). Refer to Figure 3.6 for a summary of key instrumentation used during testing.

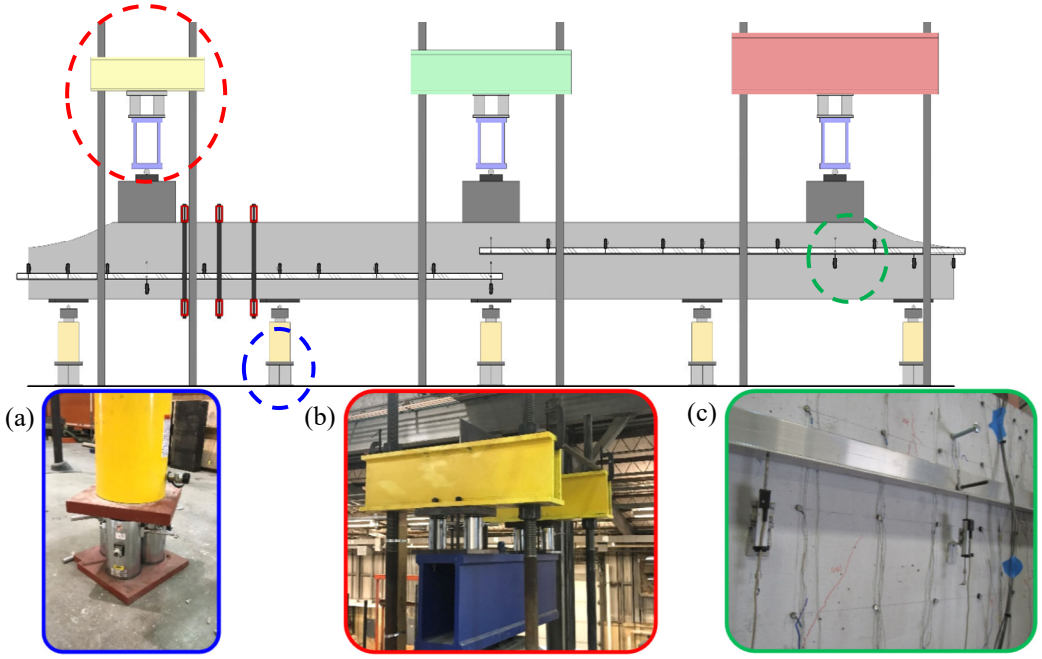

Figure 3.6. Test instrumentation; a) load cell cluster provided at each of the hydraulic rams, b) typical load cell configuration provided at top reactions, c) linear potentiometers to measure deflection along the bent cap

3.2.1.2 BC1-1: Unretrofitted Span

Test BC1-1 involved the testing of an un-retrofitted (i.e., without the application of the CFRP retrofit) interior span region of BC1. The test was performed in accordance with the testing procedure described above. It is worth noting that, upon completion of this test, it was determined that the top load cells (i.e., those comprising the column stub support reactions) did not accurately record the reactions throughout the experiment. Therefore, the data recorded by the top load cells from subsequent tests BC1-2 and BC2-1 were used to estimate the top reactions, on the basis of the applied loads, at certain load stages of test BC1-1. The proper functioning of the bottom load cells (at each of the applied GL load locations) was confirmed by monitoring the pressure of each hydraulic ram and comparing the pressure with the respective load cell readings.

Crack widths were recorded at different stages of loading. Figure 3.7 presents the crack widths and crack patterns measured in the field, under the simulated service dead load case (i.e., with an applied load of 80 kip at each GL hydraulic ram), under a 180 kip simulated lane loading scenario, and the crack pattern after the end of the test. On the basis of the crack widths presented in Figure 3.7a and 3.7b, it can be seen that the crack widths under simulated service dead load were comparable to those measured in the field, prior to extracting the bent caps from the bridges.

Figure 3.10a, 3.10b, and 3.10c show the deflection, shear, and bending moments corresponding to the 80 kip (dead load), 180 kip, and ultimate load cases respectively. Figure 3.10d shows the maximum measured shear force in the critical interior span (i.e. to the left of GL2) over the course of testing, plotted with respect the average deflection, which was calculated as shown in Figure 3.8. Note that the curve does not present all post-peak response because, during the test, the tilt saddles of the outer rams abruptly tipped, decreasing the bottom reactions by approximately 10 kips. As a result, the applied simulated dead loads were reduced to 70 kips as opposed to the 80 kip target value.

The failure of test BC1-1 was controlled by a tension-controlled shear failure. Shear cracking damage was observed on the interior span throughout the duration of the test, specifically within the concrete comprising the main strut (i.e., stemming from the location of the column stub to GL2). The development of new, but small-width, shear cracks were formed at the overhang. The failure occurred after the shear cracks of the interior span widened excessively. Concrete crushing was also observed within the concrete comprising the main interior span strut. Note that, after reaching ultimate shear, the resistance of the cap rapidly decreased and no sign of ductile behavior was observed. At 90 % of ultimate load, the major shear crack was x 1.3 the width of that measured during the field inspection. The shear cracks can be visualized in Figure 3.9c, 3.9d, 3.9e, and 3.9f.

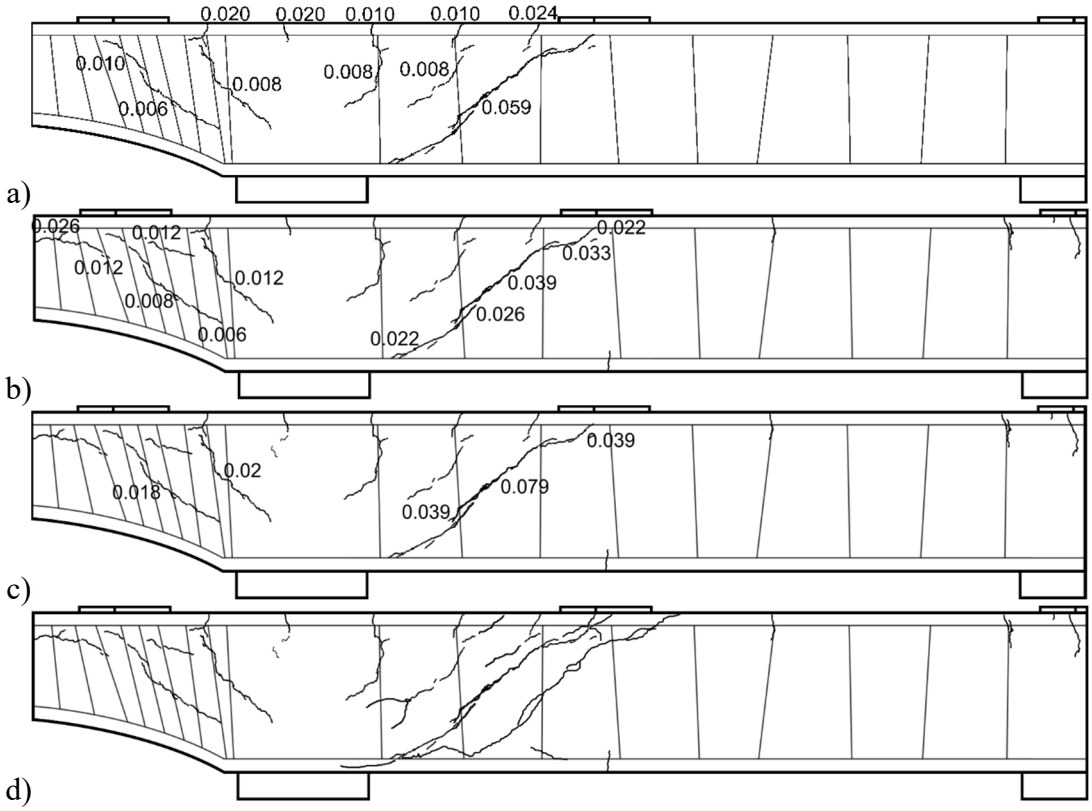

Figure 3.7. BC1-1 cracking data, and measured reinforcement placement, a) Field inspection, b) Constant dead load case, c) 180 kip load case (i.e., at approximately 90 % of the ultimate capacity), d) Crack pattern after test

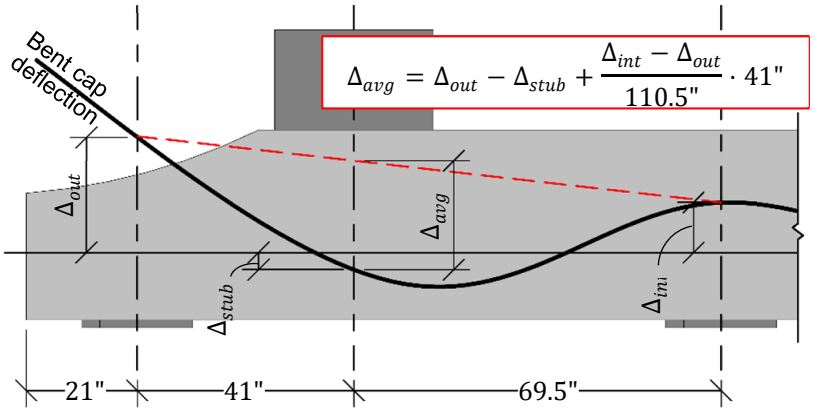

Figure 3.8. Average deflection calculation procedure for maximum shear vs. deflection plot

The maximum shear force resisted by BC1 within the interior span was estimated to be 166 kip, which corresponded to a maximum applied girder line load of 208 kip. The measured shear capacity of the interior span was comparable to that estimated by way of current AASHTO provisions, which was estimated to be 185 kip (minimum shear reinf. provided) and 171 kip (minimum shear reinf. not provided). The sectional analysis calculations performed in accordance with the AASHTO provisions are presented in Appendix C.

Note that the test results obtained for BC1-2, the other interior span region comprising BC1, yielded very similar shear capacity and was controlled by similar failure mechanisms. The shear capacity from BC1-2 was 167 kip. Additional details regarding the test results for BC1-2 are available in Appendix A.

a) Test setup

b) Crack width measurements

c) Major shear crack on the interior span after test completion (west face)

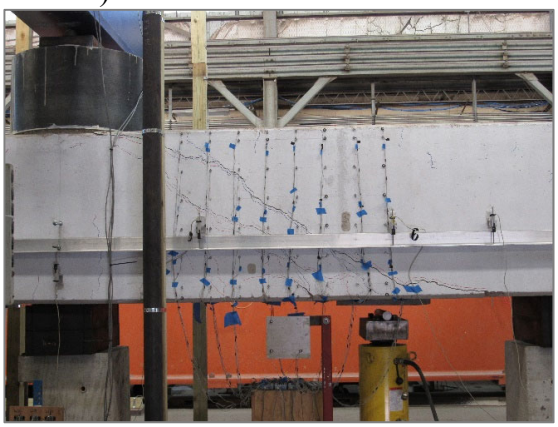

d) Major shear crack on the interior span after test completion (east face)

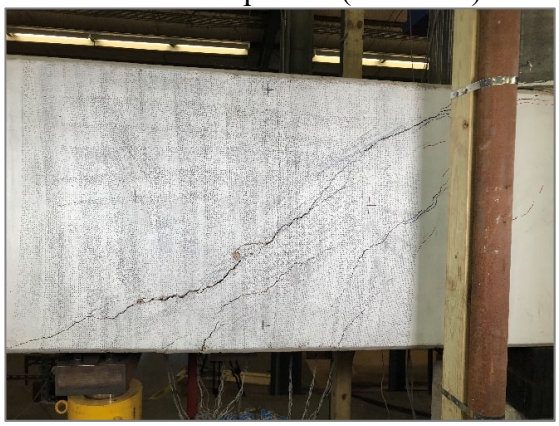

e) Major shear crack on the interior span after test completion (west face)

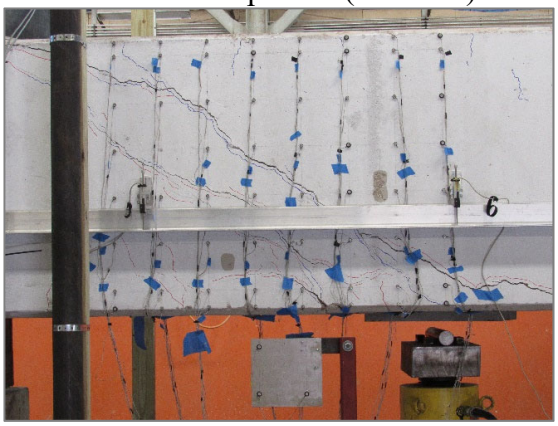

f) Major shear crack on the interior span after test completion (east face)

Figure 3.9. BC1-1 photos

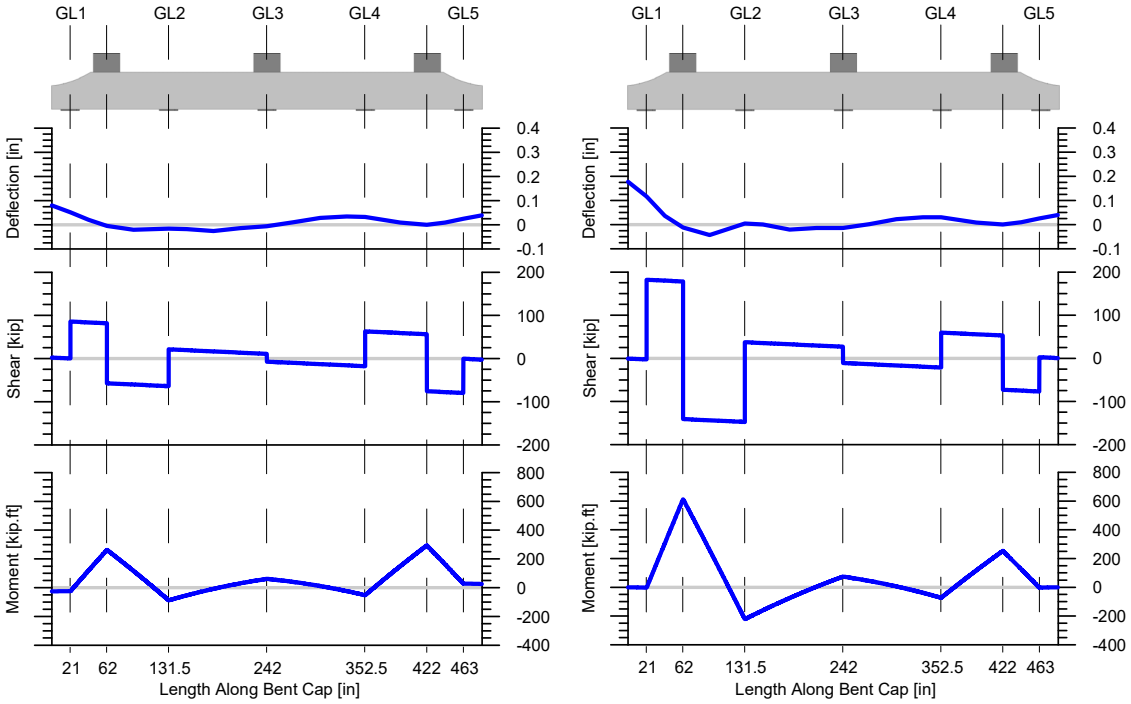

(a) 80 kip, constant dead load

(b) 180 kip monotonic load

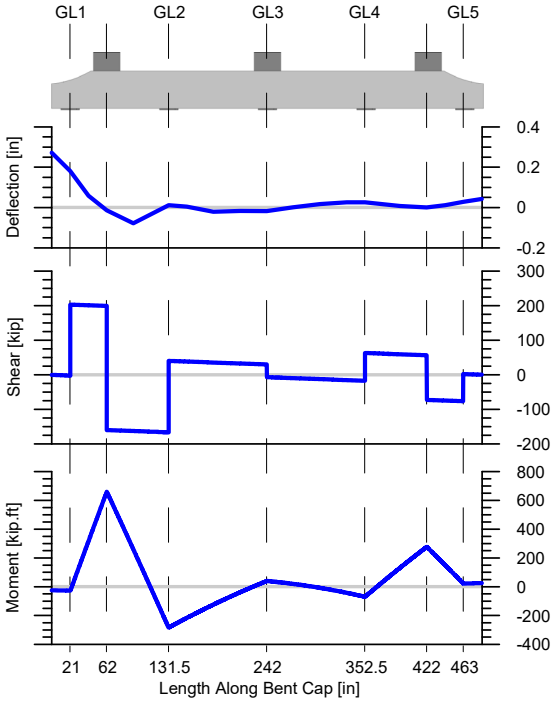

(c) ultimate load

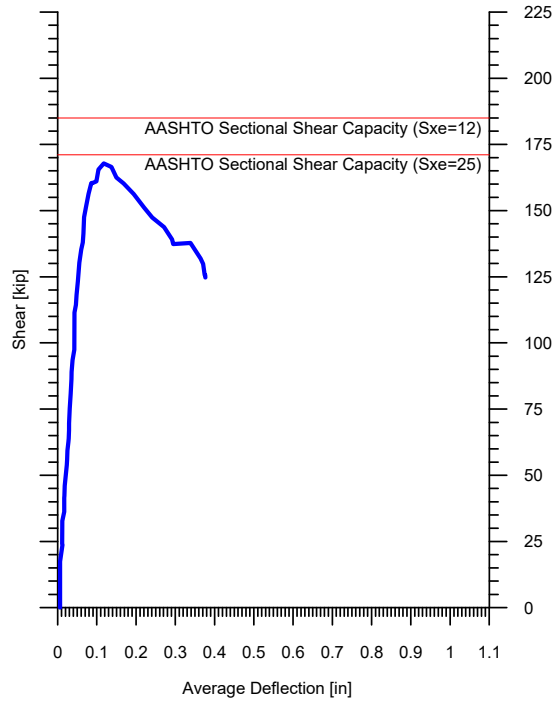

(d) shear vs. average deflection

Figure 3.10. BC1-1 moment, shear, and deflections

3.2.1.3 BC2-1: Retrofitted Interior Span

Test BC2-1 involved the testing of a retrofitted (i.e., employing CFRP wrapping) interior span region of BC2. The test was performed in accordance with the interior span test procedure previously presented, however, no external clamps were used to strengthen the previously tested interior span. The primary objective of test BC2-1 was to determine if the application of a typical CFRP retrofit would be providing adequate shear strength enhancement to mitigate the shear-controlled failure modes observed in tests BC1-1 and BC1-2, and result in more favorable flexure-controlled failure modes.

Due to the CFRP wrap having been applied to the interior spans and covering the majority of the major existing shear cracks comprising BC2, no crack width measurements from this test have been reported in this document. However, crack measurements were taken at several load cases of cracks forming in between the CFRP strips and at the overhang. Note that the crack in between the CFRP strips were covered in resin for the installation of the CFRP.

Figure 3.12a, 3.12b, and 3.12c present the bent cap deflection, measure shear force, and measured bending moments corresponding to the 80 kip (dead load), 180 kip, and ultimate load cases respectively. Figure 3.12d shows the measured shear force in the critical interior span (at a location immediately adjacent to GL2) over the course of testing, plotted with respect the average deflection, which was calculated as shown in Figure 3.8.

The failure of test BC2-1 was controlled by flexure. The formation of shear cracks was evident in the small gaps between the CFRP strips and in bent cap regions adjacent to the reaction points that were not covered with CFRP. However, the bent cap presented severe loss of stiffness when major flexural cracks formed at the face of the column stub, and at a section approximately 14 in. away from the column stub face (which may have caused the delamination and rupture of the inner edge of CFRP strip closest to the column

stub, shown in Figure 3.11a). After the formation of the first major flexural cracks, load continued to be applied to verify yielding of the longitudinal reinforcement. The bent cap was then unloaded to the constant dead load case (i.e., the pressure in each hydraulic ram was reduced to a pressure representing the 80 kip dead load) and reloaded to confirm the same unloading and reloading stiffnesses, as is shown in Figure 3.12d. During the reloading stage, the CFRP was reengaged at approximately 0.6 in. of average deflection (Figure 3.12d). As a result of continued displacement of the retrofitted span and after extensive yielding of the longitudinal reinforcement had taken place, the concrete comprising the main strut began to show some evidence of crushing.

The ultimate shear force resisted by the CFRP-retrofitted interior span was estimated to be 209 kip which corresponded to a maximum applied girder line load of 273 kip and a maximum bending moment of 678 kip-ft at the interior face of the exterior column stub. In comparison to the results obtained from BC1, the capacity of the retrofitted bent cap was approximately 30 % greater than that obtained for the non-retrofitted cap. However, it must be reiterated that the ultimate capacity obtained from test BC2-1 was limited by the flexural capacity of the bent cap and was not governed by the shear resisting performance of the retrofitted cap. The sectional moment capacity of BC2 at the interior face of the exterior column stub was estimated to be of 799 kip-ft. It is worth noting that some of the longitudinal reinforcement in tension may not have been fully developed (2-#11 and 1-#10 bars are curtailed at the interior span, refer to Figure 2.5).

Results from the digital image correlation (DIC) system data show that the largest strain in the CFRP-wrap was concentrated at a section located approximately 14-in. away from the column stub face, which coincides with the region where major flexural cracks formed. The strain profiles for the first loading stage peak load and the reloading stage peak load are shown in Figure 3.13a and 3.13b, respectively. The strain profiles show a

maximum CFRP strain on the order of 6 x 10-3 in./in. for the first loading stage and of 8 x 10-3 in./in for the reloading stage. Note that the strain differences between both load stages are a result of the large deflections and crack widening during the reloading stage. Figure 3.13b (i.e., reloading stage peak load strain profile) show wider and larger flexural and shear cracks than Figure 3.13a (i.e., first loading stage peak load strain profile), specifically at the region closest to the face of the column stub.

Note that in both of these cases, the CFRP wrap did not develop the ultimate strain value of 10 x10-3 in./in. coinciding with the manufacturer's reported rupture strain for the CFRP system. Thus, it can be confidently stated that the CFRP was not fully-utilized during the test as a result of the flexure-controlled failure mechanisms. However, it should also be noted that some local rupturing of the CFRP was observed, but was attributed to the formation of large-width flexural and shear cracks underneath the wrapping system.

Note that the test results obtained for BC2-2, the other retrofitted interior span region comprising BC2, also presented similar flexural failure mechanism. The calculated bending moment at the interior face of the exterior column stub was of 578 kip-ft, and the shear capacity was of 211 kip. Additional details regarding the test results for BC1-2 are available in Appendix B.

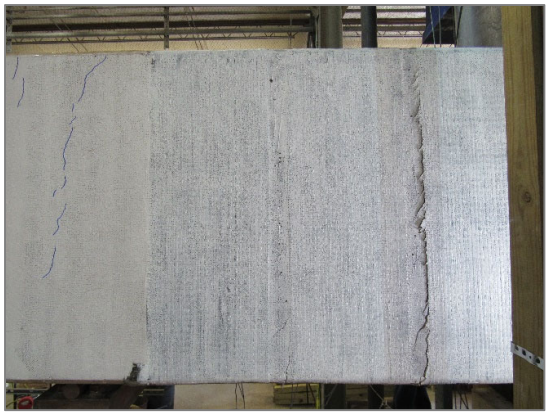

a) Major flexural cracks after unload showing flexural crack along the inner edge of CFRP strip (west face)

b) Major flexural cracks at the face of the column after reloading (west face)

c) Major flexural cracks at the face of the column after reloading (west face)

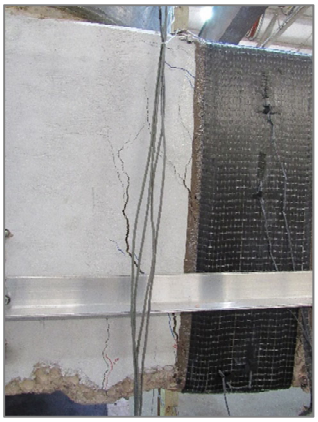

d) Shear and flexural cracks at the face of the column after test completion (east face)

e) Shear and flexural cracks at the face of the column after test completion, and ruptured CFRP shown (east face)

f) Major flexural crack at the face of the column after test completion (west face)

Figure 3.11. BC2-1 photos

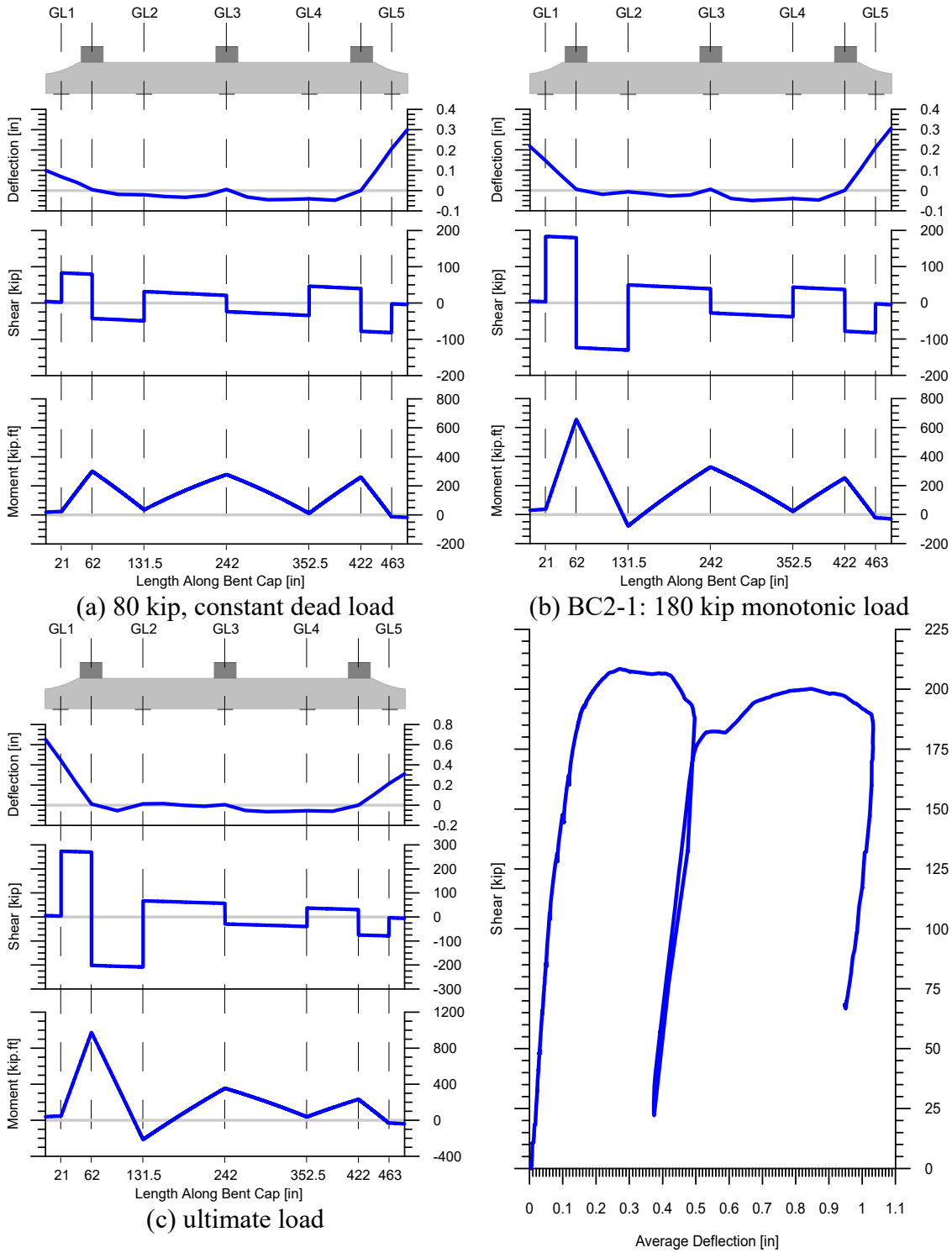

(a) 80 kip, constant dead load

(b) BC2-1: 180 kip monotonic load

(c) ultimate load

(d) shear vs. average deflection

Figure 3.12. BC2-1 moments, shear, and deflections

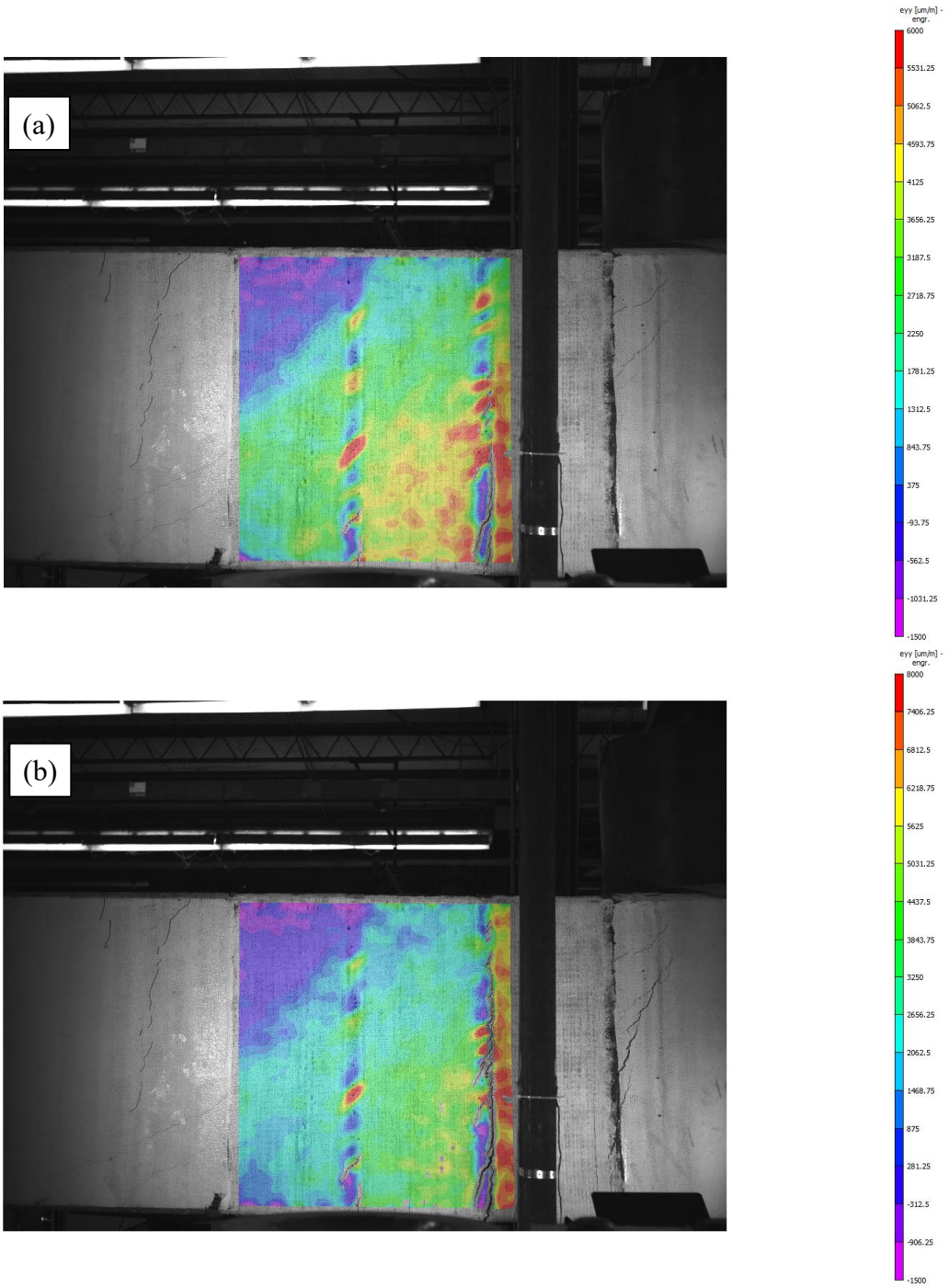

Figure 3.13. BC2-1: DIC strain contours; a) First loading stage peak load, b) Reloading stage peak load

3.2.2 OVERHANG TESTS

In addition to the interior span testing, the overhang/cantilever regions of the bent caps were also tested to failure to examine their load resisting performance. Prior to performing the overhang testing, BC1 was first cut at two locations: at the immediate right of the middle column stub and at GL4.

3.2.2.1 Test Setup

The setup of the overhang test required part of the bent cap to cantilever as shown in Figure 3.14. Hence, a shorter cantilever was beneficial to align the cut bent cap with the reaction points and to avoid the development of large stresses generated by the self-weight of the cantilever. Similar to the interior span tests, the overhangs were tested in an 'upside-down' configuration. A support was added 2 ft. to the right of the column stub centerline in an effort to prevent the already tested interior span from failing; thus, permitting investigation of the overhang failure region. External clamps were used to strengthen the already tested interior span region. A single hydraulic ram aligned with the overhang girder line (i.e., GL1 or GL5) was used to load the overhang. Load cells were placed at the locations of the hydraulic ram and at the column reaction; however, only the load cells at the hydraulic ram location were used to report data. The load cells at the top reaction were used to monitor and verify equilibrium over the course of testing.

3.2.2.1.1 Loading Procedure and Instrumentation

The testing procedure for the overhang tests consisted of monotonically loading the overhang GL. The load was intermittently paused to permit the inspection of the bent cap and the measurement concrete of crack widths. Once signs of an ensuing failure were observed, the overhang was continuously loaded to failure for the remainder of the test.

Load cells were place at the location of the hydraulic ram and at the top reaction frame in an effort to measure the applied load and the reaction at the column stub. In addition, linear potentiometers were placed along the bent cap, strategically aligning potentiometers with the centerlines of the applied load and at reaction points.

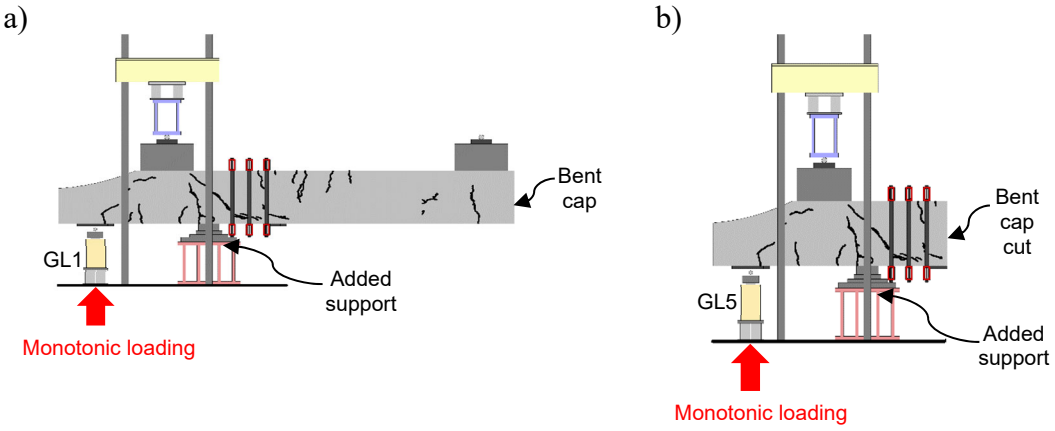

Figure 3.14. Overhang test configuration and loading conditions, a) BC1-3, b) BC1-4

3.2.2.2 BC1-3: Overhang

Test BC1-3 involved the testing of an un-retrofitted (i.e., without the CFRP wrapping) overhang of BC1. The test was performed in accordance with the overhang test procedure presented above.

Crack widths were recorded at several different stages of loading. Figure 3.15 shows crack widths and patterns for the overhang region measured in the field, under an applied load of 250 kip (78 % of ultimate), under an applied load of 300 kip (94 % of ultimate), and after completion of the test.

Figure 3.18a shows the measured bent cap deflection, measure shear forces, and measured bending moments at ultimate. Figure 3.18b shows the maximum measured shear force in the critical interior span (i.e. to the right of the outermost GL) over the course of testing, plotted with respect to the overhang deflection shown in Figure 3.16.

The failure of test BC1-3 was governed by a compression-controlled shear failure. Over the course of the test, new shear cracks formed within the overhang region (i.e., from GL1 to the column stub centerline) and at the interior span (i.e., from the column stub centerline to the added support), as shown in Figure 3.17b, 3.17c, and 3.17d. Evidence of concrete crushing was observed within the concrete comprising the main strut as shown in Figure 3.17b and Figure 3.17f. Concrete crushing also occurred at the column stub centerline, as shown in Figure 3.17b. Ultimately, the cap failed after significant widening of the shear cracks and accompanied concrete crushing comprising the overhang strut. The resultant of this damage led to appreciable stiffness degradation.

The ultimate shear force resisted by the bent cap overhang span was estimated to be 317 kip, which corresponded to a maximum applied girder line load of 319 kip (note, the slight offset is due to the self-weight of the overhang). The bending moment developed at the face of the column, immediately prior to failure, was equal to 682 kip-ft. The measured shear capacity of the interior span was comparable to that estimated by way of current AASHTO provisions, which was estimated to be 331 kip.

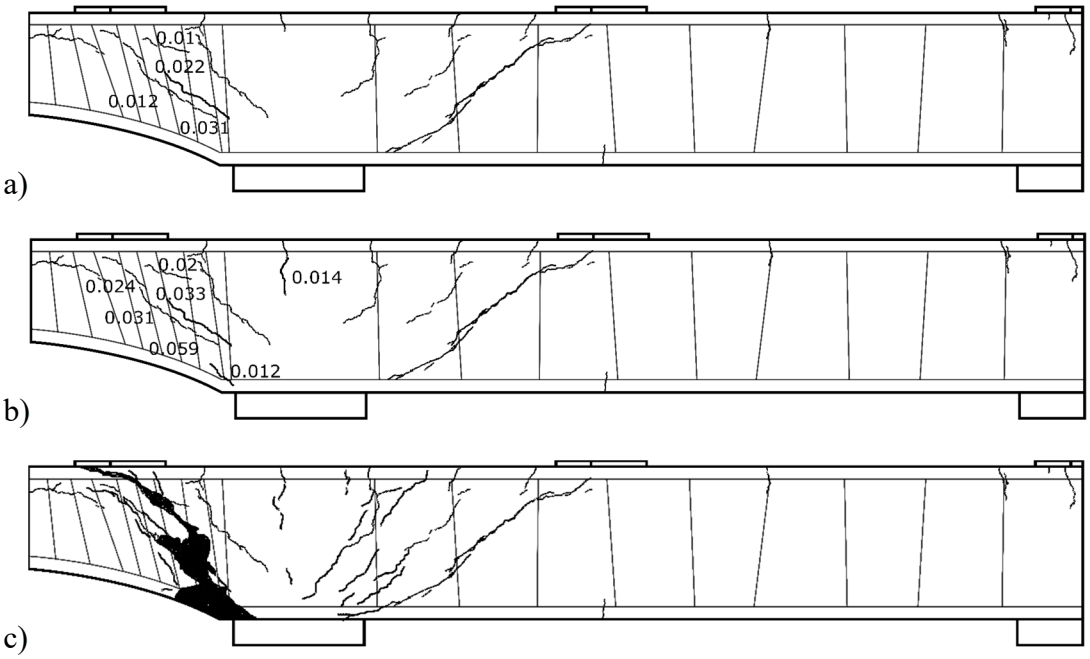

Figure 3.15. BC1-3 crack widths and pattern, and actual reinforcement, a) 250 kip load case, b) 300 kip load case, c) Crack pattern after test

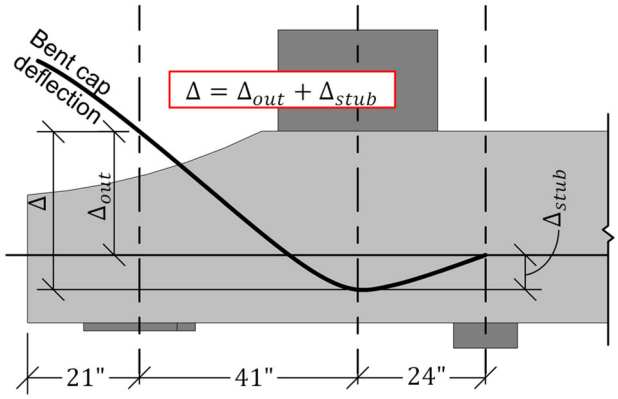

Figure 3.16. Change in deflection calculation procedure for shear vs. deflection plot

a) BC1-3 test setup

b) Shear cracks and observed concrete crushing after test completion (east face)

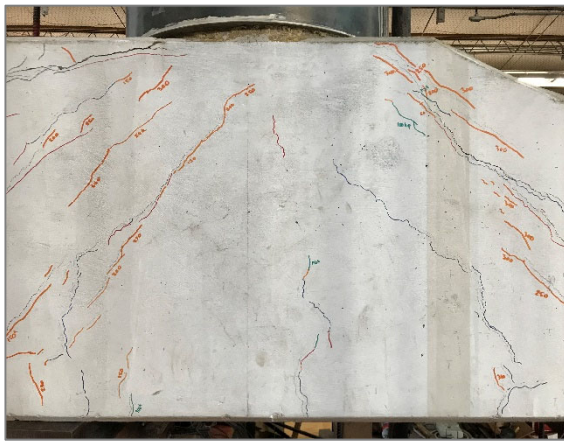

c) Crack pattern at column stub at the 300 kip load case (west face)

d) Crack pattern at overhang at the 300 kip load case (west face)

e) Shear cracks at overhang after test completion (west face)

f) Shear cracks and concrete crushing at overhang after test completion (west face)

Figure 3.17. BC1-3 photos

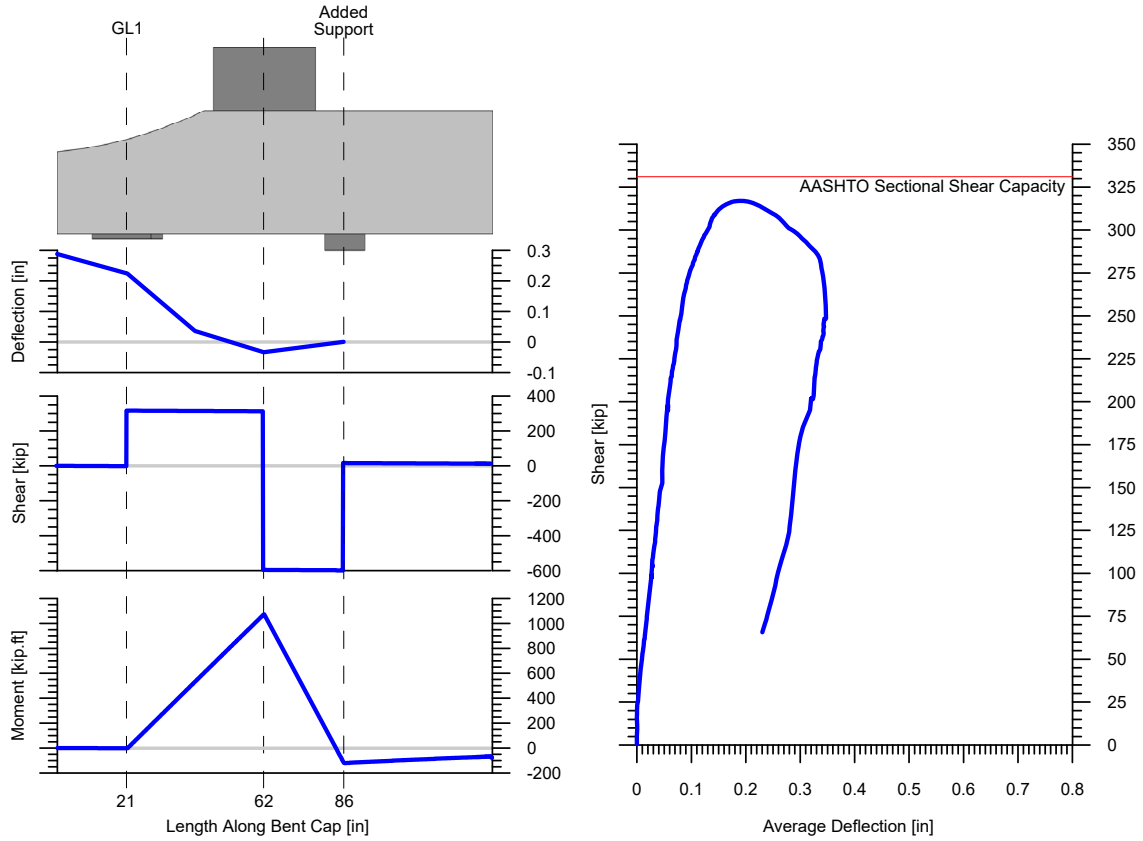

(a) ultimate load (b) shear vs. average deflection

Figure 3.18. BC1-3 moments, shear, and deflections

3.3 Chapter Summary and Discussion

Laboratory testing was performed to evaluate the load resisting performance of two shear-damaged RC bent caps. Further, the overhangs of BC1 were also tested to evaluate the shear-resisting performances. Member deflections, applied shear forces and bending moments, and concrete crack width measurements were recorded over the course of testing and briefly summarized in this chapter.

The failures of the tests performed on the interior spans of the bent caps were controlled by shear failure modes for the non-retrofitted sections, and by flexural-governed failure modes for the CFRP-retrofitted sections. The unretrofitted overhang was controlled

by shear; however, failed at a load that was only marginally lower than the estimated flexural capacity of the overhang. The retrofitted overhang test failed prematurely due to the slipping of the longitudinal reinforcement and as a byproduct of the heavily-damaged condition of the previously tested bent cap specimen. Nevertheless, it was found that the CFRP-retrofitted overhand was still able to resist loads exceeding that of the non-retrofitted overhang.

The following key findings were obtained from the ultimate load testing of the shear-damaged RC bent caps:

1. Despite the presence of the documented large-width shear cracks developed while in service, the capacity of the bent caps still permitted the application of isolated lane loading within the critical/damaged bent cap regions that greatly exceeded estimated service dead loads and provided shear resistances that were in-line with shear capacity estimates developed using the sectional shear design provisions of AASHTO LRFD. The most severe diagonal cracks developed in the bent caps while in service, significantly grew in width (e.g., 1.3 x service crack width for BC1-1; 2.5 x service crack width for BC1-2) prior to failing in shear under laboratory testing conditions. Thus, the large width diagonal cracks observed in the field were indeed the result of shear distress.
2. The use of the CFRP-wrap to retrofit the interior spans of BC2 was found to be a suitable method to improve the shear capacity of the section. The retrofitted interior spans led to a 25 % increase of shear capacity and to the caps to failing in flexure as opposed to shear. The actual shear strength enhancement provided by way of the CFRP retrofits was not evaluated through this testing program because the bent cap load resisting capabilities were limited by the flexural capacities of the caps.

3.4 Comparison of Tests Results with Nominal Design Values

The nominal shear strengths of the bent caps were estimated by means of the current AASTHO LFRD Bridge Design provisions (AASHTO). The calculation procedures used to perform these calculations are shown in Appendix C.

The shear strength capacity of three different bent cap cross sections were computed: i) a non-retrofitted interior span, ii) an non-retrofitted overhang; and the retrofitted interior spans. Non-retrofitted shear strength estimates were computed in accordance with AASHTO LRFD sectional design provisions and shear strength capacities for the CFRP-retrofitted interior spans were computed using ACI 440.2R. Key findings from the code provisions strength assessment are listed below:

- The results of the shear strength of the non-retrofitted calculated using AASHTO LRFD provisions were in-line with the experimental data if it assumed the steel reinforcement did not satisfy minimum requirements and size effects (by way of the effective crack spacing) are considered. Transverse steel reinforcement minimum requirements should also be a function of placement and spacing.
- The overhang experimental results a failure shear value of 317 kip, while the AASHTO LRFD provisions nominal shear strength value was of 331 kip. The calculated value overestimated the experimental data by only 4%.

As a means of scrutinizing the experimental data obtained, the theoretical sectional shear capacities of the bent caps were computed in accordance with the AASHTO LRFD Bridge Design Specifications and compared with the measured bent cap capacities. Considering the AASHTO General Shear Design Method, without the application of capacity resistance factors, the nominal capacity for the interior span sections of the RC bent caps was estimated to be 185 kip (minimum shear reinforcement provided) and 171

kip (minimum shear reinforcement not provided); and the nominal capacity of the cantilever sections was estimated to be 331 kip.

Note that this analysis was done on the basis of Section 5.7.3.3 of the provisions and arguably may not be entirely suitable in this case given the large cross sections of the supporting columns and the relatively small shear span-to-depth (a/d) ratios of the controlling shear spans considered. More specifically, the a/d ratio for interior span test cases was approximately 2.1 from center of the column to center of applied load; and a/d is reduced to approximately 1.7 when measured from the edge of the column stub.

For the overhang tests, the a/d was approximately 1.2 from the center of the column to the center of overhang load, and is reduced to 0.8 when measured from the edge of the column stub. Further, it must also be noted that although the large spacing and placement of the stirrups employed in the interior spans of the bent caps does not satisfy current AASHTO provisions, it was assumed that the stirrups would still remain effective and thus, were considered in the sectional shear strength calculations.

Table 3.2 presents the experimental capacity results obtained from the bent cap testing alongside the strength estimates determined on the basis of the AASHTO sectional design provisions and the estimated flexural capacities of the bent caps (refer to Appendix C for detailed calculations). Despite the arguably questionable applicability of the sectional shear design provisions being used for cases with large cross sections and relatively small shear span-to-depth ratio of the controlling span, it is encouraging to note that the sectional shear strength estimates developed using the AASHTO provisions are indeed in-line with what was observed experimentally for BC1-1 and BC1-2. This further reinforces the finding that the impact of the existing shear cracking damage on the overall load carrying capacities of the shear-cracked bent caps was likely limited.

The sectional shear capacity of the CFRP-retrofitted sections was computed according to ACI 440.2R-17 and was determined to be 297 kip for interior spans and 429 kip for the overhang. However, as discussed previously, the tests of the retrofitted bent cap sections were controlled by flexural failure mechanisms. Hence, the shear capacities of the retrofitted sections were not verified experimentally.

Table 3.2. Summary of test results

Test	Test Region	CFRP Wrap	Experiment Shear Capacity [kip]	Experiment Column-Face Moment [kip-ft.]	Observed Failure Mode	Estimated Shear Capacity* [kip]	Estimated Flexural Capacity [kip-ft.]
BC1-1	Interior	No	166	461	Shear	185 **	799
BC1-2	Interior	No	167	435	Shear	185 **	
BC1-3	Overhang	No	317	682	Shear	331	
BC1-4	Overhang	Yes	331	711	Bar slip	429	
BC2-1	Interior	Yes	209	678	Flexure	297	859
BC2-2	Interior	Yes	211	578	Flexure	297	

* shear capacity estimates on basis of AASHTO for non-retrofitted sections and ACI 440.2R-17 for retrofitted sections.

** sectional shear capacity reported calculated with $S_{xe} = 12$. Refer to Section 6.1.1.

Finally, it should be noted that the reported column-face moments for the retrofitted bent cap tests should be viewed as lower-case estimates. In all cases, flexural cracking within the column stub regions was apparent. Thus, the actual bending moments developed in the bent caps were in fact larger than the values reported at the column face. Further, as summarized in Section 2.1 several of the longitudinal bars comprising the interior span regions of the RC bent caps were curtailed at the point of the adjacent girder line (refer to Figure 2.5). The termination of these bars, and their resulting reduced development lengths, were not considered in the calculation of the estimated flexural capacities presented in Table 3.2. Combined, these two factors should be considered when comparing the experimentally-reported bending moments and the reported estimated flexural capacities. Despite the disparity between the reported column faces bending moments developed in

the tests and the estimated flexural capacities of the bent caps, the test results clearly showed that retrofitted interior span tests BC2-1 and BC2-2 were governed by flexural failure mechanisms.

CHAPTER 4 SUMMARY AND CONCLUSIONS

4.1 Summary

This thesis provided an overview of the findings obtained from the in-field inspection and subsequent laboratory testing of two 60-year old RC bent caps, which were classified as structurally deficient related to poor structural condition. This project aimed to determine the reinforced concrete shear strength of the two bent caps extracted from service. To accomplish this goal, the following tasks were accomplished:

1. Conduct visual inspections of the bent caps noting crack patterns, locations and widths.
   - A *site inspection* was conducted prior the removal of the bridge superstructures.
   - A *laboratory inspection* was conducted after the extraction and delivery of bent caps to the laboratory to determine the as-received state of damage of the specimens.
2. Pre-test characterization of concrete mechanical properties.
   - Concrete cores from the exterior faces of the bent caps were extracted and tested.
3. Retrofit of the column stubs for structural testing was performed.
4. A carbon fiber-reinforced polymer (CFRP) retrofit was employed for the interior damaged spans of BC2.
5. Conduct ultimate load testing on the decommissioned RC bent caps.
6. Post-test characterization of concrete and steel reinforcement.
   - Concrete cores were extracted from the interior of the bent caps and tested.
   - Several steel reinforcement bars were extracted from each bent cap and tested.

7. Structural assessment of the decommissioned bent caps AASHTO LRFD Bridge Design Specifications, 8th Edition and ACI 440.2R-17.

4.2 Conclusions

Existing RC structures, which were typically designed with what are now outdated design strategies/provisions, require thoughtful examination to assess the impacts of observed structural damage and degradation. In this study, it was found that the largest-width in-service diagonal shear cracks had occurred in the regions of the bent caps constructed with very light shear reinforcement and, in part, were likely the byproduct of the large stirrup spacings employed within those bent cap regions. The following presents the key findings obtained from the experimental program:

4.2.1 Mechanical Properties

- The factored compressive strengths of the concretes comprising the bent caps was on the order of about 2.3 to 2.4 ksi. In both cases, these values were less than 80 % of the design-specified strength value of 3.0 ksi for the Class A concrete (1957 AASHO) noted in the design drawings. Note that the factored compressive strengths being referred to include the strength enhancement factor specified by ASTM C42/C42M to approximately account for concrete damage that likely occurred during the core drilling process.
- Noted poor adhesion between the concrete and the steel reinforcement comprising the bent caps raises further questions regarding the concrete quality used in bent cap construction.

4.2.2 BENT CAP STRUCTURAL PERFORMANCE

- Despite the presence of the documented large-width shear cracks developed while in service, the capacity of the bent caps still permitted the application of isolated lane loading within the critical/damaged bent cap regions that greatly exceeded estimated service dead loads and provided shear resistances that were in-line with shear capacity estimates developed using the sectional shear design provisions of AASHTO LRFD. Further, the most severe diagonal cracks developed in the bent caps while in service, significantly grew in width (e.g., 1.3 x service crack width for BC1-1; 2.5 x service crack width for BC1-2) prior to failing in shear under laboratory testing conditions. Thus, the large width diagonal cracks observed in the field were indeed the result of shear distress.
- The use of the CFRP-wrap to retrofit the interior spans of BC2 was found to be a suitable method to improve the shear capacity of the section. The retrofitted interior spans led to a 25 % increase of shear capacity and resulted in the caps failing in flexure as opposed to shear. The actual shear strength enhancement provided by way of the CFRP retrofits was not evaluated through this testing program because the bent cap load resisting capabilities were limited by the flexural capacities of the caps.
- Although the shear reinforcement detailing employed in the interior spans of the bent caps does not satisfy current design requirements and the bent caps had extensive preexisting shear cracks, shear strength capacity estimates developed using the AASHTO LRFD sectional design provisions were in good agreement with measured shear strengths.

4.2.3 APPRAISAL OF BENT CAP CAPACITIES

- The results of the shear strength of the unretrofitted calculated using AASHTO LRFD provisions were in-line with the experimental data if assuming the steel reinforcement did not satisfy minimum requirements and considering aggregate size effects. Transverse steel reinforcement minimum requirements should also be a function of placing and spacing.
- The overhang testing resulted in a shear capacity of 317 kip, while the AASHTO LRFD provisions nominal shear strength value was of 331 kip. The calculated value overestimated the experimental data by only 4%.

APPENDICES

APPENDIX A Bent Cap 1 Results

The following appendix shows all the results obtained from inspections and remainder of tests not presented in the body of the thesis of Bent Cap 1.

A.1 ULTIMATE LOAD TESTS

A.1.1 BC1-2: Unretrofitted Interior Span

Test BC1-2 involved the testing of an un-retrofitted (i.e., without the CFRP wrapping) interior span region of BC1. The test was performed in accordance with the interior span test procedure presented in Section 3.2.1.1.1. Note that this test was nominally identical to BC1-1, with the exception that the initial shear cracking damage (i.e., that developed while in service) differed amongst the two interior span regions of BC1.

Crack widths were recorded over the course of testing, at different stages of loading. Figure A.1 shows crack widths and crack patterns measured in the field, under the simulated service dead load case (i.e., with an applied load of 80 kip at each GL hydraulic ram), under a 180 kip simulated lane loading scenario, and the crack pattern after completion of the test. On the basis of the crack widths presented in Figures A.1a and A.1b, it can be seen that the crack widths under simulated service dead loads were comparable to those measured in the field, prior to extracting the bent caps from the bridges. More specifically, it can be seen that the primary shear crack comprising the interior span had a maximum crack width of about 0.059 inches in the field, and under the 80 kip uniform dead load loading scenario, similar crack widths were measured in the vicinity of that same crack.

Figures A.3a, A.3b, and A.3c show the deflection, shear, and bending moments corresponding to the 80 kip (dead load), 180 kip, and ultimate load cases respectively. Figure A.3d presents the shear force measured over the course of testing in the critical interior span (i.e. to the right of GL4) over the course of testing, plotted with respect the average deflection, which was calculated as shown in Figure 3.8.

The failure of test BC1-2 was governed by a tension-controlled shear failure. Throughout the duration of the test, new shear cracks were observed to form in the overhang and interior span regions. However, the majority of the damage was located within the concrete comprising the main interior span strut, which exhibited signs of concrete crushing and extensive widening of shear cracks (see Figure A.2). A major loss of stiffness was observed immediately following the development of the shear capacity of the cap, after which the shear resistance of the interior span rapidly decreased. Note that at a load level corresponding to approximately 90 % of the ultimate capacity, the widths of the primary cracks were measured to be 2.5 times wider than those measured during the field inspection.

The maximum shear force resisted by the bent cap within the interior span was measured to be 167 kip, which corresponded to a maximum applied girder line load of 199 kip. It is worth noting that the ultimate load resisted by the interior span of the bent cap comprising test BC1-2 was within about 5 % of that obtained from test BC1-1. Thus, on the basis of the similar failure modes obtained and due to the fact that the load resisting capacities were very similar, the results obtained from the interior span testing of BC1 should be considered as a set of reliable and repeatable test results.

The measured shear capacity of the interior span was comparable to that estimated by way of current AASHTO provisions, which was estimated to be 185 kip (minimum shear reinf. provided) and 171 kip (minimum shear reinf. not provided). The sectional analysis calculations performed in accordance with the AASHTO provisions are presented in Appendix C.

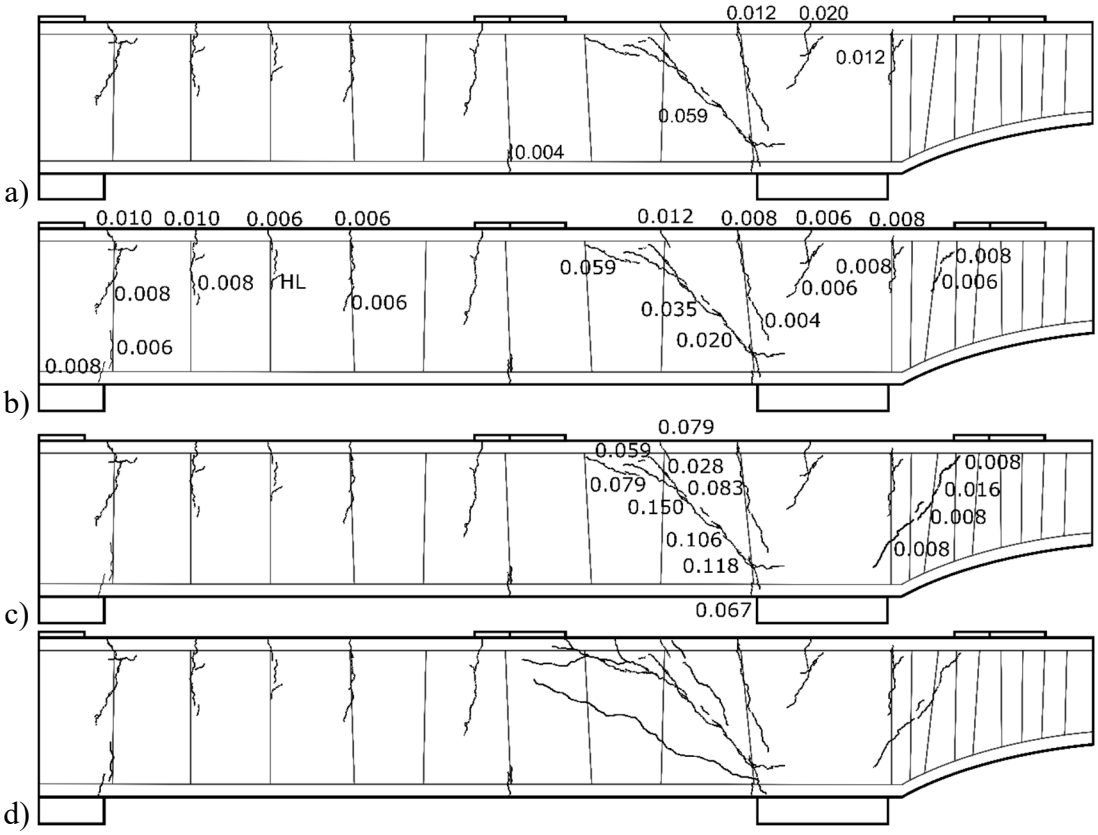

Figure A.1. BC1-2 cracking data, and measured reinforcement placement, a) Field inspection, b) Constant dead load case, c) 180 kip load case (i.e., at approximately 90 % of the ultimate capacity), d) Crack pattern after test

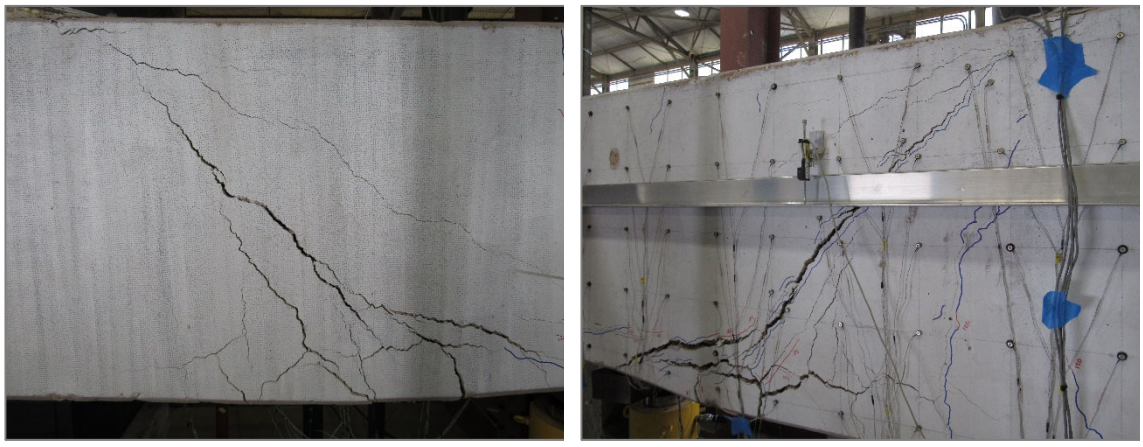

a) Major shear crack on the interior span after test completion (west face)

b) Major shear crack on the interior span after test completion (east face)

Figure A.2. BC1-2 photos

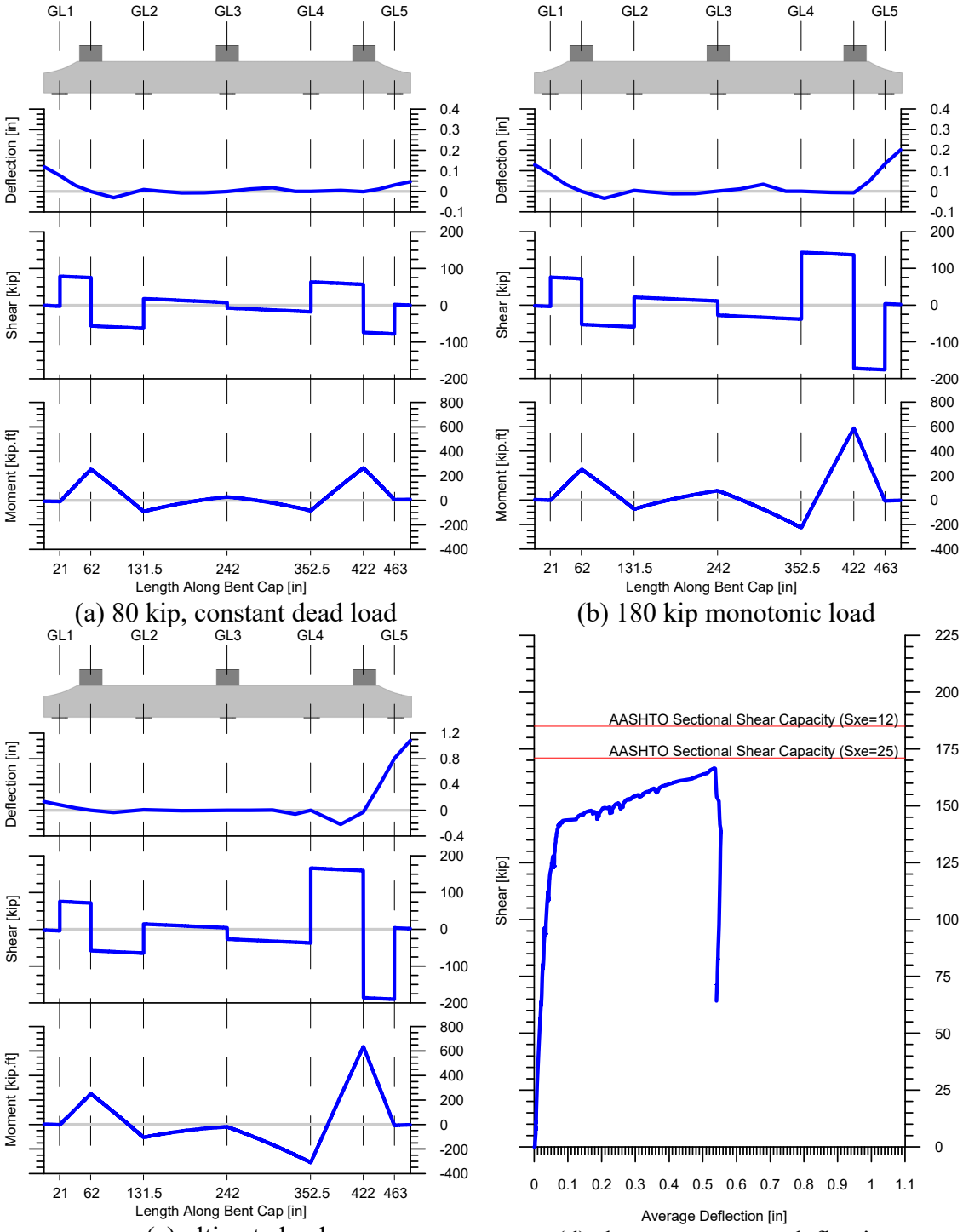

(a) 80 kip, constant dead load

(b) 180 kip monotonic load

(c) ultimate load

(d) shear vs. average deflection

Figure A.3. BC1-2 moment, shear, and deflections

A.1.2 BC1-4: Retrofitted Overhang

Test BC1-4 involved the testing of a retrofitted (i.e., with CFRP wrapping) overhang region of BC1 (refer to Figure 3.4). The test was performed in accordance with the overhang test procedure previously presented. This test was performed on a segment of BC1, after much of the bent cap had been saw-cut to permit rebar extraction for the purpose of steel coupon testing.

Figure A.5 shows the measured shear forces and measured bending moments corresponding to the ultimate load cases respectively. Note that in this test case, it was determined that the deflection measurement instrumentation did not accurately capture the overhang deflection response over initial part of the test. Thus, the deflection data have been omitted from the reporting of this test.

The failure of test BC1-3 was governed by the pullout of the longitudinal reinforcing bars and concrete crushing at the location of the added support bearing. Over the course of the test, new shear cracks formed at both the interior span and the retrofitted overhang, as visible in Figure A.4b. The failure of the overhang corresponded with the observation of extensive steel reinforcement pullout (refer to Figures A.4e and A.4f). While the primary initiator of the overhang failure was not identified in this case, the location of saw-cut made in the bent cap (which limited the development of the longitudinal steel reinforcement), the existing damage stemming from prior interior span shear testing (i.e., damage incurred previously under test BC1-2), and the concrete crushing at the added support bearing (Figure A.4d) are all likely contributors to the pullout of the longitudinal reinforcing bars.

a) BC1-4 test setup

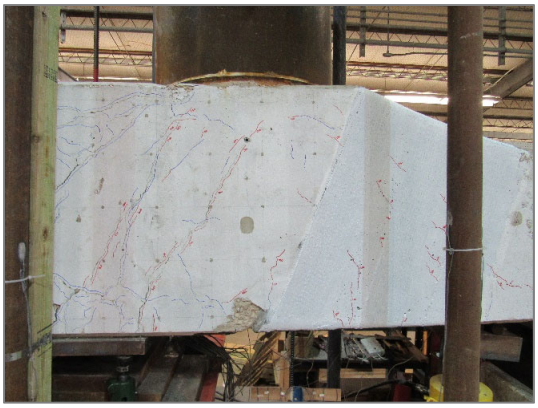

b) Shear cracks formed at 300 kip load case (west face)

c) Shear cracks after cap failure (west face)

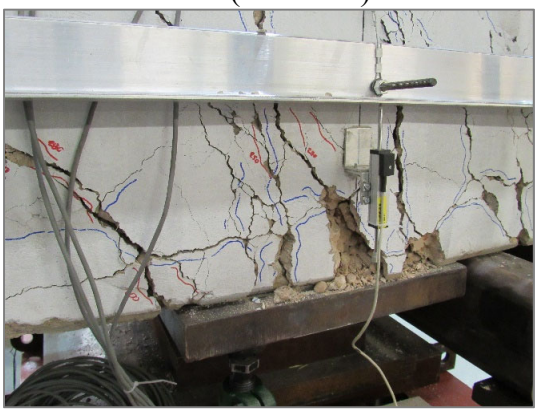

d) Concrete crushing at the added support bearing (west face) after cap failure

e) Pullout of bottom longitudinal bar after test completion

f) Pullout of bottom longitudinal bar after test completion

Figure A.4. BC1-4 photos

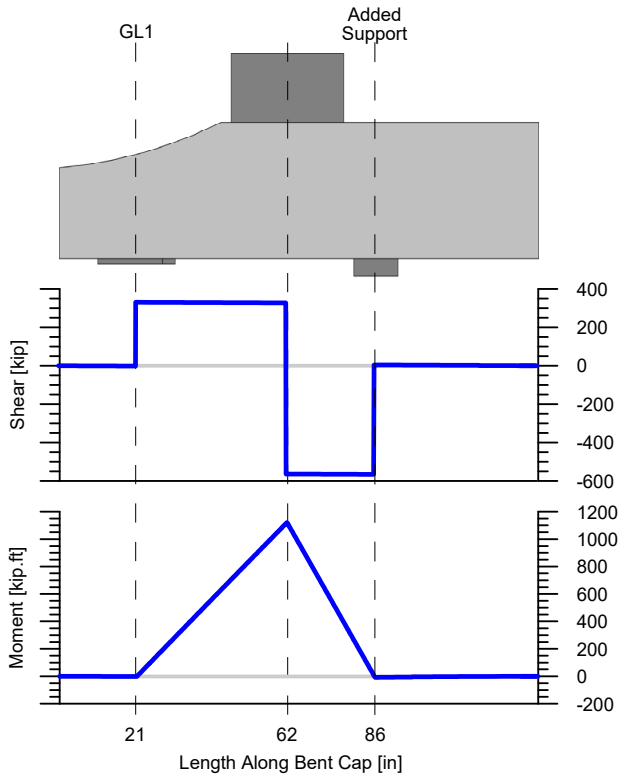

Figure A.5. BC1-4: Ultimate load

The ultimate shear force carried by the overhang was found to be 331 kip, which corresponded to a maximum applied girder line load of 333 kip and a maximum bending moment of 711 kip-ft at the face of the column stub closest to the overhang. Thus, it is worth noting that, even with the premature pull-out failure, an increase in the capacity of the overhang was attained by way of the CFRP retrofit. Further, for comparative purposes, note that the nominal flexural capacity of the overhang was estimated to be 799 kip-ft. at face of the column stub. Note that the such nominal capacity assumes that the full height if the bent cap provides flexural resistance (i.e., does not account the tapering of the overhang).

A.2 INSPECTION DRAWINGS

The following digital drawings summarize the crack locations and widths measured in the field and while in service. Additionally, the GPR-located steel reinforcement is also shown with respect the crack patterns.

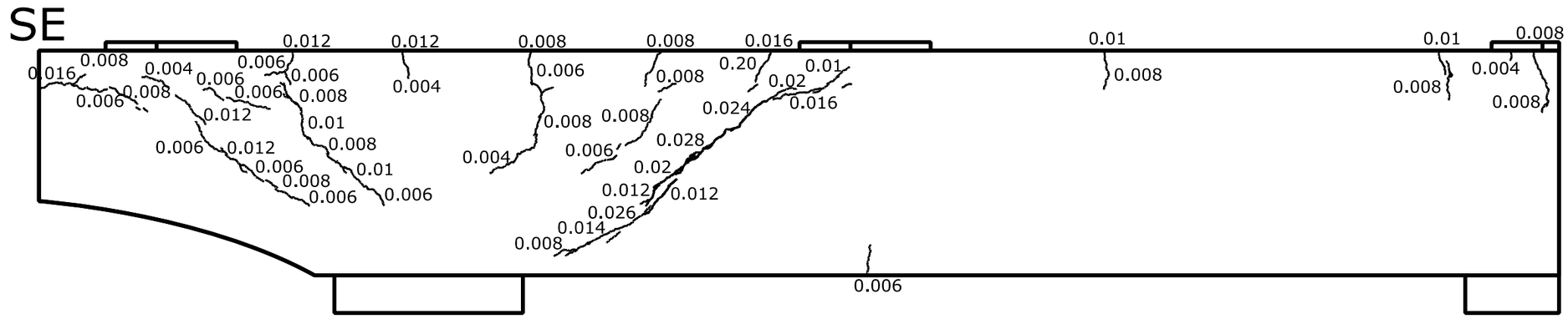

Figure A.6. East face of BC1: cracking measured from laboratory inspection; crack widths reported using units of inches

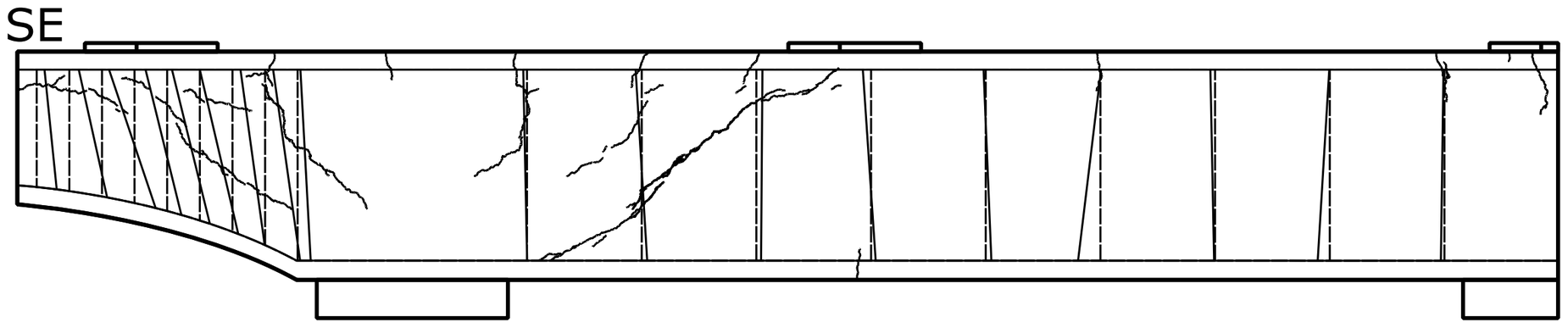

Figure A.7. East face of BC1 as-built steel reinf. (solid lines) and design drawings steel reinf. (dashed lines)

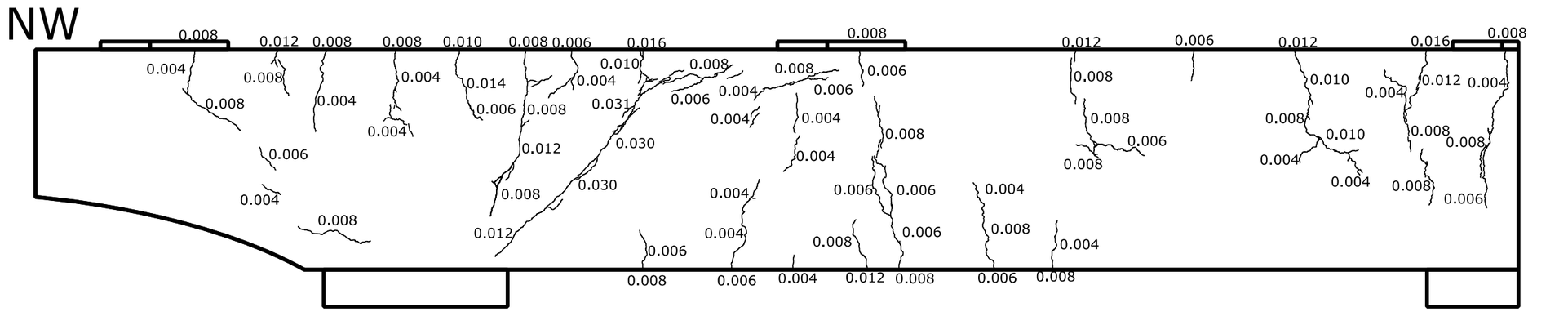

Figure A.8. West face of BC1: cracking measured from laboratory inspection; crack widths reported using units of inches

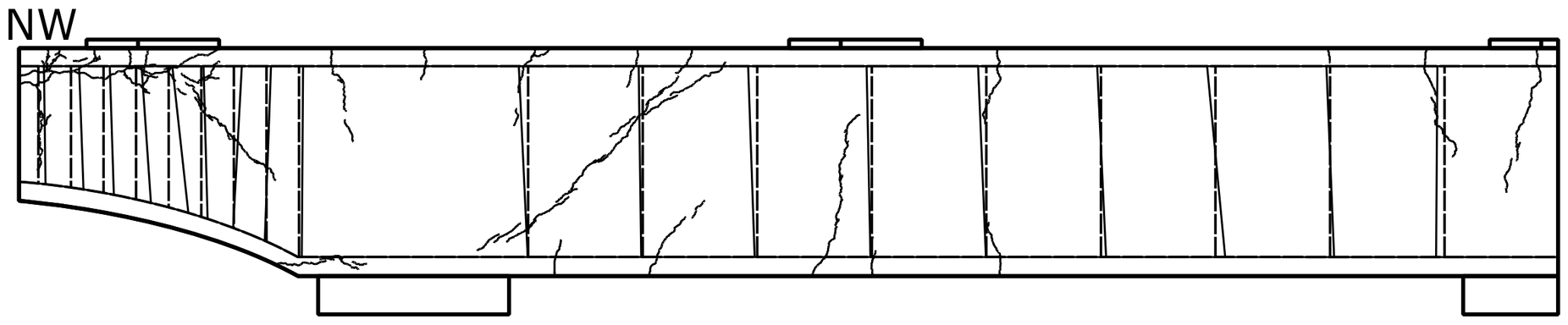

Figure A.8. East face of BC1 as-built steel reinf. (solid lines) and design drawings steel reinf.(dashed lines)

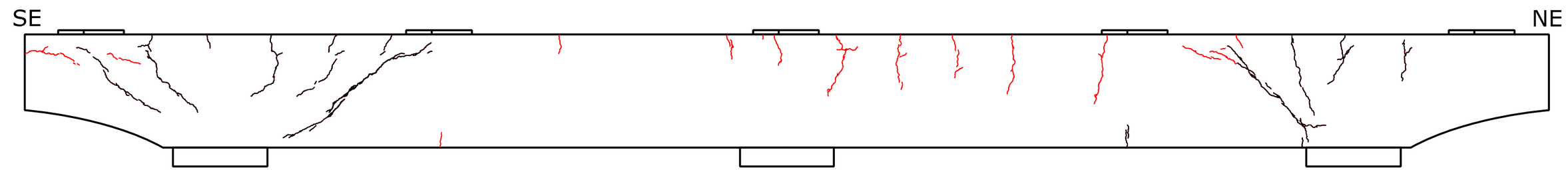

Figure A.9. East face of BC1 additional crack pattern found in FSEL (represented in red)

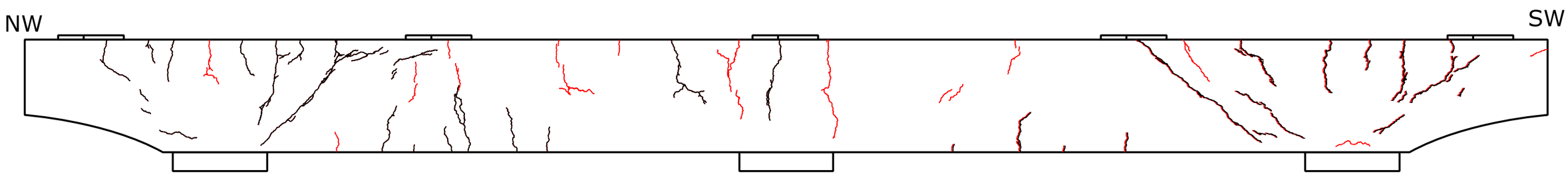

Figure A.10. West face of BC1 additional crack pattern found in FSEL (represented in red)

APPENDIX B Bent Cap 2 Results

The following appendix shows all the results obtained from inspections and remainder of tests not presented in the body of the thesis of Bent Cap 2.

B.1 ULTIMATE LOAD TESTS

B.1.1 BC2-2.A: Retrofitted Interior Span

Test BC2-2A involved the testing of a retrofitted (i.e., with the application of the CFRP wrap) interior span region of BC2. The test was performed in accordance with the interior span test procedure previously presented; however, no external clamps were used to strengthen the previously tested interior span. This test was nominally identical to that presented above for BC2-1. It must also be noted that this test was terminated prematurely due to the fact that, during testing, the bent cap began to bear on a temporary support used to stabilize the bent cap before and after testing, as is shown in Figure B.2c. The large bent cap deflections developed during this test led to the bottom surface of the bent cap reacting against the temporary support, invalidating the intended loading conditions of the test, from that point forward. However, it is important to note that the bent cap had already showed signs of stiffness degradation and flexural yielding prior to engaging the temporary support. Thus, the key findings presented for this test remain valid and can be used to characterize the overall response of the retrofitted bent cap span.

Due to the CFRP-wrapping, which was applied over the majority of the interior span region, covering the majority of the major existing shear cracks, no crack width measurements of this test are provided in this document. However, crack measurements were taken at several load cases of cracks forming in between the CFRP strips and within the overhang region of the cap. Note that the cracks in between the CFRP strips were covered in resin for the installation of the CFRP.

Figures B.3a, B.3b, and B.3c show the measured bent cap deflection, measured shear forces, and measured bending moments corresponding to the 80 kip (dead load), 180 kip, and ultimate load cases respectively. Figure B.3d presents the measured shear force in

the critical interior span (at a location immediately adjacent to GL2) over the course of testing, and plotted with respect the average deflection, which was calculated as shown in Figure 3.8.

The failure of test BC2-2A was controlled by flexure. The formation of shear cracks was visible in between the CFRP strips and close to the reaction points. However, the bent cap presented a severe loss of stiffness when major flexural cracks formed at the face of the column stub, and at a section located approximately 14-in. away from the column stub face (which may have caused the delamination and rupture of the inner edge of CFRP strip closest to the column stub, shown in Figure B.2a). After the formation of the first major flexural cracks, load continued to be applied to verify yielding of the longitudinal bars. As noted above, the test was terminated when the bent cap was observed to bear on the temporary support structure of the test. Immediately prior to unloading the cap, some limited rupturing and delamination of the CFRP was observed at the location where the bent cap engaged the temporary support.

While this test was terminated prematurely, the ultimate capacity of the retrofitted bent cap and the governing failure mode were effectively measured. The ultimate shear force resisted by the interior span of the cap was estimated to be 211 kip, which corresponded to a maximum applied girder line load of 262 kip and a maximum bending moment of 578 kip-ft. at the interior face of the column stub. The sectional moment capacity of BC2 at the interior face of the exterior column stub was estimated to be of 859 kip-ft. It is worth noting that some of the longitudinal reinforcement in tension may not have been fully developed (2-#11 and 1-#10 bars are curtailed at the interior span).

Results from the DIC data show that the largest strain in the CFRP-wrap was concentrated a section approximately 14-in. away from the column stub face, which coincides with the region where major flexural cracks formed. The strain profile for the

ultimate load is shown in Figure B.1 The strain contour shows a maximum CFRP strain of 3.5 x 10-3 in./in. Thus, in comparison to the manufacturer's reported ultimate strain capacity of 10 x 10-3 in./in. for the CFRP system, it is evident that only limited CFRP strain development had occurred. Note that rupture of the CFRP was observed as a function of the formation of flexural and shear cracks underneath the wrapping system and was likely mostly attributed to the widening of the flexural cracks.

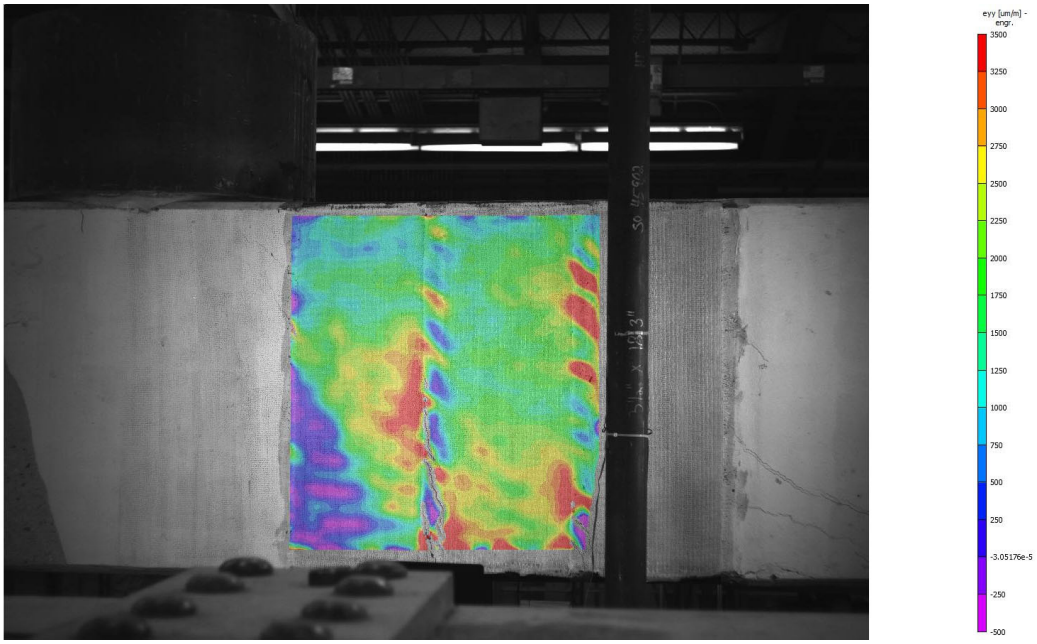

Figure B.1. BC2-2A: DIC strain contour at ultimate load

a) Formation of major flexural and shear cracks (west face)

b) Delamination and rupture of CFRP at location of major flexural crack (east face)

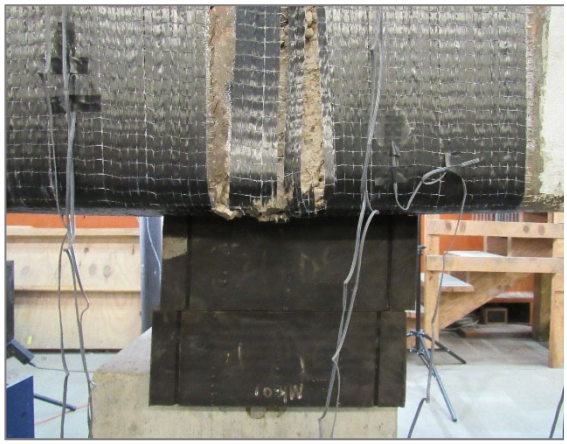

c) Temporary support in contact with bent cap bottom surface (west face)

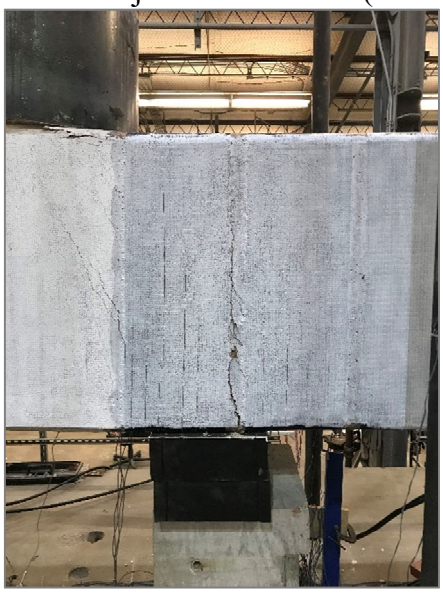

d) CFRP retrofitted span after test completion (west face)

Figure B.2. BC2-2A photos

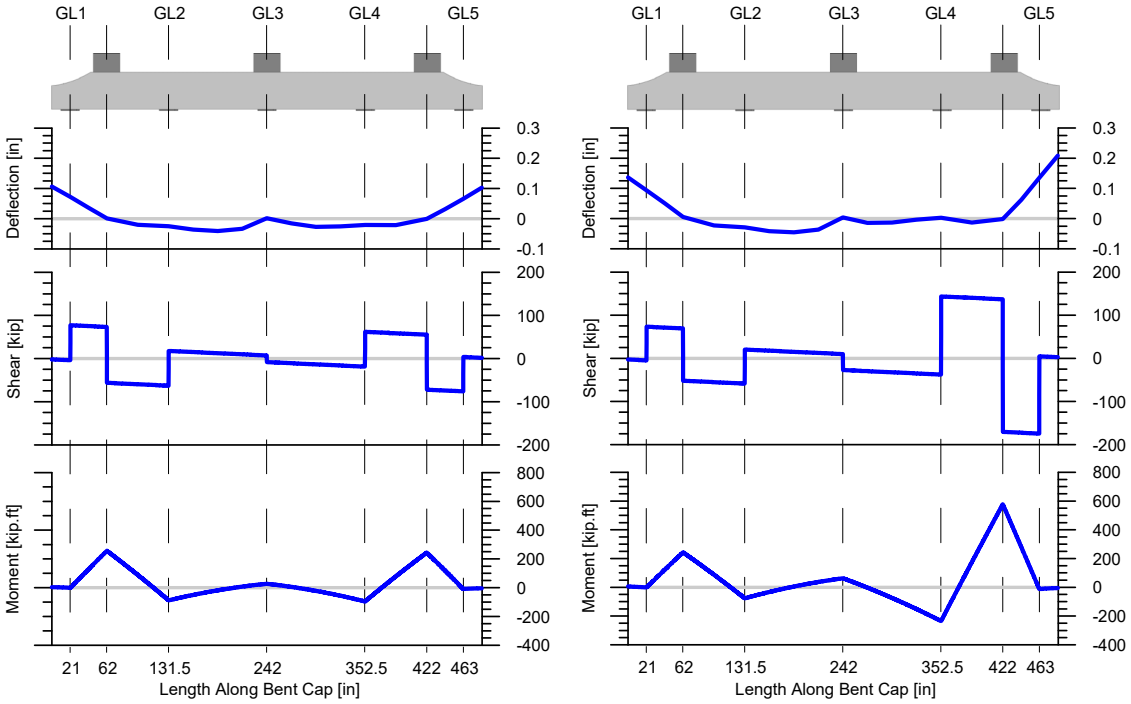

(a) 80 kip, constant dead load

(b) 180 kip monotonic load

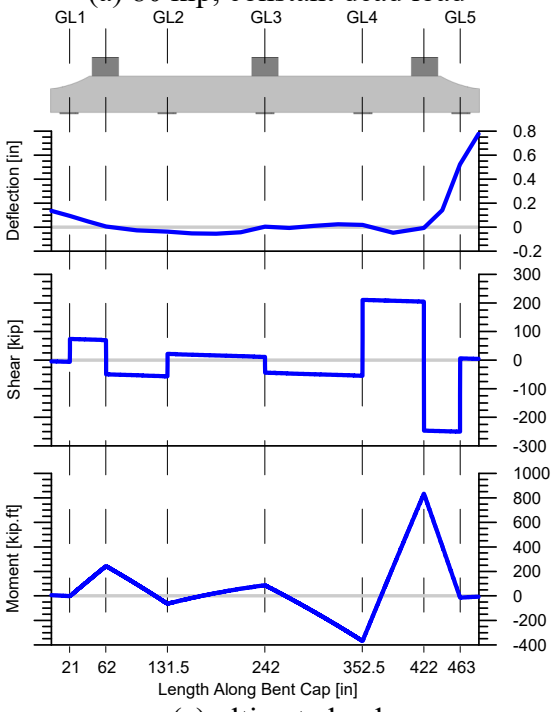

(c) ultimate load

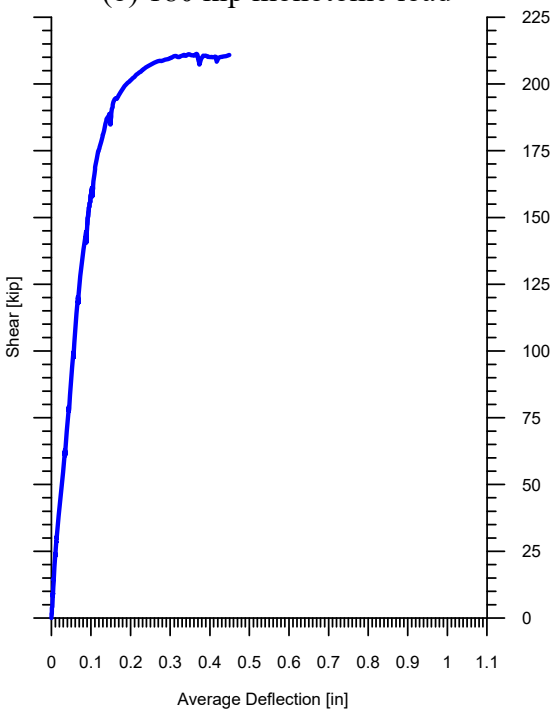

(d) shear vs. average deflection

Figure B.3. BC2-2A moments, shear, and deflections

B.1.2 BC2-2.B: Retrofitted Interior Span

Test BC2-2B involved the testing of the same bent cap region as that tested in BC2-2A (refer to B.1.1), and was done in an effort to confirm the ultimate strength of the section. Recall that in BC2-2A, the test was prematurely terminated due to inadvertent bearing with a temporary support. Test BC2-2B effectively repeated the testing of the same interior span region with all temporary support structures removed. The test was performed in accordance with the interior span test procedure previously presented, however, no external clamps were used to strengthen the previously tested interior span.

Figure B.5a, B.5b, and B.5c the measured bent cap deflection, measured shear forces, and measured bending moments corresponding to the 80 kip (dead load), 180 kip, and ultimate load cases respectively. Figure B.5d shows the measured shear force in the critical interior span (at a region immediately adjacent to GL2) over the course of testing, plotted with respect the average deflection, which was calculated as shown in Figure 3.8.

a) Major shear and flexural cracks after test completion (west face)

b) Major shear and flexural cracks after test completion (west face)

Figure B.4. BC2-2B photos

As was initially observed in test BC2-2A, the failure of this test region was controlled by flexural failure mechanisms. Because this section of the bent cap had been tested previously, part of the CFRP strip closest to the column stub was already ruptured

and the section already contained severe flexural and shear cracks (see Figure B.2). After reloading the previously tested bent cap, the flexural cracks at the face of the column widened significantly as can be seen from Figure B.4.

The ultimate shear force resisted by the interior span was estimated to be 187 kip, which corresponded to a maximum applied girder line load of 231 kip and a maximum bending moment of 510 kip-ft at the interior face of the column stub. The retesting of this section confirmed that the flexural failure modes observed were no a byproduct of the interference with the temporary support structure (refer to test summary of BC2-2A).

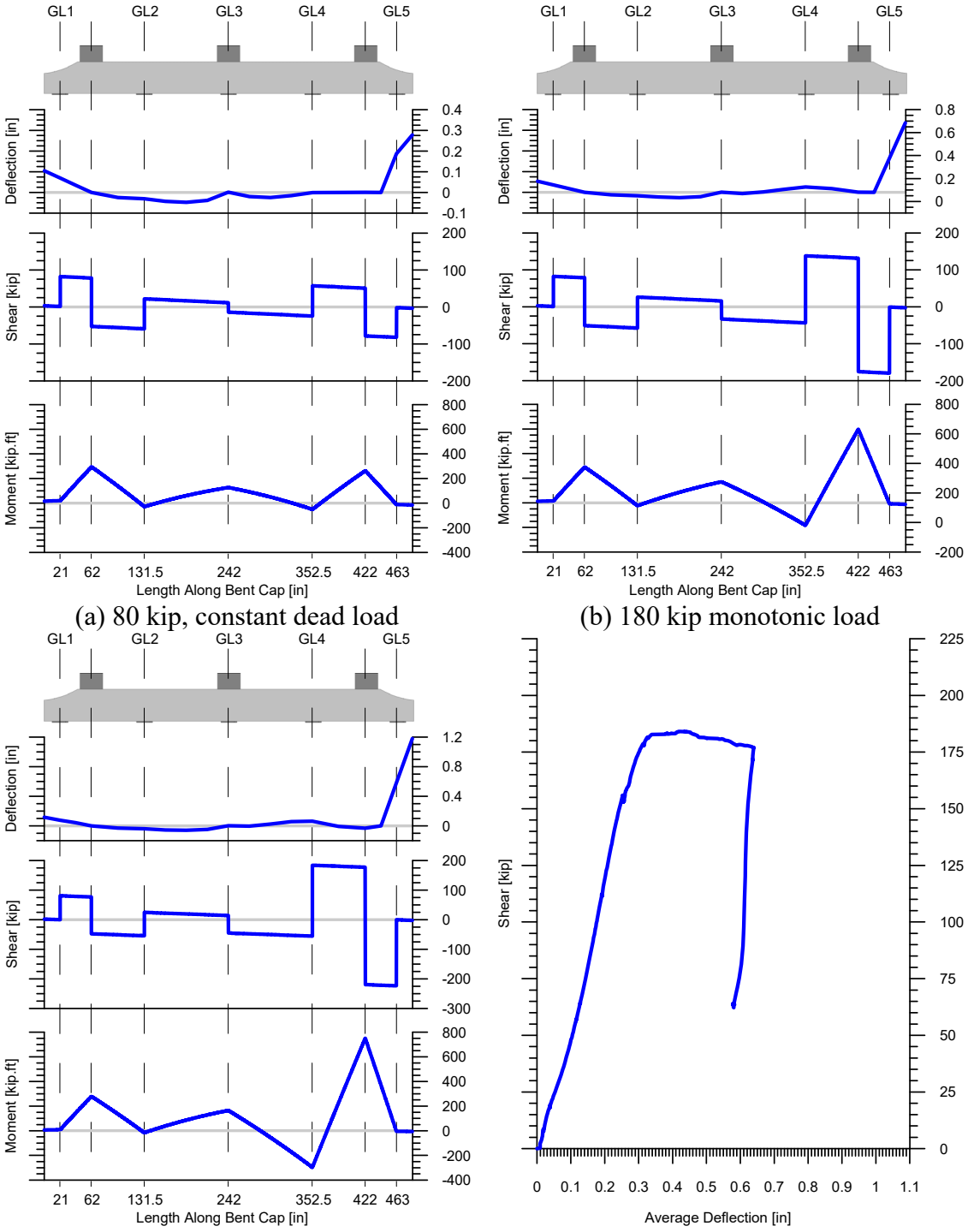

(a) 80 kip, constant dead load

(b) 180 kip monotonic load

(c) ultimate load

(d) shear vs. average deflection

Figure B.5. BC2-2B moment, shear, and deflections

B.2 INSPECTION DRAWINGS

The following digital drawings summarize the crack locations and widths measured in the field and while in service. Additionally, the GPR-located steel reinforcement is also shown with respect the crack patterns.

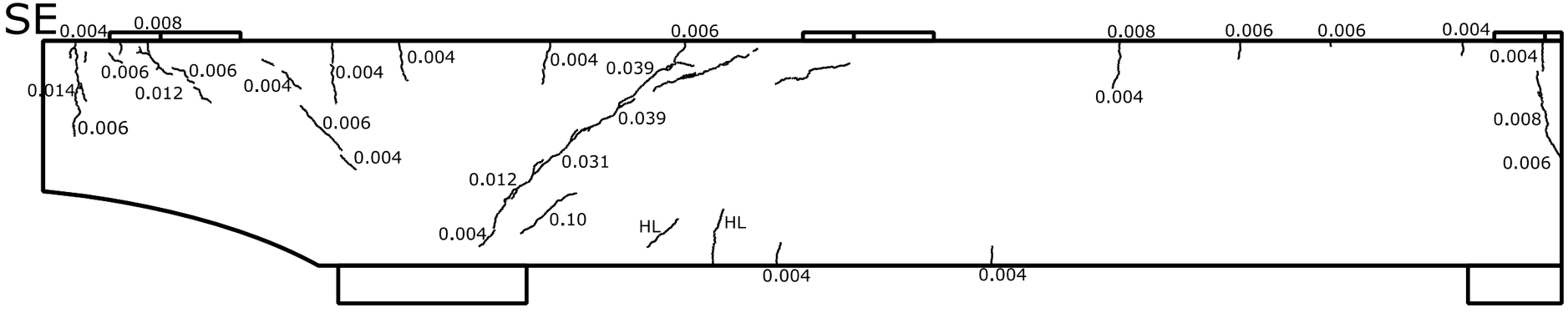

Figure B.6. East face of BC2: cracking measured from laboratory inspection; crack widths reported using units of inches

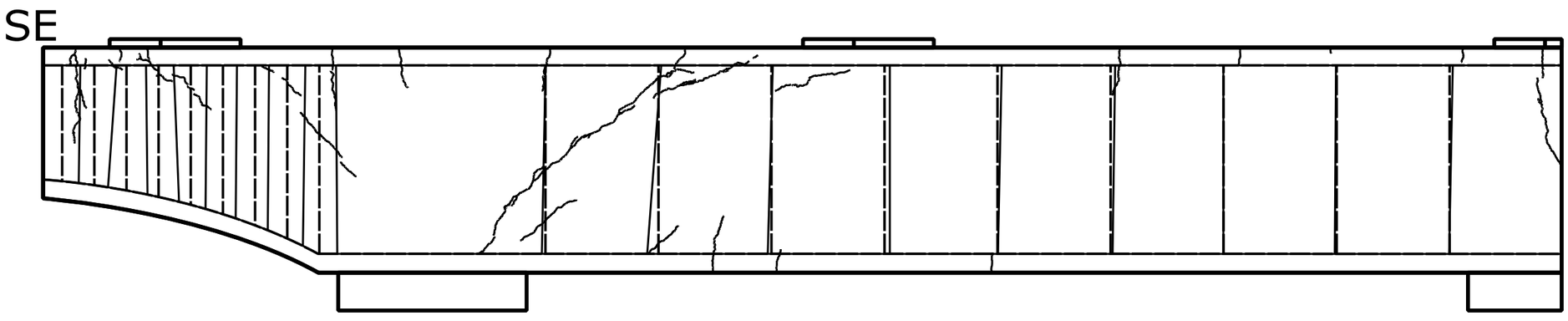

Figure B.7. East face of BC2 as-built steel reinf. (solid lines) and design drawings steel reinf. (dashed lines)

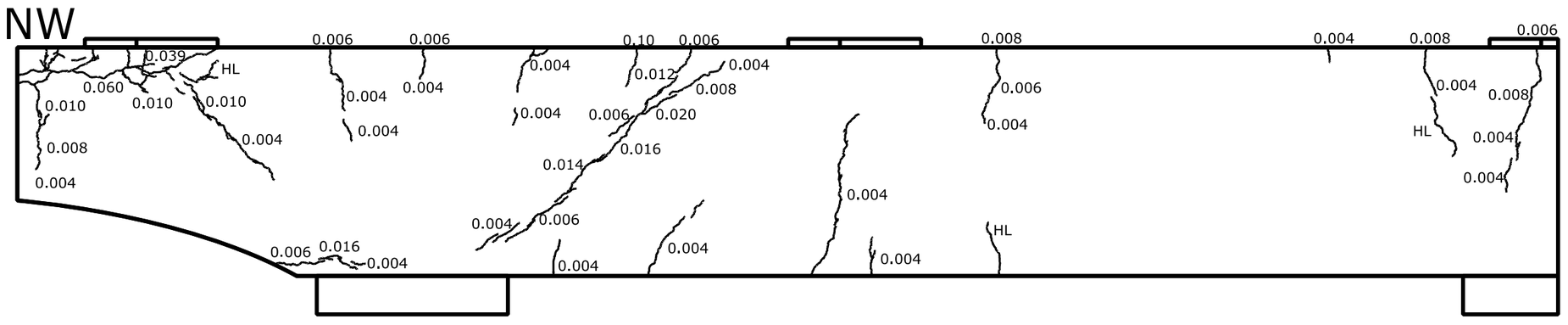

Figure B.8. West face of BC2: cracking measured from laboratory inspection; crack widths reported using units of inches

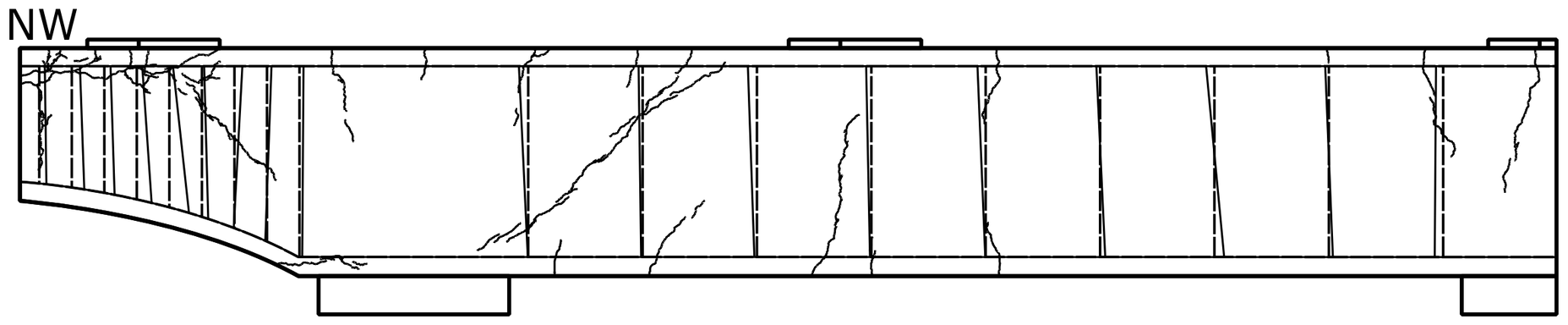

Figure B.9. West face of BC2 as-built steel reinf. (solid lines) and design drawings steel reinf.(dashed lines)

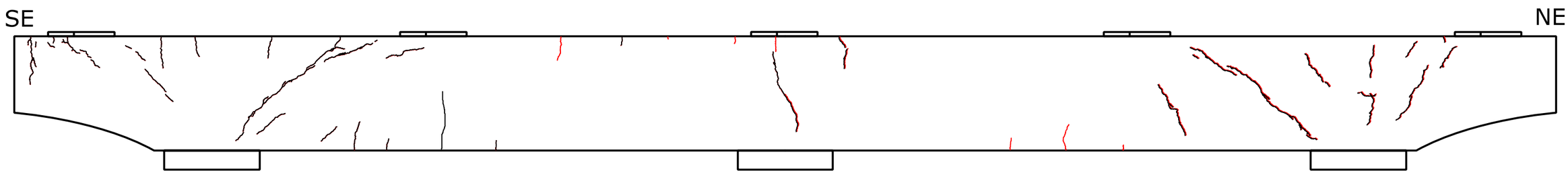

Figure B.10. East face of BC2 additional crack pattern found in FSEL (represented in red)

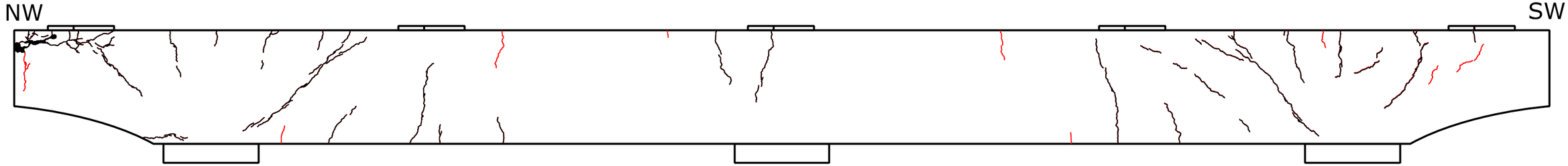

Figure B.11. West face of BC2 additional crack pattern found in FSEL (represented in red)

APPENDIX C Appraisal of experimental capacities

C.1 AASHTO (2017) AASHTO LRFD BRIDGE DESIGN SPECIFICATIONS

In this section, the shear strength of the interior spans of the RC bent caps are calculated using the test-evaluated mechanical properties of the concrete and the steel reinforcement. Additionally, the CFRP manufacturer's properties are used in the shear strength evaluation of the retrofitted interior spans.

C.1.1 AASHTO LFRD Bridge Design Provisions: Unretrofitted Interior Span

Two sets of calculations were performed on the basis of Section 5.7.3.3 of the AASHTO LRFD sectional design provisions in an effort to evaluate the shear strength of the bent caps. The first one uses an effective crack spacing of $S_{xe} = 12$ because the minimum transverse steel reinforcement was provided per Equation C.9. However, although the minimum transverse steel reinforcement was provided, the large stirrup placement and location raises questions about the adequacy of the formula. Therefore, another shear strength calculation was performed considering the crack spacing parameter influenced by aggregate size, assuming minimum shear reinforcement and/or proper shear reinforcement detailing was not provided.

C.1.1.1 Interior Span Shear Strength Calculation: $S_{xe} = 12$

$$V_u = 185.2\ kip \tag{C.1}$$

$$M_u = V_u \frac{M_{u,test}}{V_{u,test}} = (185.2\ kip)(31.32 \frac{kip - in}{kip}) = 5800\ kip - in \tag{C.2}$$

$$\varepsilon_s = \frac{\frac{M_u}{d_v} + V_u}{E_s A_s} = \frac{\frac{5800\ kip - in}{29.7"} + 185.2\ kip}{(29{,}000 ksi)(7.51 in^2)} = 0.00174 \tag{C.3}$$

$$\beta = \frac{4.8}{(1 + 750\varepsilon_s)} \frac{51}{(39 + S_{xe})} = \frac{4.8}{(1 + 750(0.00174))} \frac{51}{(39 + 12)} = 2.08 \tag{C.4}$$

$$\theta = 29 + 3500\varepsilon_s = 29 + 3500(0.00174) = 35.11 \tag{C.5}$$

$$V_c = 0.0316\beta\lambda\sqrt{f_c'}b_v d_v = 0.0316(2.08)\sqrt{2.4ksi}(30")(29.7") = 90.6\ kip \quad (C.6)$$

$$V_s = \frac{A_v f_y d_v \cot(\theta)}{s} = \frac{(0.62in^2)(66ksi)(29.7")\cot\left(\frac{35.11\pi}{180}\right)}{18"} = 94.6\ kip \quad (C.7)$$

$$V_n = V_c + V_s = 185.2\ kip \quad (C.8)$$

Minimum Transverse Shear Reinforcement

$$A_v \geq\ 0.0316\lambda\sqrt{f_c'}\frac{b_v s}{f_y}$$

$$A_v = 0.62\ in^2 \geq\ 0.41\ in^2 = 0.0316\sqrt{2.4ksi}\frac{(30")(18")}{65ksi} \quad (C.9)$$

It is worth noting that the large stirrup spacing makes it arguable that minimum shear reinforcement was being provided adequately.

C.1.1.2 Interior Span Shear Strength Calculation: $S_{xe} = 25.14$

$$V_u = 171.4\ kip \quad (C.10)$$

$$M_u = V_u\frac{M_{u,test}}{V_{u,test}} = (171.4\ kip)(31.32\frac{kip-in}{kip}) =\ 5369kip-in \quad (C.11)$$

$$\varepsilon_s = \frac{\frac{M_u}{d_v} + V_u}{E_s A_s} = \frac{\frac{5369\ kip-in}{29.7"} + 171.4\ kip}{(29{,}000ksi)(7.51in^2)} = 0.00162 \quad (C.12)$$

$$S_{xe} = S_x\frac{1.38}{(a_g + 0.63)} = (29.7")\frac{1.38}{(1+0.63)} = 25.14 \quad (C.13)$$

$$\beta = \frac{4.8}{(1+750\varepsilon_s)}\frac{51}{(39+S_{xe})} = \frac{4.8}{(1+750(0.00162))}\frac{51}{(39+25.14)} = 1.72 \quad (C.14)$$

$$\theta = 29 + 3500\varepsilon_s = 29 + 3500(0.00162) = 34.7 \quad (C.15)$$

$$V_c = 0.0316\beta\lambda\sqrt{f_c'}b_v d_v = 0.0316(1.72)\sqrt{2.4ksi}(30")(29.7") = 75.2\ kip \quad (C.16)$$

$$V_s = \frac{A_v f_y d_v \cot(\theta)}{s} = \frac{(0.62in^2)(65ksi)(29.7")\cot\left(\frac{34.7\pi}{180}\right)}{18"} = 96.2\ kip \quad (C.17)$$

$$V_n = V_c + V_s = 171.4\ kip \tag{C.18}$$

The second iteration, which assumed no minimum shear reinforcement was provided, gave results that were more in-line with the experimental data.

C.1.2 AASHTO LFRD Bridge Design Provisions: Unretroffited Overhang

The overhang shear capacity was evaluated using Section 5.7.3.3. To assess the tapered region, the height of the bent cap was considered to be 30 in., the median height between the outermost girder line and the adjacent column stub centerline.

$$V_u = 331.4\ kip \tag{C.19}$$

$$M_u = V_u(20.5") = (331.4kip)(20.5") = \ 6794\ kip - in \tag{C.20}$$

$$\varepsilon_s = \frac{\frac{M_u}{d_v} + V_u}{E_s A_s} = \frac{\frac{6794\ kip - in}{27"} + 331.4\ kip}{(29{,}000ksi)(7.51in^2)} = 0.0027 \tag{C.21}$$

$$\beta = \frac{4.8}{(1 + 750\varepsilon_s)}\frac{51}{(39 + S_{xe})} = \frac{4.8}{(1 + 750(0.0027))}\frac{51}{(39 + 12)} = 1.60 \tag{C.22}$$

$$\theta = 29 + 3500\varepsilon_s = 29 + 3500(0.0027) = 38.37 \tag{C.23}$$

$$V_c = 0.0316\beta\lambda\sqrt{f_c'}b_v d_v = 0.0316(1.60)\sqrt{2.4ksi}(30")(27") = 63.3kip \tag{C.24}$$

$$V_s = \frac{A_v f_y d_v \cot(\theta)}{s} = \frac{(0.62in^2)(66ksi)(29.7")\cot\left(\frac{38.37\pi}{180}\right)}{5.125"} = 268.2\ kip \tag{C.25}$$

$$V_n = V_c + V_s = 331.4\ kip \tag{C.26}$$

The obtained calculated overhang shear capacity is comparable to the overhang test ultimate strength of 317 kip. Both values only differ by 4%.

C.1.2.1 ACI 440.2R-17 Design Provisions: Retrofitted Interior Span

The calculations below show the shear strength results of the retrofitted bent caps. Note that the ultimate load testing of the retrofitted spans resulted in flexural failure. Therefore, no experimental data from this research project can be used in contrast with the code provisions.

$$V_c = 2\sqrt{f_c'}b_w d = 2\sqrt{2400psi}(30")(33") = 97\ kip \quad \text{(C.27)}$$

$$V_s = \frac{A_{vs}f_{yt}d}{s} = \frac{(0.62in^2)(65ksi)(33")}{18"} = 74\ kip \quad \text{(C.28)}$$

$$V_f = \frac{A_{vf}f_{fe}d}{s_f} = \frac{2(12")(0.04")(55.6ksi)(33")}{14"} = 126\ kip \quad \text{(C.29)}$$

$$f_{fe} = \varepsilon_{fe}E_f = (0.004)(13900ksi) = 55.6\ ksi \quad \text{(C.30)}$$

$$V_n = V_c + V_s + V_f = 297\ kip \quad \text{(C.31)}$$

It should also be noted that the total quantity of the vertical reinforcement provided (existing steel stirrups + CFRP) results in a shear reinforcement ratio of approximately 0.34 %, which is comparable to the minimum vertical crack control reinforcement requirements of AASHTO LRFD for deep beams (Cl. 5.8.2.6-1).

Crack Control Reinforcement per AASHTO LFRD Bridge Design 8th Ed.

$$\frac{A_v}{b_w s_w} \geq 0.003\ ,\ \ \frac{0.62in^2}{(30")(18")} + \frac{0.96in^2}{(30")(14")} = \ 0.0034 \geq 0.003 \quad \text{(C.32)}$$

APPENDIX D Material Preparation and Retrofits Procedure

D.1 PREPARATION OF CONCRETE CORES

- The 4-in. diameter concrete core specimens were cut to a length of 8 in. using a lapidary slab saw.
- Large imperfections and weak cover concrete were removed from the ends of the cores using a concrete cylinder grinding machine.
- Core diameters and lengths were measured using digital calipers and documented. Diameters were measured at the top surface, mid-height, and bottom surface of the specimens. Lengths of the cores were measured at 120-degree increments and averaged.
- Prior to testing, sulfur end-capping was done to eliminate effects associated with remaining/small surface imperfections.

D.2 REBAR EXTRACTION PROCEDURE

The steel reinforcement was extracted by cutting the concrete around the steel reinforcement using a circular concrete saw. After cutting, bent cap prisms containing the rebar were removed from the bent caps as shown in Figure D.1.

(a) extraction of stirrups (b) extraction of longitudinal bars

Figure D.1. Extracted concrete-encased reinforcing bars

D.3 CFRP COUPONS PREPARATION

The following procedure was used to prepare the CFRP laminates that were tested to verify reported manufacturer's CFRP properties:

1. Base plate preparation: A 24 x 12-in. dimension, 28-gauge, steel plate was used as a mold and covered with a 0.03 in. thick polythene plastic (see Figure D.2).
2. Placing of CFRP ply on base plate: A 23 x 11-in. dimension CFRP ply was used to prepare the laminate, leaving 0.5-in. clear distance from the base plate edges. The resin was mixed and applied at the surface of the base plate. The CFRP ply was placed on the base plate and resin was applied on top of the CFRP, as shown in Figure D.3.
3. CFRP ply saturation and curing: A trowel was used to spread the resin along the direction of the CFRP fibers. The process was repeated until the resin could no longer be removed and air pockets were no longer visible. A plastic sheet was placed on top of the plies to allow the curing of the CFRP for a minimum of 48 hours (refer to Figure D.4).
4. Cutting of CFRP strips: To maintain the same amount of fibers in each coupon, the 'folding' method was used, which consists on folding the CFRP laminate along the direction of the fiber and in between the strips of the CFRP (Pham). A total of 3 strips per coupon was achieved using the folding method, as visible in Figure D.5. Subsequently, a heavy-duty paper guillotine was used to cut the coupons in the direction perpendicular to the CFRP fiber.
5. Dimension measurements: Calipers of a 0.001 in. resolution were used to measure the widths and thicknesses of each coupon. The dimensions were taken at three points throughout the length of the specimens: one at the mid-point and the other two at the ends of the specimens, close to the grip area.

(a) steel plates used as molds

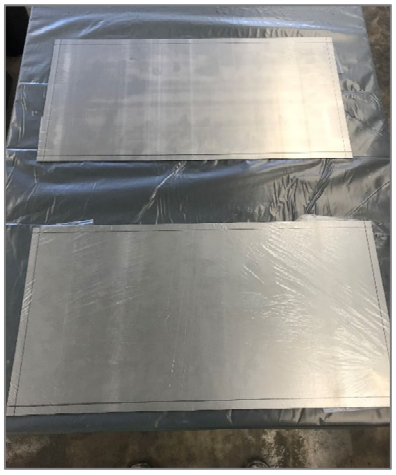

(b) molds covered with plastic

Figure D.2. Base plate preparation

(a) epoxy applied to base plate surface

(b) placement of CFRP

Figure D.3. Placing of CFRP fiber wrap ply on base plate

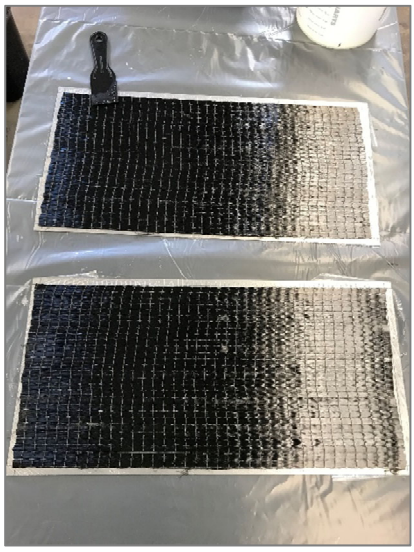

(a) saturated CFRP plies

(b) plastic placed on top

Figure D.4. Saturated CFRP plies and curing

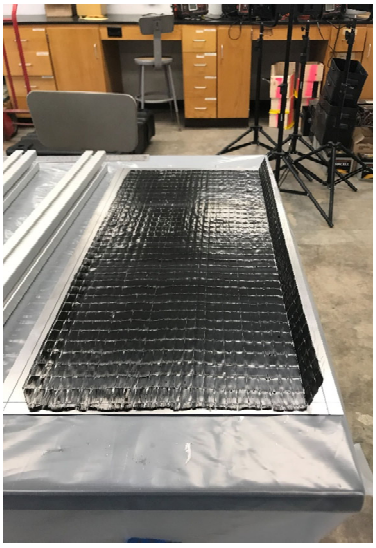

(a) folding of CFRP laminate parallel to the fiber direction for coupon preparation

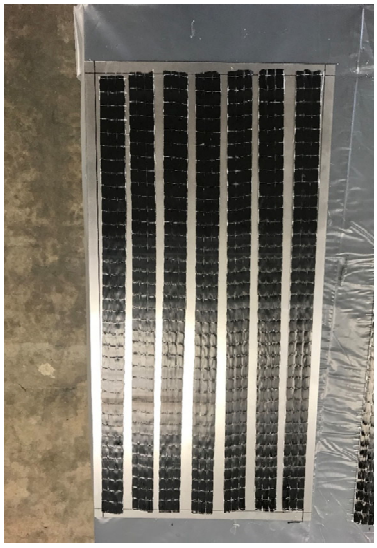

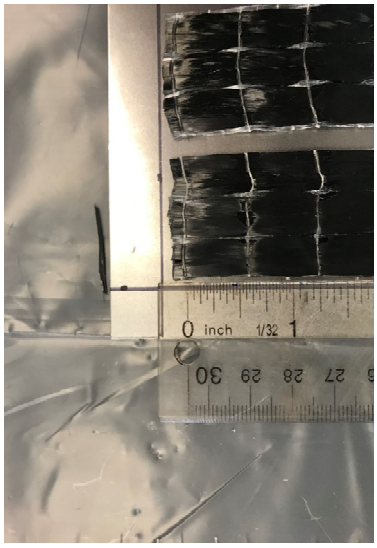

(b) CFRP coupons showing 3 unidirectional strips per specimen

Figure D.5. Cutting of CFRP laminates

D.4 COLUMN STUB RETROFIT PROCEDURE

The following outlines the procedure used to retrofit the bent cap column stubs. The key steps comprising the procedure are as follows:

1. Column stub concrete cover removal: Concrete was chipped off from the side surfaces of the column stubs until the column spiral reinforcement was exposed along the perimeter, over the height of the stub. An approximate 2 to 3-in. height of concrete cover was left in-tact at the base of the column stub to ensure that the column stub-bent cap connection geometries of the specimens remained unaltered from that provided in service. Loose concrete and debris were removed from the exposed cores of the column stubs and the resulting roughened surface was maintained to ensure maximum adhesion of the grout to the column stub core concrete. Figure D.6 shows the column stub concrete cover removal process and the exposed column spiral reinforcement.

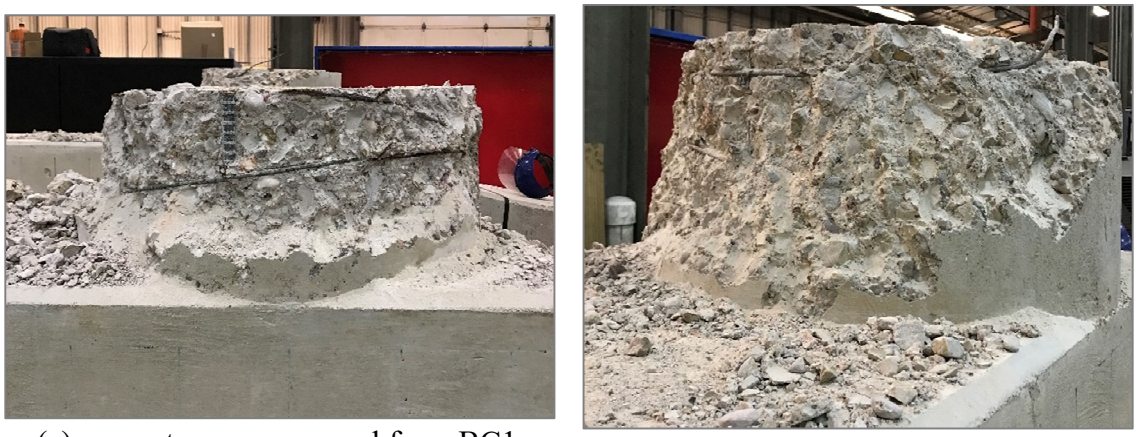

(a) concrete cover removal from BC1 middle column stub

(b) concrete cover removal from BC1 south column stub

Figure D.6. Concrete cover removal

2. Medium density fibreboard (MDF) forms preparation: ¾-in. thick MDF boards were used to enclose the perimeters of the column stubs and function as supports for the steel tubes. The MDF boards were placed on the surfaces of the bent caps to

provide separation of the stub retrofits from the surfaces of the bent caps. The separation of the steel tube and the bent cap surface ensured that the stub column-bent cap connection geometry remained unchanged from that provided in service.

3. Gap waterproofing: Spray foam insulation was applied to close the gaps between the MDF support base and the column stubs, as can be seen from Figure D.7a. Leftover foam was cut flush with the top surface of the MDF and silicone caulking was used to seal any remaining gaps and mitigate leakage during the grouting operations (refer to Figure D.7b).
4. Steel tube placement: The ¼-in. thick steel tubes were placed on top of the MDF support boards and centered with respect the east-west and north-south centerlines of the existing column stubs. After they were correctly positioned, they were secured in place using a series of clamps (refer to Figure D.8).

(a) foam application between MDF form and column stub outer face

(b) caulk application to waterproof waterproof gaps

Figure D.7. Gap closure between MDF form and column stub

5. Waterproofing of Steel Tubes Base: Prior to grouting, caulking was applied along the outside perimeters at the bases of the steel tubes to avoid water leakage during the grouting process. The caulking of the steel tube-MDF support board connections can be seen in Figure D.7.

6. High-performance Grout Application: SikaGrout 328 was mixed and used to fill the steel tubes comprising the retrofits and enclose the bent cap column stubs. Prior to grouting, the concrete comprising the existing column stubs was pre-saturated with water to minimize leakage of grout moisture to existing concrete and to maximize the adhesion of cured grout-column stub interface. Note that the specific grouting material employed in this case was a non-shrink product which ensured that the level top surface of the retrofitted stubs created during casting would be maintained after curing, and it also maximized the positive stub confining effects provided by the steel tubes encasing the retrofits.

Figure D.8. Waterproofing of steel tube base and clamping of steel tube

D.5 CFRP INSTALLATION PROCEDURE

The following section summarizes the key steps taken to install the CFRP retrofit developed:

1. Surface preparation: To ensure proper adhesion of the concrete with the CFRP, the laitance (i.e., the thin weak layer of fine aggregate, dirt, and loose debris on the concrete surface) was removed. A diamond grinder was used to remove the laitance. The concrete was ground until aggregate was exposed, typically removing about ¼ in. thick layer of concrete, as visible in Figure D.9a Note that this initial stage of surface preparation was arguably not required for the 'contact critical' (i.e., the strength of the CFRP develops by bonding back into itself) full-wrap CFRP configuration that was employed. Nevertheless, was carried-out to maximize the effectiveness of retrofit.

   Two additional items for the surface preparation were completed, as described below.

   - Corner rounding: The corners of the bent cap cross-section were ground-down to achieve a minimum corner radius of ¾ in. (refer to Figure D.9b). The curved corners are used to minimize the development of stress concentrations developed within the retrofit.
   - Corner grouting: As a result of the chain straps that were used to secure the bent caps during transportation from the bridge site to the laboratory, some of the bent cap corners comprising the to-be-retrofitted regions and localized spalls and concrete damage. These were grouted using SikaGrout 328 (i.e., a high-strength non-shrink grout). The grout was ground smooth after curing to provide the desired ¾-in. corner radius. This provided the

proper geometry for the CFRP installation. Refer to Figure D.9.c and Figure D.9d.

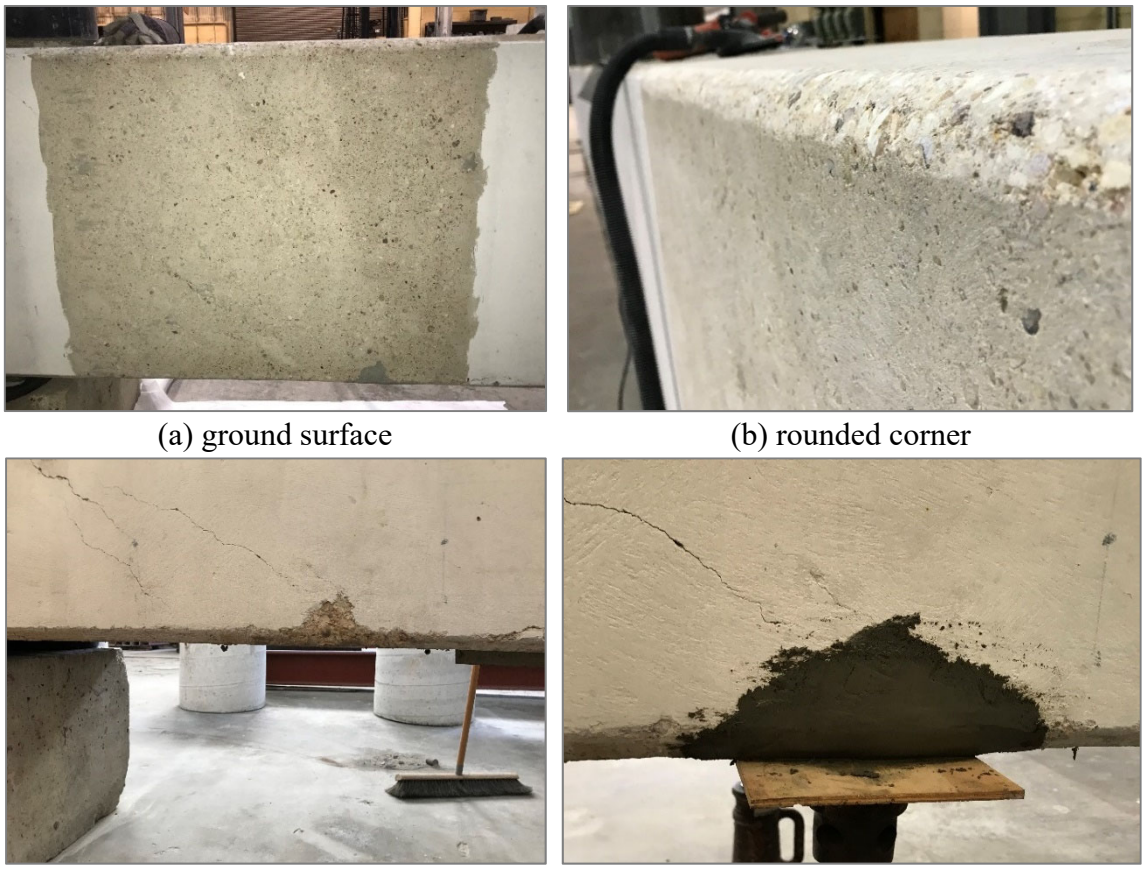

(a) ground surface (b) rounded corner

(c) damaged corner (d) grouted corner

Figure D.9. Surface preparation for CFRP application

2. CFRP cutting: The Tyfo SCH-41 material comes in 24-in. wide rolls. Therefore, 6 strips of dimensions 12 in. by 84 in. were cut using standard office scissors. Note that Fyfe recommended the use of either 12-in. or 24-in. wide CFRP strips to minimize separation of the fibers at the edges, and to ease handling during installation.
3. Bent cap surface cleaning: Using a nylon brush and air nozzle, dust and impurities were removed from the previously grinded surfaces.

4. CFRP location marking: The target installation locations of the CFRP were initially marked on the surface of the bent cap. Surface priming: After mixing the Tyfo S Epoxy, a thin layer was applied with a roller on the target zones for the CFRP application. On uneven surfaces (i.e., at locations of existing cracks, cured concrete voids, damaged areas, etc.) a thicker epoxy was used to level the surface using a trowel (refer to Figure D.10).

(a) thickened epoxy on crack (b) thickened epoxy on uneven surface

Figure D.10. Resin application on cracked and uneven surfaces

5. CFRP manual saturation: A 'bath frame' was built to saturate the CFRP strips. Within the frame, the CFRP strips were placed on the surface and saturated using rollers, as shown in Figure D.11. Both sides of the CFRP were saturated. Using a 2-in. diameter PVC tube, the CFRP strip was spooled and transported for installation.

6. CFRP installation: The CFRP strips were placed in their respective positions as per the design presented in Section 3.1.2. A trowel was used to eliminate entrapped air bubbles and ensure proper adhesion to the concrete surface, as shown in Figure D.12.

Figure D.11. Saturation of CFRP strip using a roller

7. Edge epoxy application: A final coat of epoxy was applied to the edges of the installed strips to avoid fabric delamination at these locations. Figure D.13 presents the completed retrofit.

(a) CFRP strip application

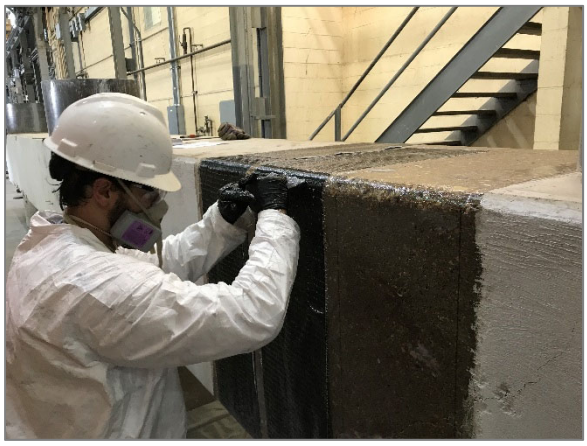

(b) elimination of entrapped air bubbles

Figure D.12. FRP strip application and elimination of entrapped bubbles

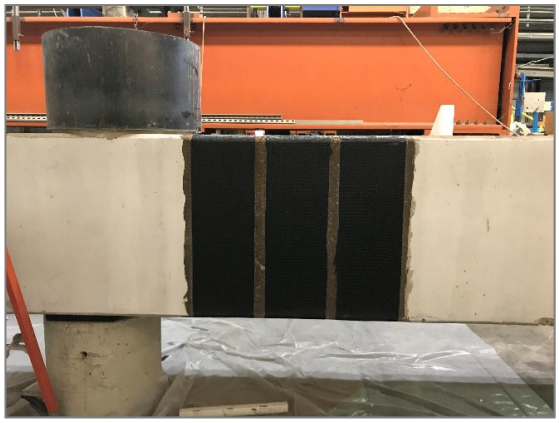

(a) front view of finished retrofit

(b) overview of finished retrofit

(c) bottom of finished retrofit

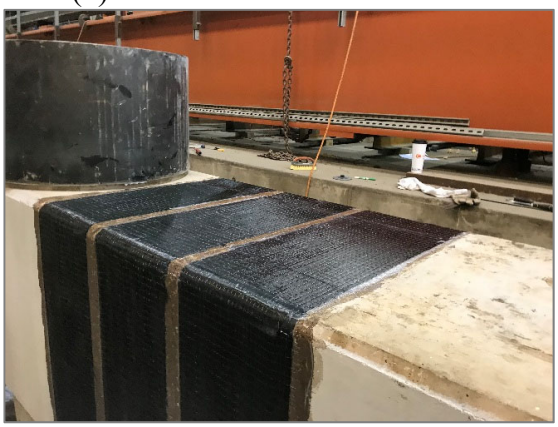

(d) top of finished retrofit

Figure D.13. Finished CFRP retrofit

APPENDIX E Design Drawings

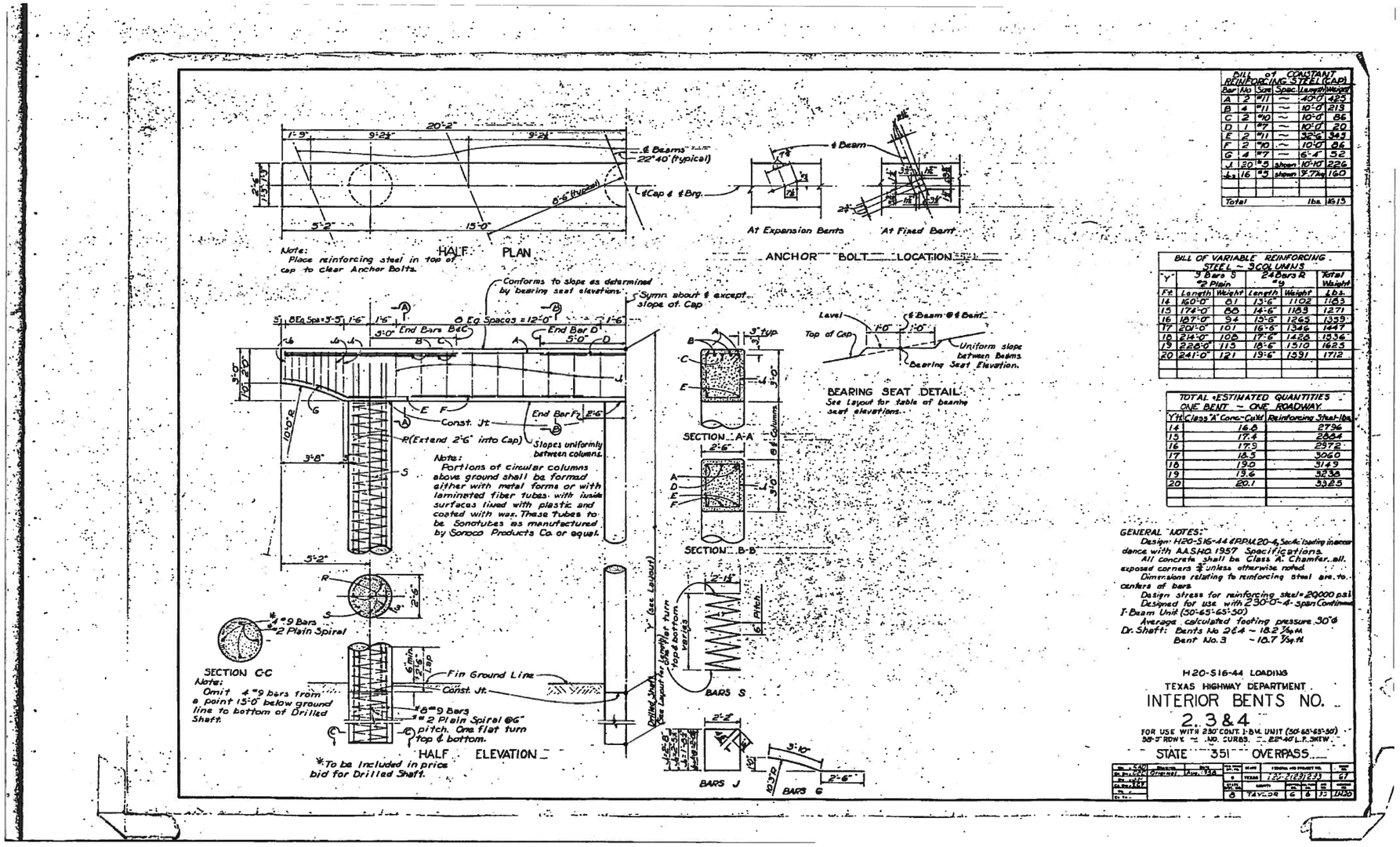

BILL of CONSTANT REINFORCING STEEL (CAP)

Bar	No	Size	Spac.	Length	Weight
A	2	#11	—	40'-0	455
B	4	#11	—	10'-0	219
C	2	#10	—	10'-0	86
D	1	#9	—	10'-0	20
E	2	#11	—	32'-6	343
F	2	#10	—	10'-0	86
G	4	#7	—	6'-4	52
J	20	#5	shown	10'-10	226
Js	16	#5	shown	9'-7	160
Total					lbs 1615

BILL OF VARIABLE REINFORCING STEEL - 3 COLUMNS

Y	3 Bars S #2 Plain		2 Bars R #9		Total Weight
Ft	Length	Weight	Length	Weight	Lbs
14	160'-0"	81	13'-6"	1102	1183
15	174'-0"	88	14'-6"	1183	1271
16	187'-0"	94	15'-6"	1265	1359
17	201'-0"	101	16'-6"	1346	1447
18	214'-0"	108	17'-6"	1428	1536
19	228'-0"	115	18'-6"	1510	1625
20	241'-0"	121	19'-6"	1591	1712

TOTAL ESTIMATED QUANTITIES ONE BENT - ONE ROADWAY

Y'ft	Class "A" Conc. - Cu.Yd.	Reinforcing Steel - lbs.
14	16.0	2756
15	17.4	2884
16	17.9	2972
17	18.5	3060
18	19.0	3149
19	19.6	3238
20	20.1	3325

GENERAL NOTES:
Design H20-S16-44 & PPM 20-4, Specific loading in accordance with AASHO 1957 Specifications.
All concrete shall be Class A. Chamfer all exposed corners ¾" unless otherwise noted.
Dimensions relating to reinforcing steel are to centers of bars.
Design stress for reinforcing steel = 20000 p.s.i.
Designed for use with 230'-0"-4-span Continuous I-Beam Unit (50'-65'-65'-50')
Average calculated footing pressure 30 t/s.f.
Dr. Shaft: Bents No 2 & 4 ~ 18.2 ⅞ q.m.
Bent No. 3 ~ 18.7 ⅞ q.m.

H20-S16-44 LOADING
TEXAS HIGHWAY DEPARTMENT
INTERIOR BENTS NO. 2, 3 & 4
FOR USE WITH 230' CONT. I-BM. UNIT (50'-65'-65'-50')
38'-3" ROW'S - NO. CURBS. - 22'-40' L.P. SKEW.
STATE 351 OVERPASS

Designed	Detailed	Checked	Quantities	Date
Original	Rev. 1-58			

Dist.	County	Sheet No.	Total Sheets
6	TAYLOR	6	32

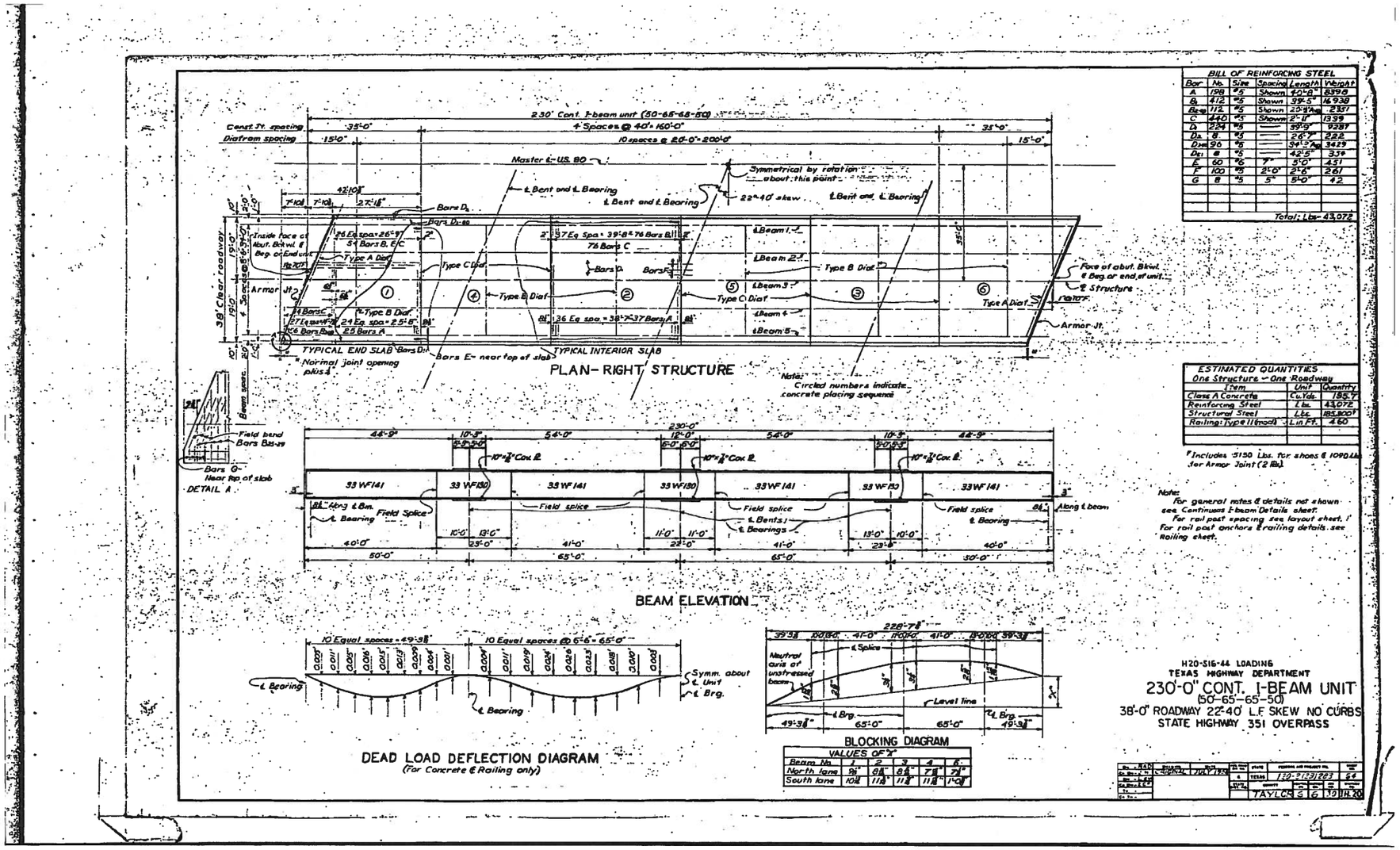
PLAN- RIGHT STRUCTURE
TYPICAL END SLAB
TYPICAL INTERIOR SLAB
Bars E- near top of slab
Normal joint opening plus ¼"
Notes: Circled numbers indicate concrete placing sequence
DETAIL A
Field bend Bars Bb1-39
Bars G- Near top of slab
BEAM ELEVATION
33 WF 141
33 WF 130
Field splice
Bents
Bearings
DEAD LOAD DEFLECTION DIAGRAM
(For Concrete & Railing only)
Symm. about ℄ Unit
℄ Bearing
BLOCKING DIAGRAM
Neutral axis of unstressed beam
Level line
℄ Brg.
VALUES OF "X"
Beam No. 1 2 3 4 5
North lane 9½" 6⅞" 6¼" 7⅛" 7½"
South lane 10¼" 11⅜" 11⅜" 11⅜" 11"-0"
BILL OF REINFORCING STEEL
Total: Lbs- 43,072
ESTIMATED QUANTITIES
One Structure — One Roadway
Item Unit Quantity
Class A Concrete Cu.Yds. 185.7
Reinforcing Steel Lbs. 43,072
Structural Steel Lbs. 183,800†
Railing: Type 411 (mod) L.in Ft. 460
† Includes 3150 Lbs. for shoes & 1090 Lbs. for Armor Joint (2 lbs.)
Note: For general notes & details not shown see Continuous I-beam Details sheet. For rail post spacing see layout sheet. For rail post anchors & railing details see Railing sheet.
H20-S16-44 LOADING
TEXAS HIGHWAY DEPARTMENT
230'-0" CONT. I-BEAM UNIT
(50'-65'-65'-50')
38'-0" ROADWAY 22°40' L.F. SKEW NO CURBS
STATE HIGHWAY 351 OVERPASS
TAYLOR 3 16 1951 20

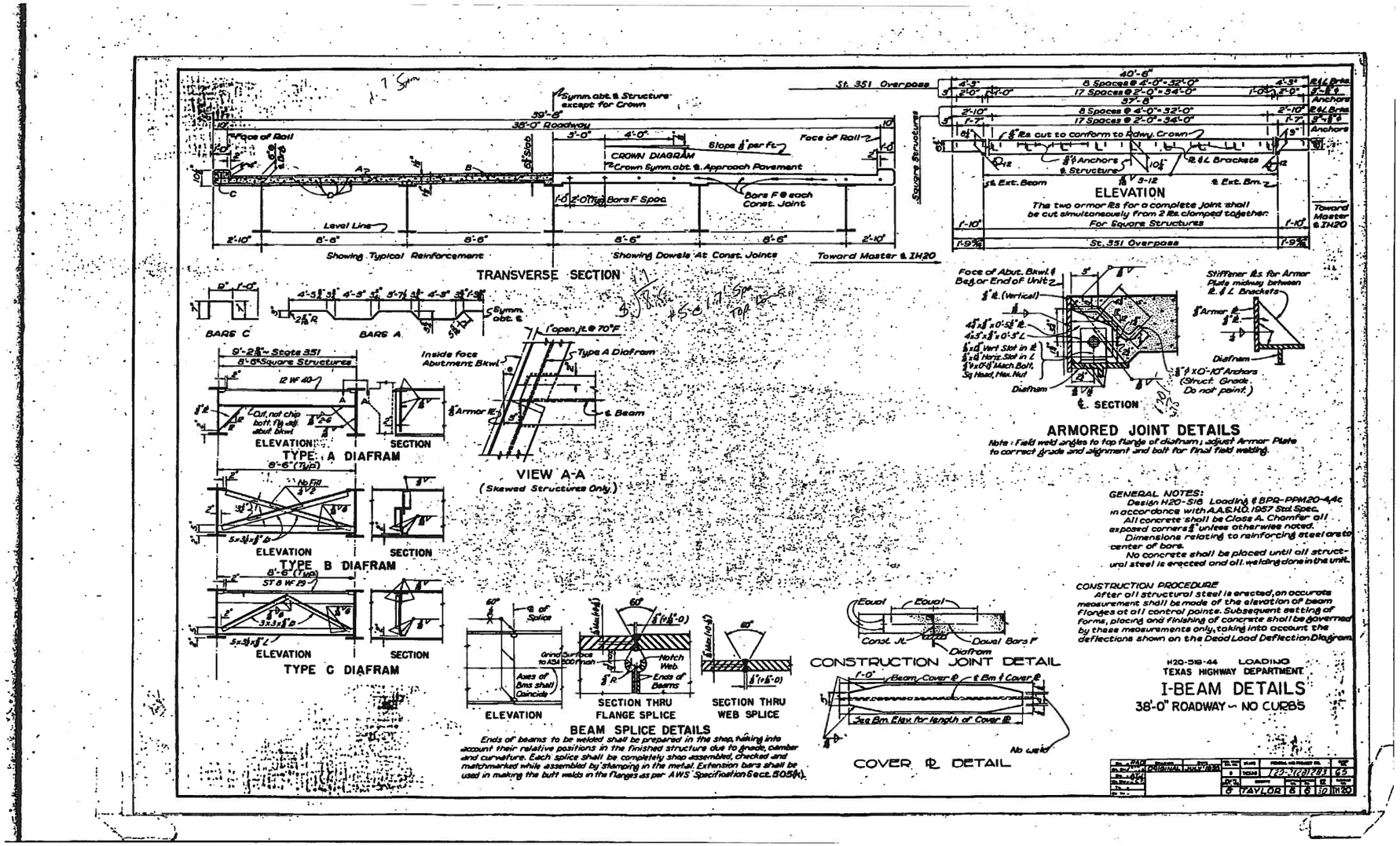
TRANSVERSE SECTION
Showing Typical Reinforcement
Showing Dowels At Const. Joints
Toward Master ℄ IH20
38'-0" Roadway
Face of Rail
CROWN DIAGRAM
Slope ⅛" per Ft.
Level Line
Bars F @ each Const. Joint
St. 351 Overpass
ELEVATION
The two armor ℞s for a complete joint shall be cut simultaneously from 2 ℞s clamped together.
For Square Structures
BARS C
BARS A
TYPE A DIAFRAM
TYPE B DIAFRAM
TYPE C DIAFRAM
ELEVATION
SECTION
VIEW A-A
(Skewed Structures Only)
Inside face Abutment Bkwl.
Type A Diafram
℄ Beam
Armor ℞
ARMORED JOINT DETAILS
Note: Field weld angles to top flange of diafram; adjust Armor Plate to correct grade and alignment and bolt for final field welding.
GENERAL NOTES:
Design H20-S16 Loading & BPR-PPH20-44c in accordance with A.A.S.H.O. 1957 Std. Spec.
All concrete shall be Class A. Chamfer all exposed corners ¾" unless otherwise noted.
Dimensions relating to reinforcing steel are to center of bars.
No concrete shall be placed until all structural steel is erected and all welding done in the unit.
CONSTRUCTION PROCEDURE
After all structural steel is erected, an accurate measurement shall be made of the elevation of beam flanges at all control points. Subsequent setting of forms, placing and finishing of concrete shall be governed by these measurements only, taking into account the deflections shown on the Dead Load Deflection Diagram.
H20-S16-44 LOADING
TEXAS HIGHWAY DEPARTMENT
I-BEAM DETAILS
38'-0" ROADWAY — NO CURBS
Grind Surface to 454 300 finish
Axes of Bms shall Coincide
Notch Web
Ends of Beams
SECTION THRU FLANGE SPLICE
SECTION THRU WEB SPLICE
BEAM SPLICE DETAILS
Ends of beams to be welded shall be prepared in the shop, taking into account their relative positions in the finished structure due to grade, camber and curvature. Each splice shall be completely shop assembled, checked and matchmarked while assembled by stamping in the metal. Extension bars shall be used in making the butt welds in the flanges as per AWS Specification 5 sect. 505(k).
CONSTRUCTION JOINT DETAIL
Const. Jt.
Dowel Bars F
Diafram
COVER ℞ DETAIL
No weld
TAYLOR
IH 20

APPENDIX F Petrography report

A Twining Company

3200 Carbon Place #104
Boulder, CO 80301
T: 303.938.0166
www.drpcinc.com

Petrographic Investigation of Concrete Cores From a Bridge Bent Cap on Interstate Highway 20 in Abilene, Texas

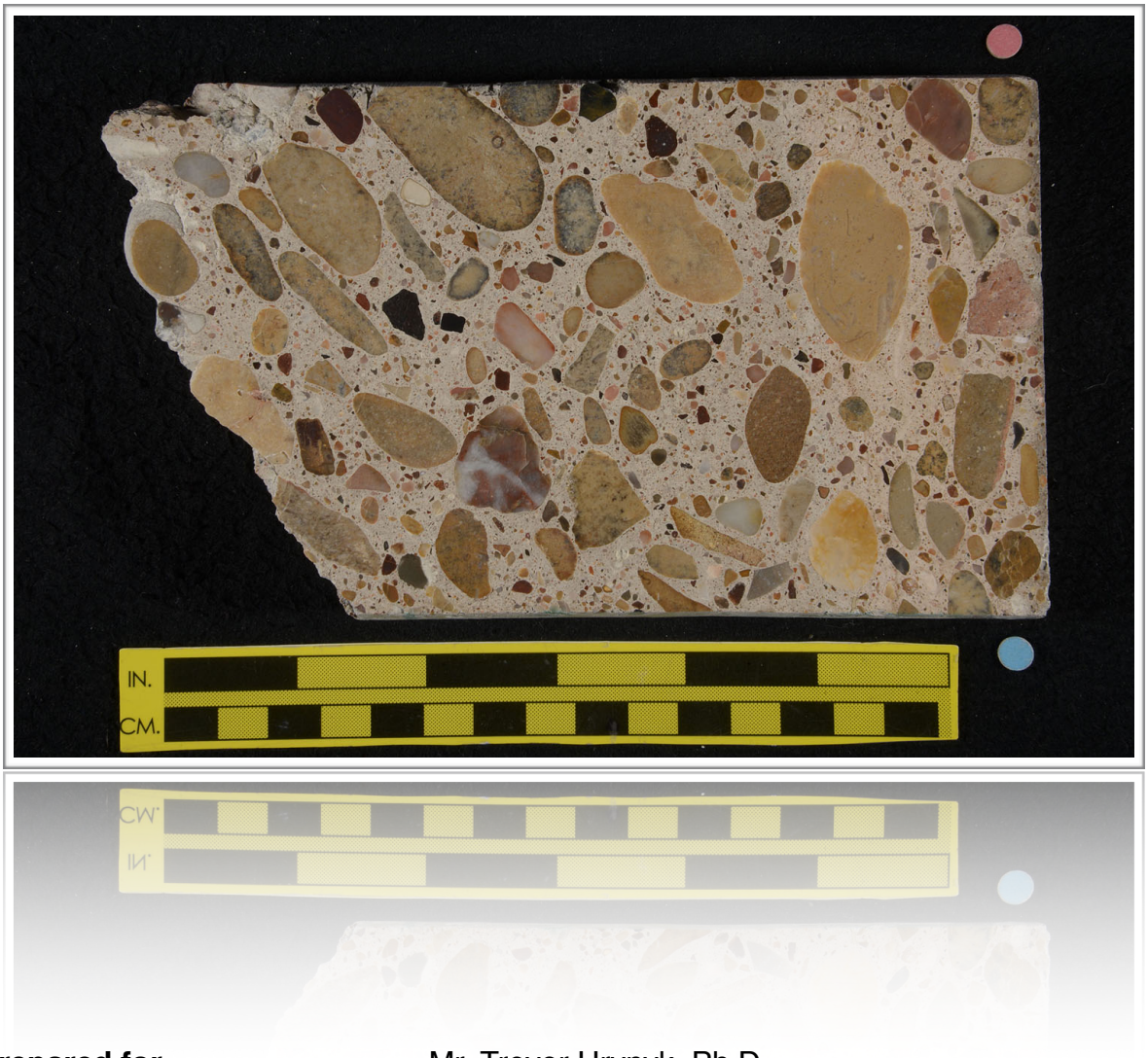

Prepared for

Mr. Trevor Hrynyk, Ph.D.
Ferguson Structural Engineering Laboratory
The University of Texas at Austin
Austin, Texas

Prepared by

David Rothstein, Ph.D., P.G., FACI
Report No. 177091.d
1 December 2017

EXECUTIVE SUMMARY

Two (2) cores extracted from the bent caps of a bridge on Interstate Highway 20 in Abilene, Texas are subjects of petrographic examination to characterize the general composition and condition of the concrete represented by the cores. The findings from this scope of work indicate that both cores are similar in terms of the components used to produce the concrete and the proportioning of those components. The paste contains hydrated portland cement with no fly ash, slag cement or other supplemental cementitious materials observed. Both cores are non-air-entrained and contain less than 3% total air as estimated from visual and microscopical observations. Both cores have a natural gravel coarse aggregate with a nominal top size of 25 mm (1 in.). The coarse aggregate is mostly carbonate in composition and consists primarily of limestones but chert and quartzite are also present. The fine aggregate is a natural sand that consists mostly of quartzite and chert with minor limestone. Chert and quartzite are potentially susceptible to alkali-silica reaction (ASR) but no evidence of such reactions was observed beyond minor internal microcracking and reaction rims on chert particles. Neither core contains embedded steel.

Both cores show numerous hairline cracks and microcracks, particularly in the outer 19 mm (¾ in.) of the core. These hairline cracks and microcracks are not typical of drying shrinkage and are clearly not from an internal expansion mechanism such as ASR. As such, they may likely be related to structural issues. Both cores show deep carbonation that reaches up to 50 mm (2 in.) from the formed surface. The depth of carbonation is most likely a function of the abundance of cracking and microcracking along with the nature of the concrete mixture, which appears relatively lean by modern standards.

1.0 INTRODUCTION

Mr. Trevor Hrynyk, Ph.D., of the University of Texas Ferguson Structural Engineering Laboratory (**UT**) located in Austin, Texas requested DRP, A Twining Company (**DRP**) to perform petrographic examinations on two (2) concrete cores extracted from bent caps on a bridge on Interstate Highway 20 in Abilene, Texas. On 20 October 2017 **DRP** received two (2) cores from **UT**. The cores were designated as Core 12T1 and Core 1T2 and assigned **DRP** sample numbers 21YD8927 and 21YD8928, respectively.

The purpose of the examination was to characterize the general composition and condition of the concrete. Mr. Brown indicated that the bridge was constructed approximately 60 years ago and was recently removed from service. Elements within the bridge reportedly exhibited structural damage that manifested as diagonal cracking near support points. Aggregate particles reportedly broke free easily from cores that were extracted from the bent caps and tested for compressive strength. No information was available regarding the original concrete mix design information.

2.0 SCOPE OF WORK

The testing involved petrographic examinations according to ASTM C856 [**1**] on both cores; hardened air content was estimated from visual and microscopical observations but was not measured according to ASTM C457 [**2**]. *Appendix A* and *Appendix B* contain the notes, photographs and micrographs from the petrographic examinations and *Appendix C* describes the procedures used to perform this scope of work.

1 *Standard Practice for Petrographic Examination of Hardened Concrete.* Annual Book of ASTM Standards, Vol. 4.02., ASTM C856-17.

2 *Standard Test Method for Microscopical Determination of Parameters of the Air-Void System in Hardened Concrete*, Annual Book of ASTM Standards, Vol. 4.02, ASTM C457-16.

3.0 FINDINGS

3.1 ***Orientation, Dimensions & As-Received Condition*** Both cores are horizontal in orientation and measure 100 mm (4 in.) in diameter. Both cores span from intact formed surfaces to fracture surfaces such that they represent partial thicknesses of the bent caps. Core 12T1 is 125-175 mm (5-7 in.) long and Core 1T2 is 190-210 mm (7 ½-8 ⅜ in.) long. Neither core contains reinforcing steel or other embedded objects. **Figure 1** contains photographs of the cores in their as-received condition and the polished surfaces from the cores.

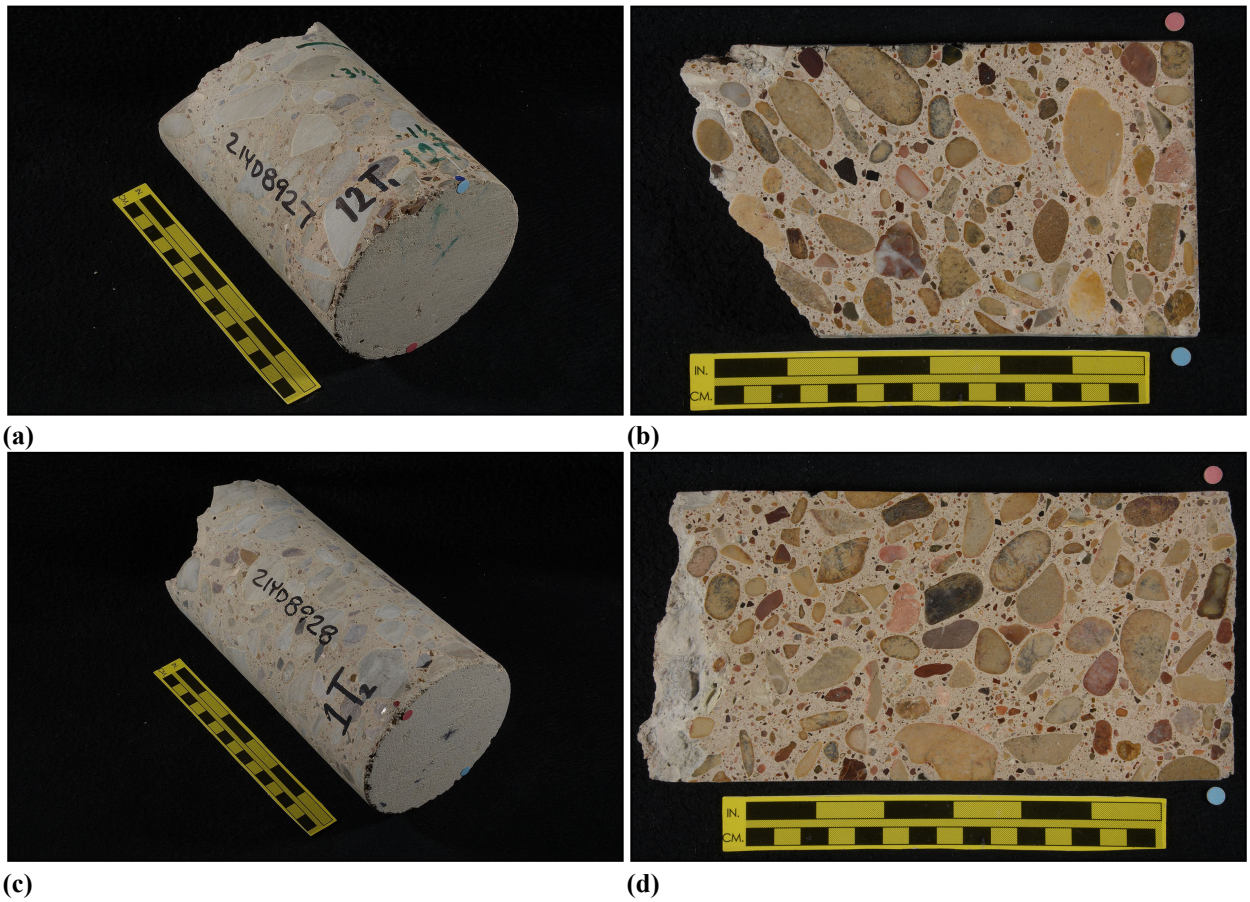

(a) (b)

(c) (d)

Figure 1. (a) Photograph of Core 12T1 showing oblique view of the top and side of the core. (b) Photograph of polished surface of Core 12T1. (c) Photograph of Core 1T2 showing oblique view of the top and side of the core. (d) Photograph of the polished surface of Core 1T2. The yellow scale is ~ 150 mm (6 in.) long in all of the photos. The red and blue dots in (a) and (c) indicate the orientation of the saw cuts used to prepare the sample.

3.2 ***Components: Paste*** The paste fraction of both samples is similar in terms of composition. The paste consists of hydrated portland cement with no fly ash; no slag cement or other supplemental cementitious materials were observed. The hydration is normal to somewhat less advanced than anticipated for concrete that is ~ 60 years old. Calcium hydroxide is medium to coarse-grained and distributed evenly. The paste is light gray to pale yellow with a granular texture and dull luster. The paste is moderately soft (Mohs 2.5-3). **Figure 2** shows photographs and photomicrographs of the paste from Core 12T1 as an example of the paste properties. Both cores showed slightly darker paste at the outer end of the core.

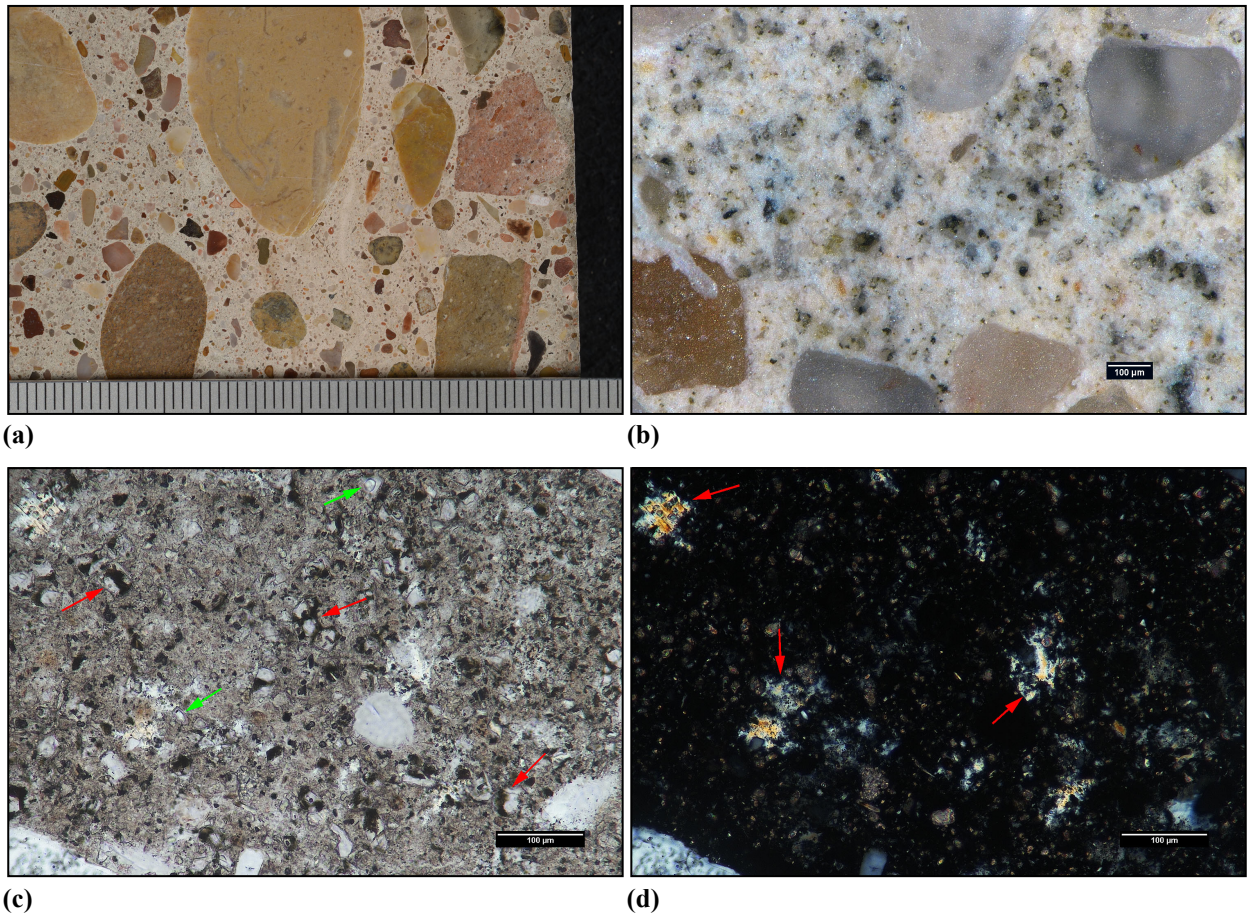

(a) **(b)**

(c) **(d)**

Figure 2. Examples of paste properties in Core 12T1. (a) Photograph of the polished surface showing overview of paste at the top of the core. (b) Reflected light photomicrograph of polished surface showing detail of paste in the middle of the core. Transmitted light photomicrographs of thin section showing detail of the paste in (c) plane-polarized and (d) cross-polarized light. The red and green arrows in (c) indicate relict and residual cement grains and fly ash, respectively.

3.3 ***Components: Air*** Both cores are non-air-entrained and contain less than 3% total air as estimated from visual and microscopic observations. The concrete is well consolidated with no major entrapped voids or water voids observed.

3.4 ***Components: Aggregates*** The cores contain similar aggregates (**Figure 5**). The coarse aggregate is a natural gravel with a nominal top size of 25 mm (1 in.). The grading and distribution are relatively even. The aggregate consists of a mixture of carbonate and siliceous sedimentary rocks that consist mostly of limestone (~ 85%) with minor amounts of chert (~ 10%) and quartzite (~ 5%). The fine aggregate is a natural sand that consists mostly of quartzite and chert with minor limestones similar to those observed in the coarse aggregate. Chert and quartzite are potentially susceptible to alkali-silica reaction (ASR) but no evidence of such reactions were observed in either core apart from some internal microcracks and reaction rims on chert particles. No deposits of gel were observed.

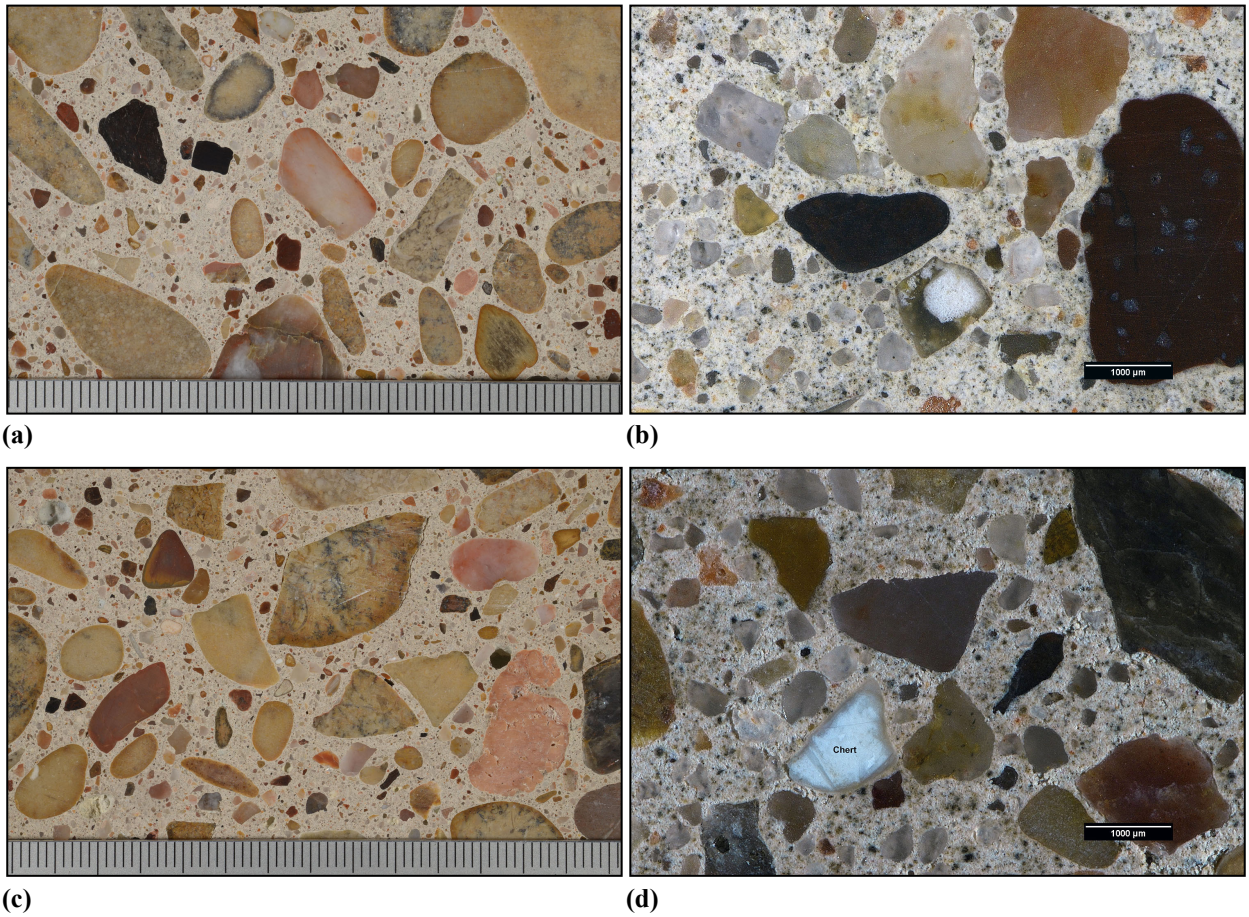

(a) **(b)**

(c) **(d)**

Figure 5. (a) Photograph and (b) reflected light photomicrograph of polished surface of Core 12T1 showing coarse and fine aggregate, respectively. The scale is in millimeters in (a). (c) Photograph and (d) reflected light photomicrograph of polished surface of Core 1T2 showing coarse and fine aggregate, respectively. The scale is in millimeters in (c).

3.5 ***Cracking and microcracking*** Both cores show extensive hairline cracking and microcracking. In Core 12T1 hairline cracks were observed throughout the core but were most prominent in the outer 19 mm (¾ in.). These cracks are up to 500 µm (20 mil) wide and 6 mm (¼ in.) long. Core 1T2 also shows numerous hairline cracks; these are mostly in the outer 25-38 mm (1-1 ½ in.) of the core. A sub-horizontal crack cuts from the formed surface to 30 mm (1 ⅛ in.); this crack is up to 175 µm (7 mil) wide. Occasional microcracks were observed throughout the length of both cores but were most abundant in the outer 19 mm (¾ in.). The cracks and microcracks consistently cut around aggregate particles and are free of secondary deposits. **Figure 6** shows examples of cracks and microcracks in the cores.

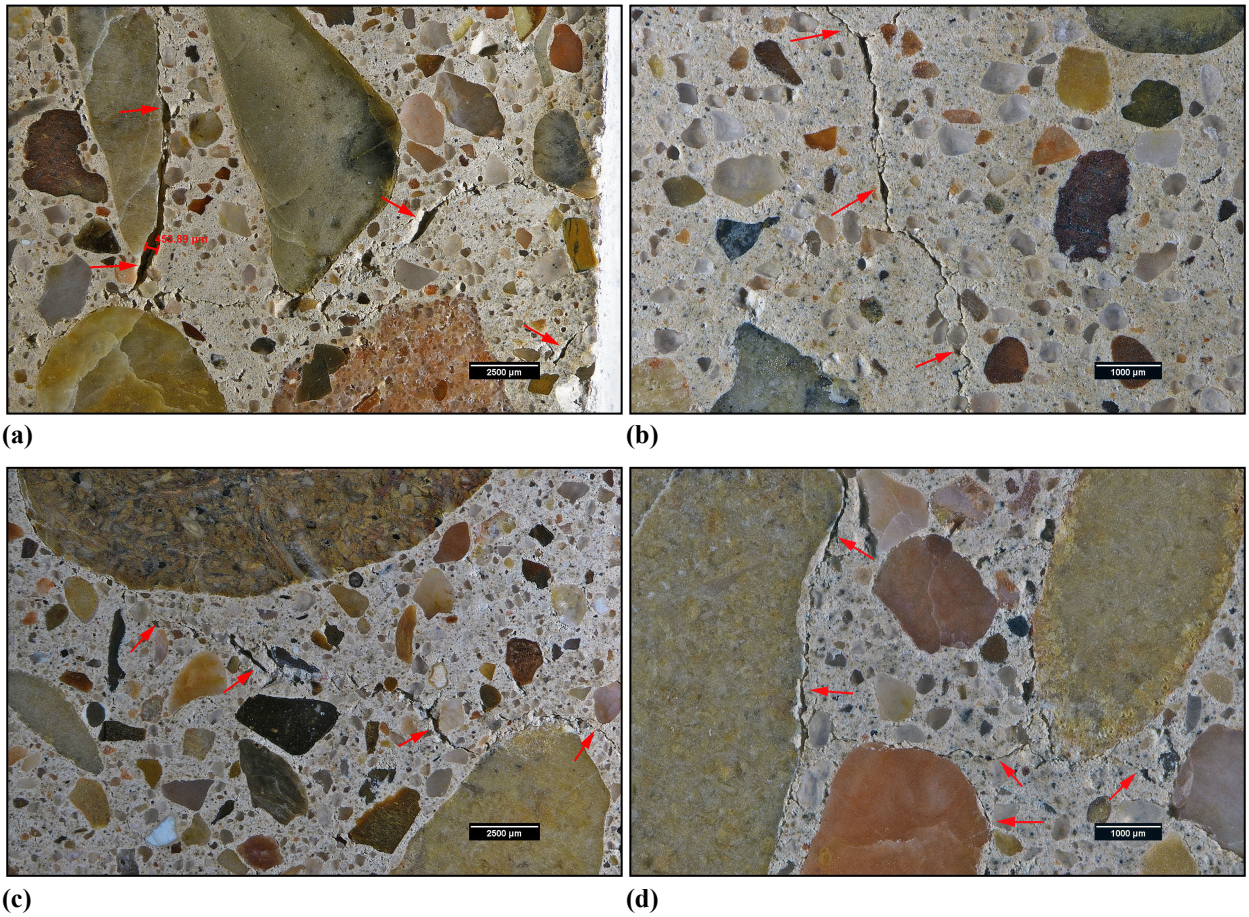

(a) **(b)**

(c) **(d)**

Figure 6. (a) Reflected light photomicrograph of the polished surface of Core 12T1 showing hairline cracks (red arrows) at the outer end of the core. (b) Reflected light photomicrograph of the polished surface of Core 12T1 showing microcracks (red arrows) about 25 mm (1 in.) from the outer surface. (c) Reflected light photomicrograph of the polished surface of Core 1T2 showing hairline cracks (red arrows) about 25 mm (1 in.) from the outer surface. (d) Reflected light photomicrograph of the polished surface of Core 1T2 showing microcracks (red arrows) about 19 mm (¾ in.) from the outer surface.

3.6 ***Secondary Deposits*** Both cores show deep carbonation as detected by phenolphthalein staining and thin section microscopy that reaches a depth of ~ 50 mm (2 in.). **Figure 7** contains photographs showing the phenolphthalein-stained surfaces. No other secondary deposits were observed.

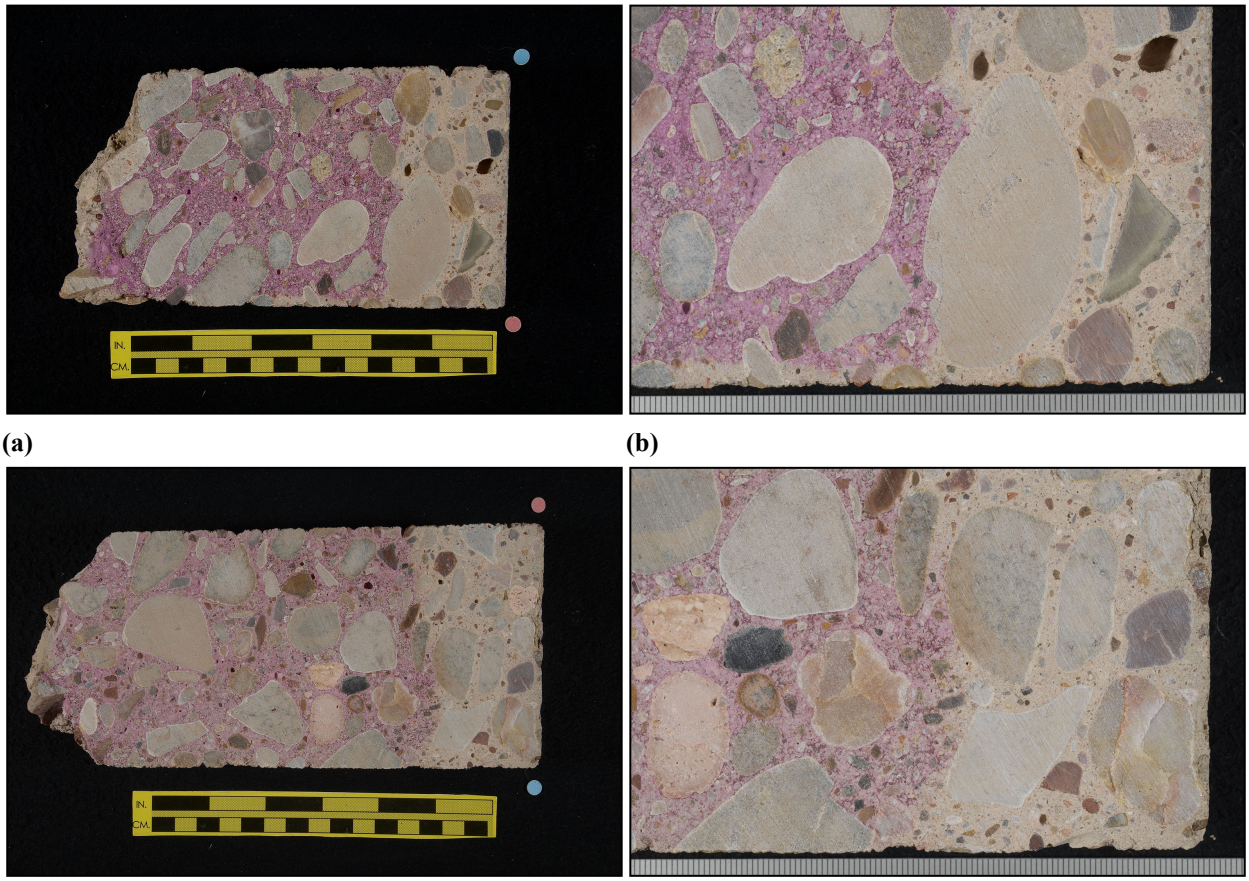

(a) **(b)**

(c) **(d)**

Figure 7. Photographs showing (a) overview of phenolphthalein-stained surface from Core 12T1 and (b) detail of the surface near the outer surface of the Core 12T1. The yellow scale in (a) is ~ 150 mm (6 in.) long and the scale in (b) is in millimeters. Photographs showing (c) overview of phenolphthalein-stained surface from Core 1T2 and (d) detail of the surface near the outer surface of the Core 1T2. The yellow scale in (c) is ~ 150 mm (6 in.) long and the scale in (d) is in millimeters.

4.0 Discussion & Conclusions

Based on the observations described above, both cores are similar in terms of the components used to produce the concrete and the proportioning of those components. The paste contains hydrated portland cement with no fly ash, slag cement or other supplemental cementitious materials observed. Both cores are non-air-entrained and contain less than 3% total air as estimated from visual and microscopical observations. Both cores have a natural gravel coarse aggregate with a nominal top size of 25 mm (1 in.). The coarse aggregate is mostly carbonate in composition and consists primarily of limestones but chert and quartzite are also present. The fine aggregate is a natural sand that consists mostly of quartzite and chert with minor limestone. Chert and quartzite are potentially susceptible to alkali-silica reaction (ASR) but no evidence of such reactions was observed beyond minor internal microcracking and reaction rims on chert particles. Neither core contains embedded steel.

Both cores show numerous hairline cracks and microcracks, particularly in the outer 19 mm (¾ in.) of the core. These hairline cracks and microcracks are not typical of drying shrinkage and are clearly not from an internal expansion mechanism such as ASR. As such, they may likely be related to structural issues. Both cores show deep carbonation that reaches up to 50 mm (2 in.) from the formed surface. The depth of carbonation is most likely a function of the abundance of cracking and microcracking along with the nature of the concrete mixture, which appears relatively lean by modern standards.

This concludes work performed on this project to date.

David Rothstein, Ph.D., P.G., FACI

Interstate Highway 20 Bridge Bent Cap Core Petrography

Appendices

1. Received Condition	
Orientation & Dimensions	Horizontal core through bent cap panel measures 100 mm (4 in.) in diameter and 125-175 mm (5-7 in.) long (**Figure A1**, **Figure A2**).
Surfaces	The outer surface is formed and the inner surface is a fracture such that the core represents a partial thickness of the bent cap. The outer surface is smooth and intact (**Figure A3**).
General Condition	The concrete is hard and compact and rings lightly when sounded with a hammer.

2. Embedded Objects	
General	None observed.

3. Cracking	
Macroscopic	Numerous hairline cracks were observed in the outer ~ 19 mm (¾ in.) of the core (**Figure A4**). Most of these cracks are sub-vertical to oblique in orientation, range up 500 µm (20 mil) wide and 6 mm (¼ in.) long. Occasional cracks of similar dimensions were observed throughout the core. These cracks pass around aggregate particles and are free of secondary deposits.
Microscopic	Microcracks are also abundant in the outer ~ 19 mm (¾ in.) of the core; these range up to 100 µm (4 mil) wide and 3 mm (⅛ in.) long (**Figure A5**). Occasional microcracks of similar dimensions cut sub-horizontally from the formed surface. A sub-vertical microcrack ranging from 50-100 µm wide cuts sub-vertically through the paste over a 15 mm (⅝ in.) strike length about 25 mm (1 in.) from the formed surface. All microcracks cut around aggregate particles and lack secondary deposits.

4. Voids	
Void System	Concrete is non-air-entrained and contains less than 3% total air as estimated from visual and microscopic observations (not determined in accordance with ASTM C457). The concrete is well consolidated with no major entrapped voids or bleed voids observed.
Void Fillings	None observed.

5. Coarse Aggregate	
Physical Properties	The coarse aggregate is a natural gravel with a nominal top size of 25 mm (1 in.; **Figure A6**). The rocks are hard and competent. Most particles are slightly elongated with rounded to sub-angular edges. The gradation and distribution are relatively even.
Rock Types	The aggregate consists of a mixture of siliceous and carbonate sedimentary rocks. Most of the aggregate consists of limestones (~ 85%) with minor amounts of chert (~ 10%) and quartzite (~ 5%). Most of the limestones range in color from buff to pale brown to brownish green to red. The textures range from massive and micritic to rocks with abundant intraclasts to rocks with minor amounts of fossiliferous material. Occasional carbonaceous limestones were observed. None of the limestones show textures typical of rocks that are susceptible to alkali-carbonate reaction (ACR). Most of the quartzites are arenitic. Quartzite and chert are potentially susceptible to alkali-silica reaction (ASR).
Other Features	No deleterious coatings or incrustations observed. No low w/c mortar coatings were observed. No evidence of ASR or ACR was observed.

6. Fine Aggregate

Physical Properties	The fine aggregate is a natural sand that consists of rocks that are hard and competent (**Figure A7**). The particles are sub-equant to slightly elongated in shape with sub-rounded to angular edges. The grading and distribution are relatively even.
Rock Types	The sand consists primarily of siliceous rocks that include quartzite, chert and fragments of quartz with minor amounts of limestone similar to those observed in the coarse aggregate. Chert and quartzite are potentially susceptible to ASR.
Other Features	No deleterious coatings or incrustations observed. No low w/c mortar coatings observed. No evidence of ASR was observed involving the fine aggregate.

7. Paste Observations

Polished Surface	Paste is light gray (Munsell 2.5Y/7/1) to pale yellow (2.5Y/8/4), has a granular texture and a dull luster (**Figure A8**). The paste is moderately soft (Mohs 2.5-3). The paste is gray for up to 2 mm (80 mil) from the formed surface.
Fresh Fracture	Fracture surface is light gray, has a punky texture and a dull luster (**Figure A9**). The fracture cuts mostly around coarse aggregate particles.
Thin Section*	The paste contains hydrated portland cement with no fly ash, slag cement or other SCM observed. The hydration is normal with relict and residual cement grains that consist mostly of belite making up 3-7% of the paste (**Figure A10**). CH is medium to coarse grained and evenly distributed.

** Abbreviations as follows: RRCG = relict and residual cement grains; SCM = supplemental cementitious materials; CH = calcium hydroxide; ITZ = interfacial transition zone. Modal abundances are based on visual estimations.*

8. Secondary Deposits

Phenolphthalein	No staining for up to 50 mm (2 in.) from the outer surface and up to 5 mm (200 mil) from the sides of the core (**Figure A11**).
Deposits	No significant secondary deposits were observed apart from carbonation.

FIGURES

(a)

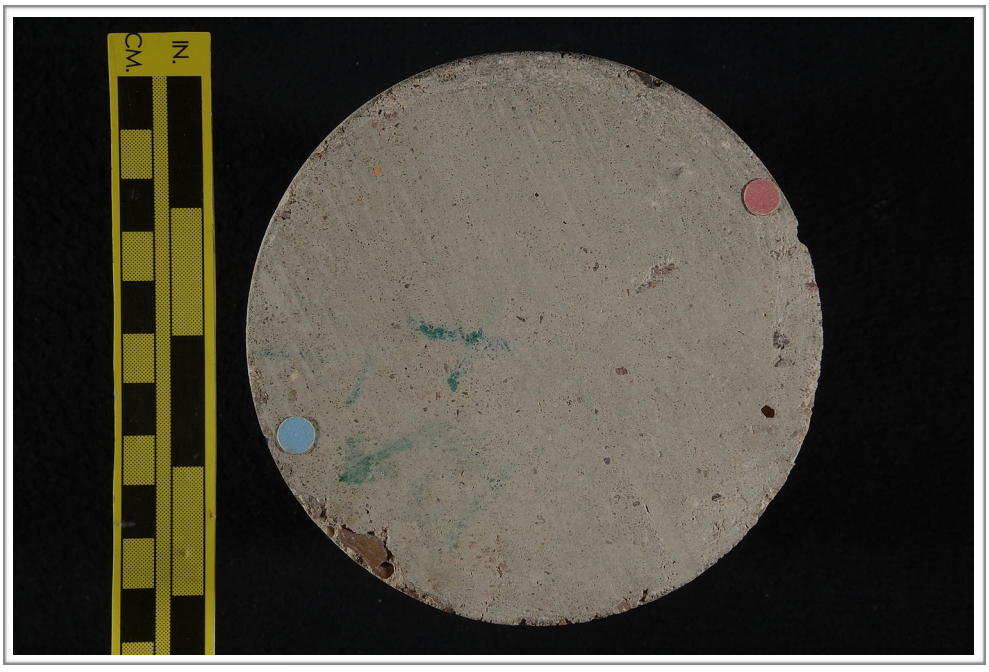

(b)

Figure A1. Photographs showing (a) oblique view of the outer surface and side of the core with identification labels and (b) the outer surface of the core. The red and blue dots show the orientation of the saw cuts used to prepare the sample. The yellow bar in (a) is ~ 150 mm (6 in.) long; the large and small divisions on the yellow scale in both photos are in inches and centimeters, respectively.

(c)

(d)

Figure A1 (cont'd). Photographs of the core in as-received condition showing the (c) side of the core and (d) the inner surface of the core. The yellow scale in (c) is ~ 150 mm (6 in.) long; the large and small divisions on the yellow scale in both photos are in inches and centimeters, respectively.

Figure A2. Photograph showing the polished surface of the core. The large and small divisions on the yellow scale are in inches and centimeters, respectively.

Figure A3. Photograph showing detail of the outer surface; scale in millimeters.

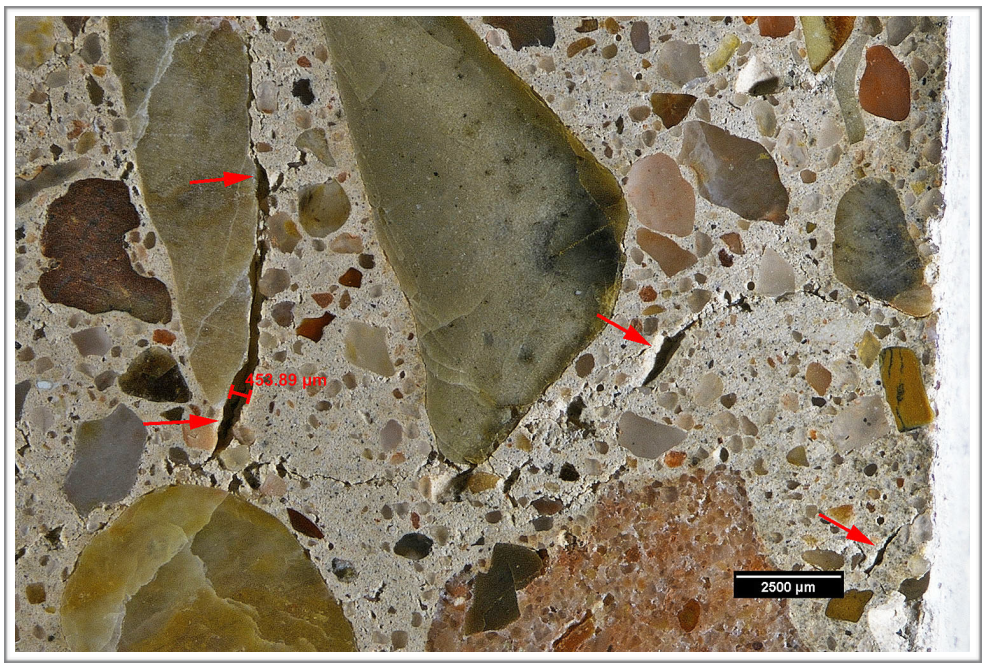

(a)

(b)

Figure A4. Reflected light photomicrographs of the polished surface showing hairline cracks (red arrows) near the outer surface of the core. The green bar in (b) measures the thickness of the zone of darker paste.

(c)

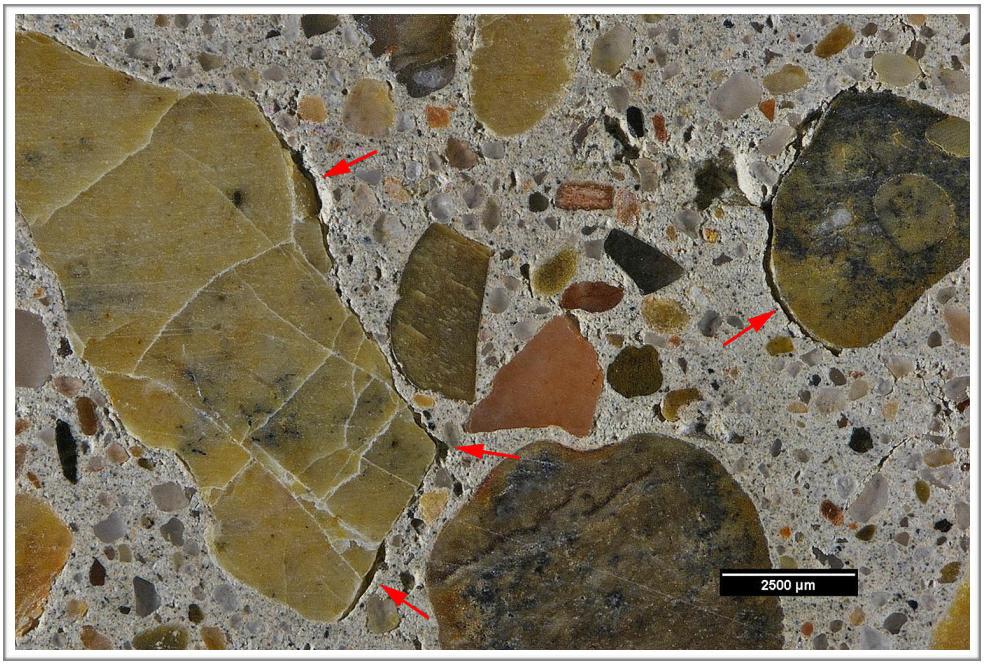

Figure A4 (cont'd). (c) Reflected light photomicrograph of the polished surface showing hairline cracks (red arrows) about 55 mm (2 ⅛ in.) from the outer surface of the core.

(a)

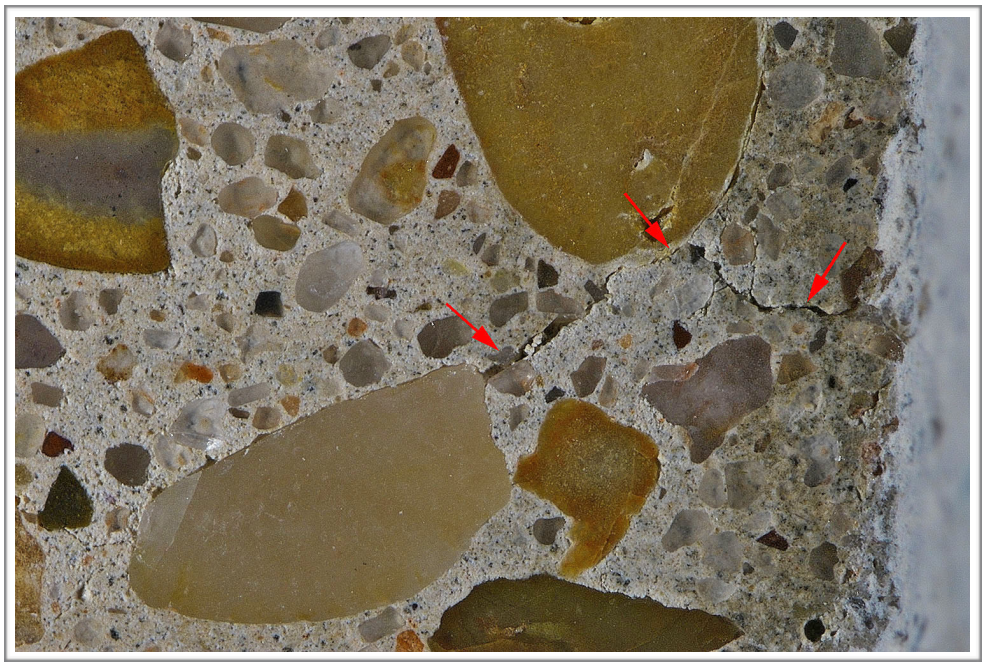

Figure A5. Reflected light photomicrograph of the polished surface showing microcracks (red arrows) near the outer surface of the core.

(b)

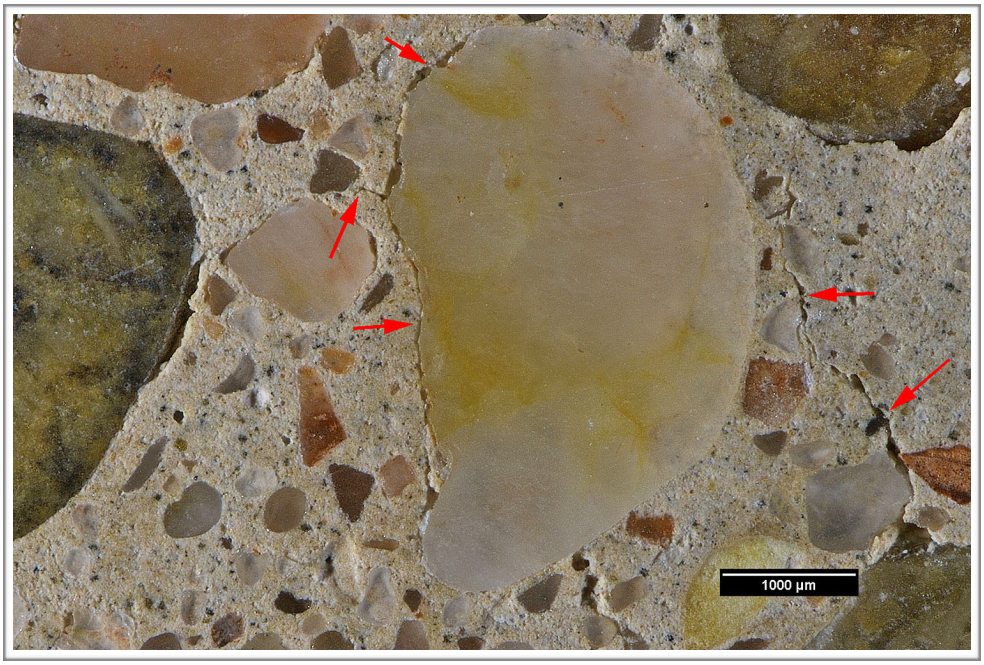

(c)

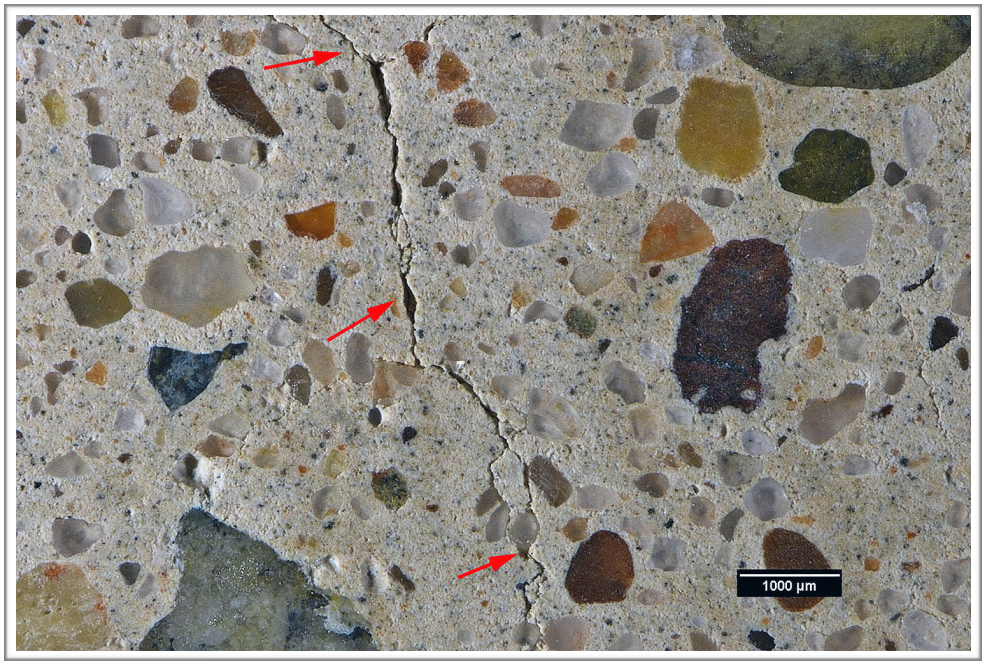

Figure A5 (cont'd). Reflected light photomicrographs of the polished surface showing microcracks (red arrows) cutting through the paste (b) ~ 19 mm (¾ in.) and (c) ~ 25 mm (1 in.) from the outer surface of the core.

Figure A6. Photograph of the polished surface showing overview of coarse aggregate; scale in millimeters.

Figure A7. Reflected light photomicrograph of the polished surface showing the fine aggregate.

(a)

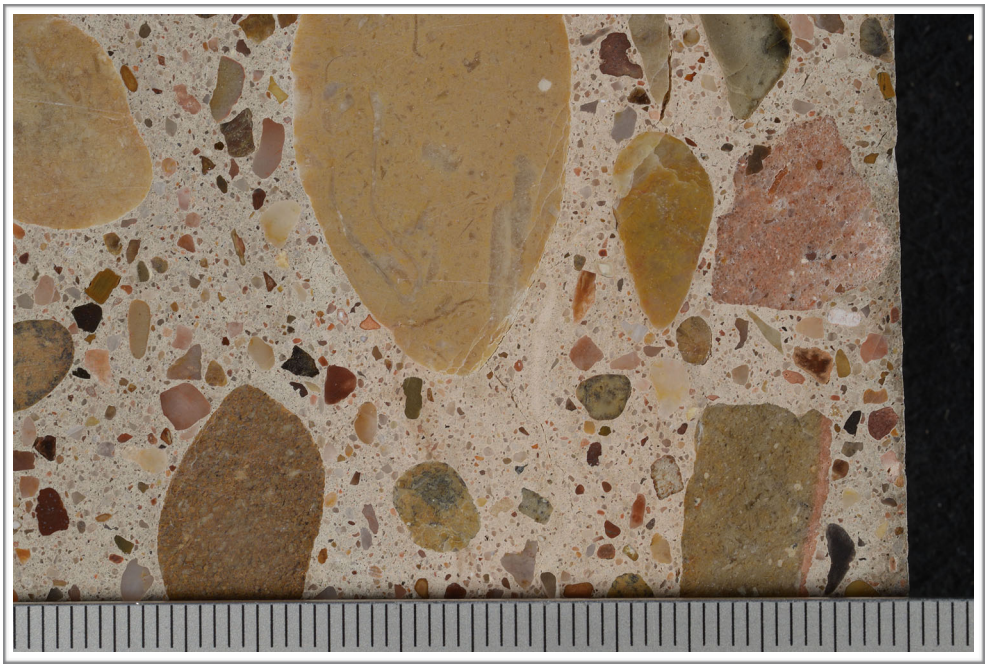

(b)

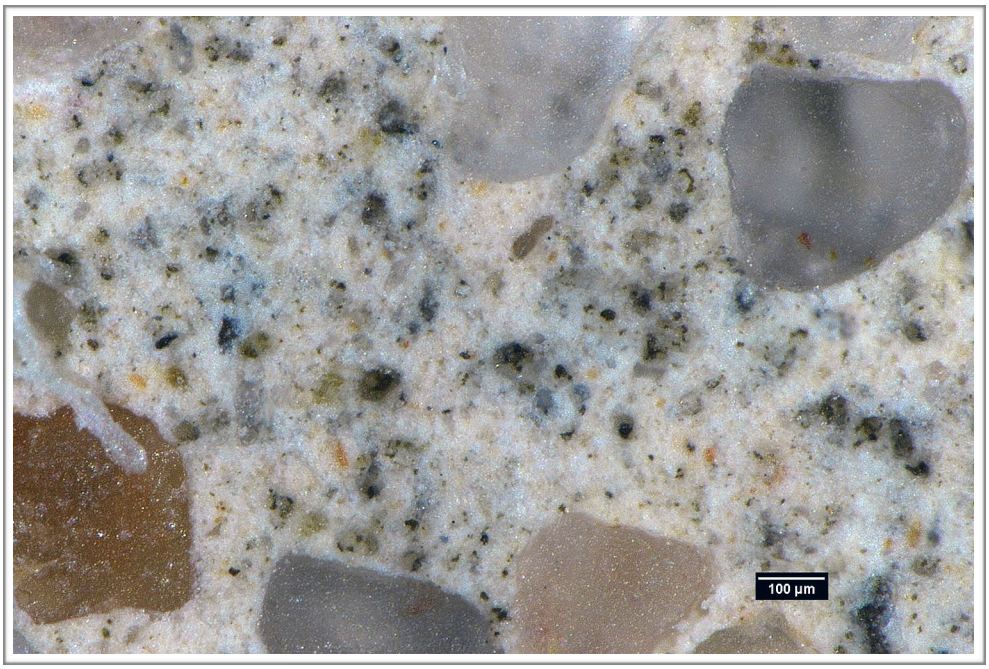

Figure A8. (a) Photograph of the polished surface showing overview of the paste at the outer end of the core. Scale in millimeters. (b) Reflected light photomicrograph of the polished surface showing detail of paste in the middle of the core.

(a)

(b)

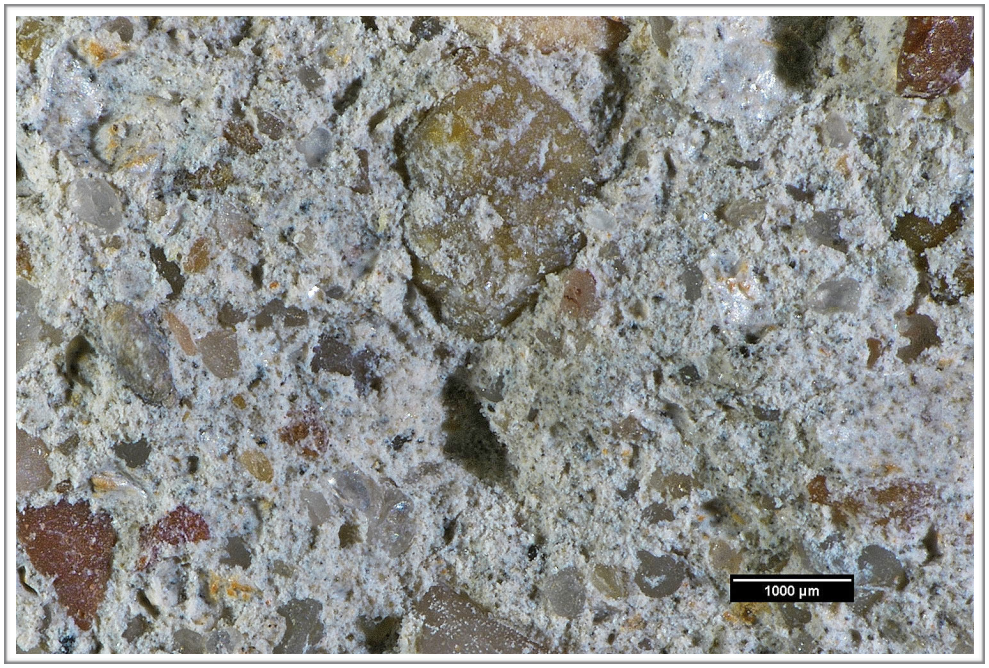

Figure A9. (a) Photograph and (b) reflected light photomicrograph of fresh fracture surface. The scale is in millimeters in (a).

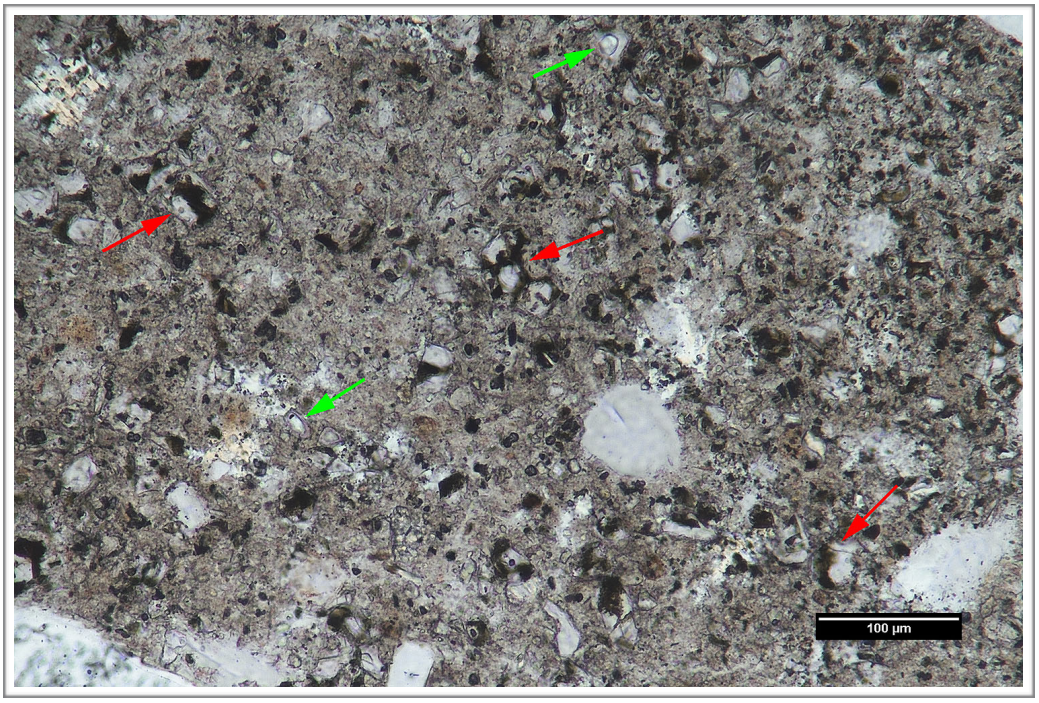

(a)

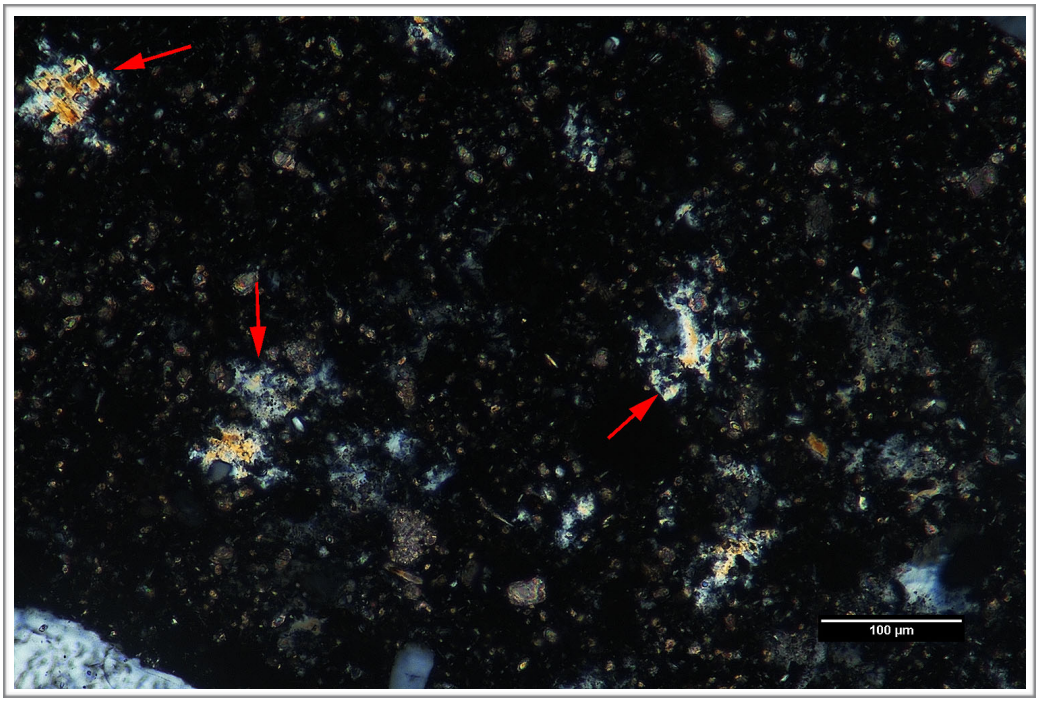

(b)

Figure A10. Transmitted light photomicrographs of thin section showing detail of paste in (a) plane-polarized and (b) cross-polarized light. The red arrows in (a) indicate RRCG; in (b) they indicate CH. The green arrows in (a) indicate particles of fly ash.

(a)

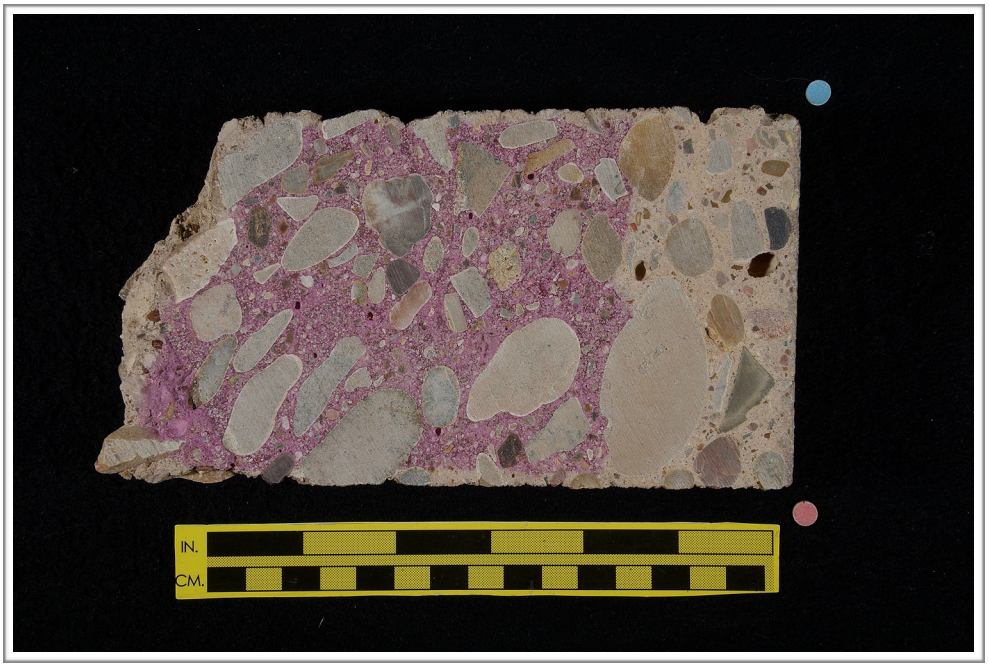

(b)

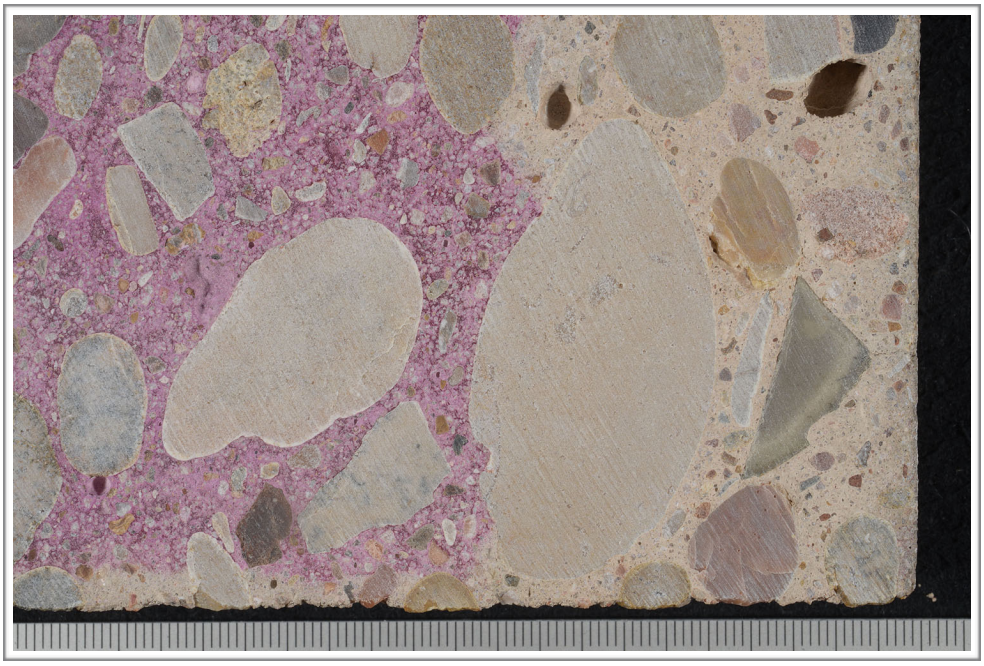

Figure A11. Photographs showing (a) overview of phenolphthalein-stained surface and (b) detail of surface near the outer end of the core. The large and small divisions on the yellow scale in (a) are in inches and centimeters, respectively. The scale in (b) is in millimeters.

1. Received Condition	
Orientation & Dimensions	Horizontal core through bent cap panel measures 100 mm (4 in.) in diameter and 190-210 mm (7 ½ - 8 ⅜ in.) long (**Figure B1**, **Figure B2**).
Surfaces	The outer surface is formed and the inner surface is a fracture such that the core represents a partial thickness of the bent cap. The outer surface is smooth and intact (**Figure B3**).
General Condition	The concrete is hard and compact and rings lightly when sounded with a hammer.

2. Embedded Objects	
General	None observed.

3. Cracking	
Macroscopic	Numerous hairline cracks were observed (**Figure B4**). A sub-vertical crack that measures ~ 250 µm (10 mil) wide and ~ 19 mm (¾ in.) long was observed in the outer 2-3 mm (40-125 mil) of the core; the crack follows an elongated aggregate particle just inboard of the formed surface. A few other randomly scattered hairline cracks were observed in the outer 25-38 mm (1-1 ½ in.) of the core. A sub-horizontal hairline crack measuring up to 175 µm (7 mil) wide was observed that cuts from the formed surface to ~ 30 mm (1 ⅛ in.). All of the cracks cut around aggregate particles and are free of secondary deposits.
Microscopic	Occasional microcracks were observed throughout the core but are most abundant in the outer 19 mm (¾ in.). These are 50-100 µm (2-4 mil) wide, cut around aggregate particles and are free of secondary deposits (**Figure B5**).

4. Voids	
Void System	Concrete is non-air-entrained and contains less than 3% total air as estimated from visual and microscopic observations (not determined in accordance with ASTM C457). The concrete is well consolidated with no major entrapped voids or bleed voids observed.
Void Fillings	None observed.

5. Coarse Aggregate	
Physical Properties	The coarse aggregate is a natural gravel with a nominal top size of 25 mm (1 in.; **Figure B6**). The rocks are hard and competent. Most particles are slightly elongated with rounded to sub-angular edges. The gradation and distribution are relatively even.
Rock Types	The aggregate consists of a mixture of siliceous and carbonate sedimentary rocks. Most of the aggregate consists of limestones (~ 85%) with minor amounts of chert (~ 10%) and quartzite (~ 5%). Most of the limestones range in color from buff to pale brown to brownish green to red. The textures range from massive and micritic to rocks with abundant intraclasts to rocks with minor amounts of fossiliferous material. Occasional carbonaceous limestones were observed. None of the limestones show textures typical of rocks that are susceptible to alkali-carbonate reaction (ACR). Most of the quartzites are arenitic. Quartzite and chert are potentially susceptible to alkali-silica reaction (ASR).
Other Features	No deleterious coatings or incrustations observed. No low w/c mortar coatings were observed. No evidence of ASR or ACR was observed.

6. Fine Aggregate

Physical Properties	The fine aggregate is a natural sand that consists of rocks that are hard and competent (**Figure B7**). The particles are sub-equant to slightly elongated in shape with sub-rounded to angular edges. The grading and distribution are relatively even.
Rock Types	The sand consists primarily of siliceous rocks that include quartzite, chert and fragments of quartz with minor amounts of limestone similar to those observed in the coarse aggregate. Chert and quartzite are potentially susceptible to ASR.
Other Features	No deleterious coatings or incrustations observed. No low w/c mortar coatings observed. No evidence of ASR was observed involving the fine aggregate.

7. Paste Observations

Polished Surface	Paste is light gray (Munsell 2.5Y/7/1) to pale yellow (2.5Y/8/4), has a granular texture and a dull luster (**Figure B8**). The paste is soft (Mohs ~ 2.5).
Fresh Fracture	Fracture surface is light gray, has a punky texture and a dull luster (**Figure B9**). The fracture cuts mostly around coarse aggregate particles.
Thin Section*	The paste contains hydrated portland cement with no fly ash, slag cement or other SCM observed. The hydration is normal with relict and residual cement grains that consist mostly of belite making up 3-7% of the paste (**Figure B10**). CH is medium to coarse grained and evenly distributed.

** Abbreviations as follows: RRCG = relict and residual cement grains; SCM = supplemental cementitious materials; CH = calcium hydroxide; ITZ = interfacial transition zone. Modal abundances are based on visual estimations.*

8. Secondary Deposits

Phenolphthalein	No staining for up to 50 mm (2 in.) from the outer surface (**Figure B11**).
Deposits	No significant secondary deposits were observed apart from carbonation.

FIGURES

(a)

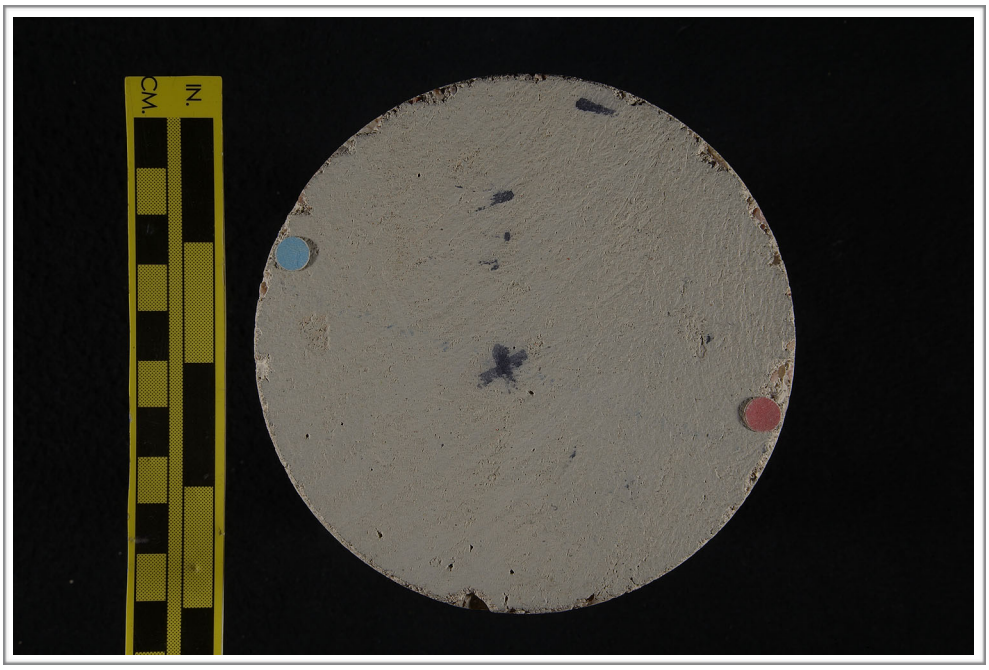

(b)

Figure B1. Photographs showing (a) oblique view of the outer surface and side of the core with identification labels and (b) the outer surface of the core. The red and blue dots show the orientation of the saw cuts used to prepare the sample. The yellow bar in (a) is ~ 150 mm (6 in.) long; the large and small divisions on the yellow scale in both photos are in inches and centimeters, respectively.

(c)

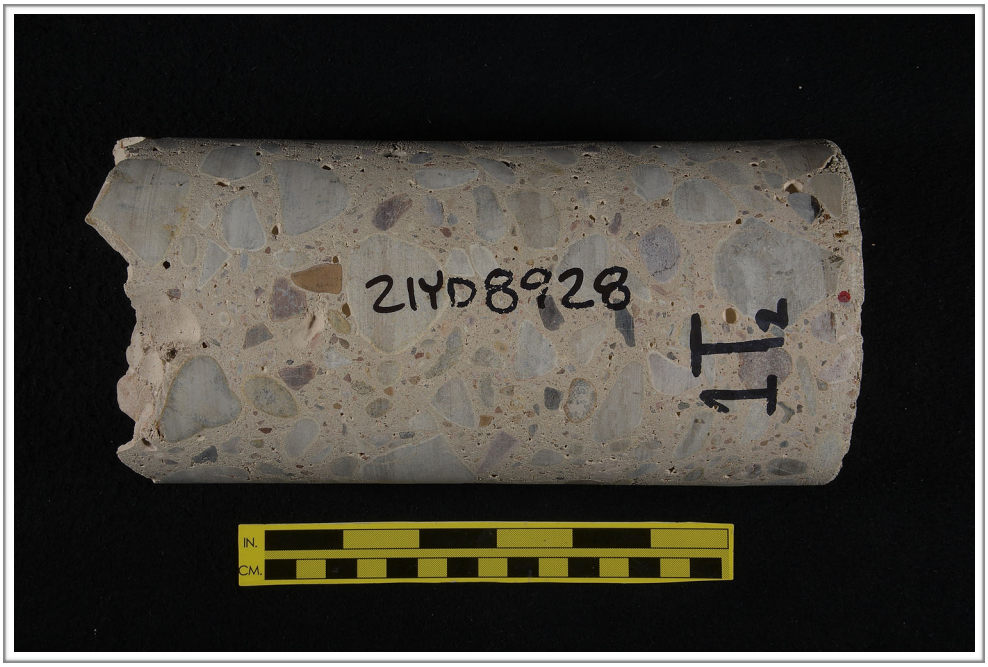

(d)

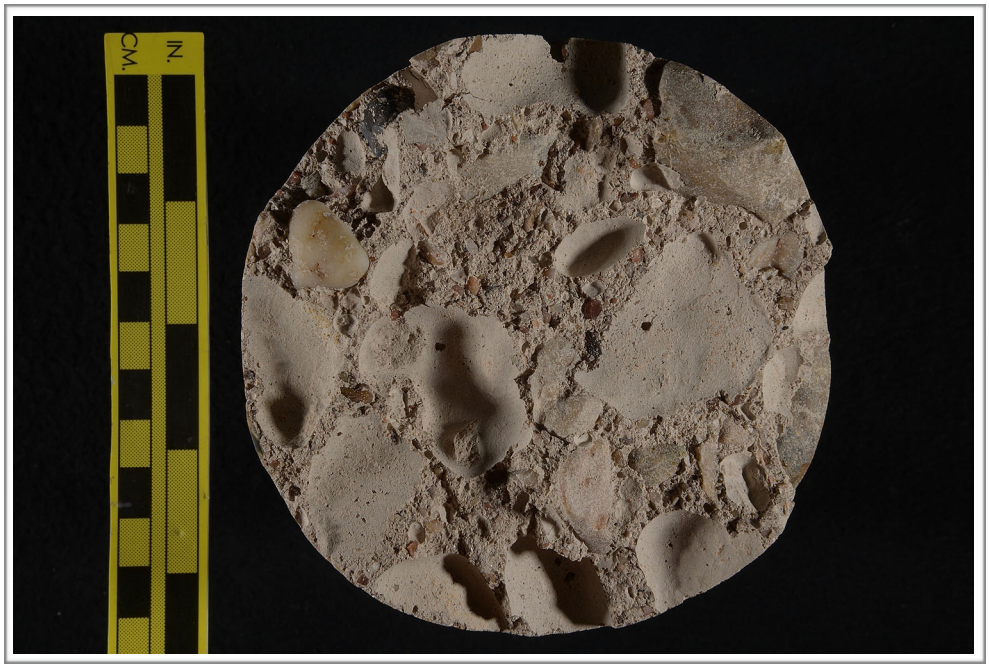

Figure B1 (cont'd). Photographs of the core in as-received condition showing the (c) side of the core and (d) the inner surface of the core. The yellow scale in (c) is ~ 150 mm (6 in.) long; the large and small divisions on the yellow scale in both photos are in inches and centimeters, respectively.

Figure B2. Photograph showing the polished surface of the core. The large and small divisions on the yellow scale are in inches and centimeters, respectively.

Figure B3. Photograph showing detail of the outer surface; scale in millimeters.

(a)

(b)

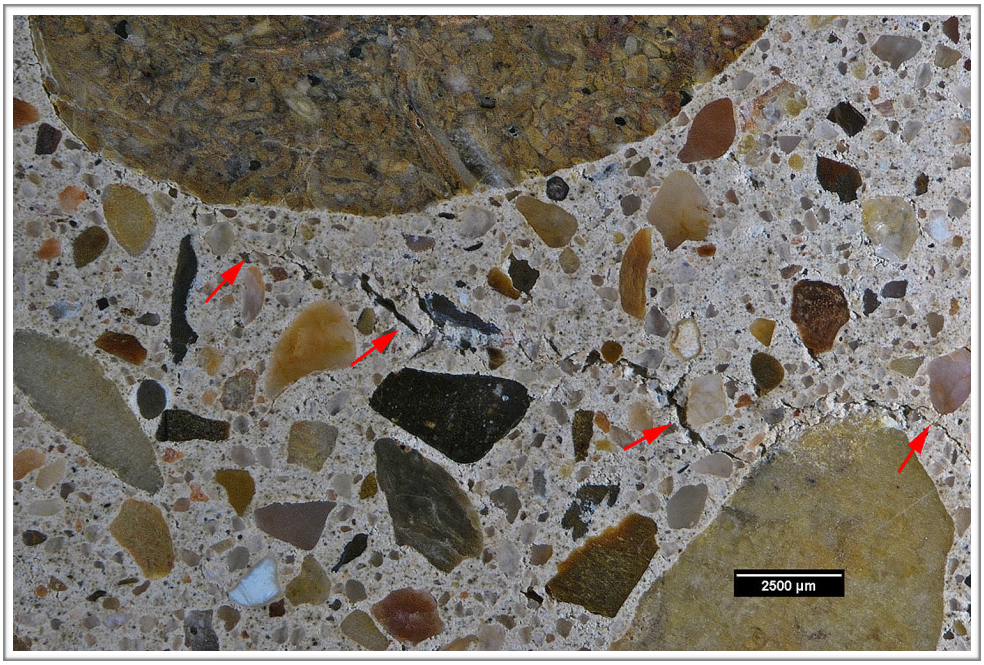

Figure B4. Reflected light photomicrographs of the polished surface showing hairline cracks (red arrows) near the outer surface of the core.

(a)

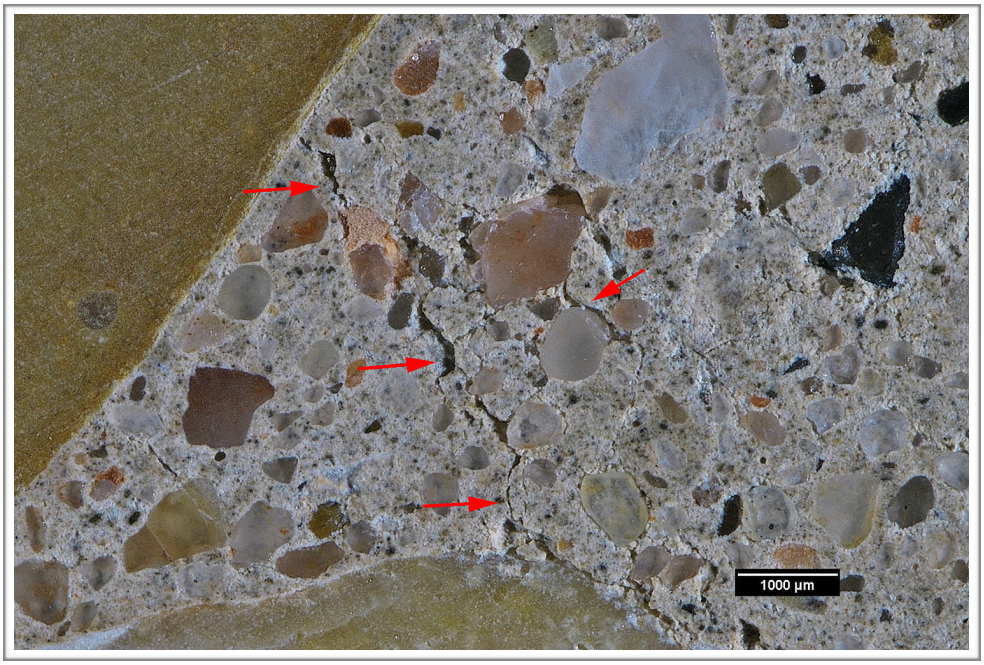

(b)

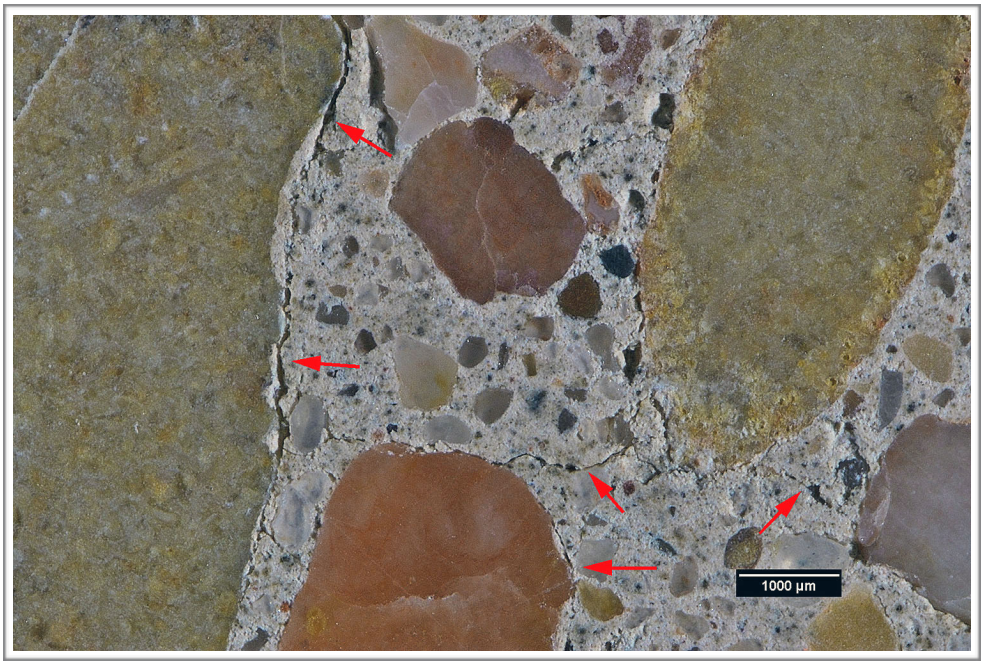

Figure B5. Reflected light photomicrograph of the polished surface showing microcracks (red arrows) cutting through the paste about (a) 12.5 mm (½ in.) and (b) 19 mm (¾ in.) from the outer surface of the core.

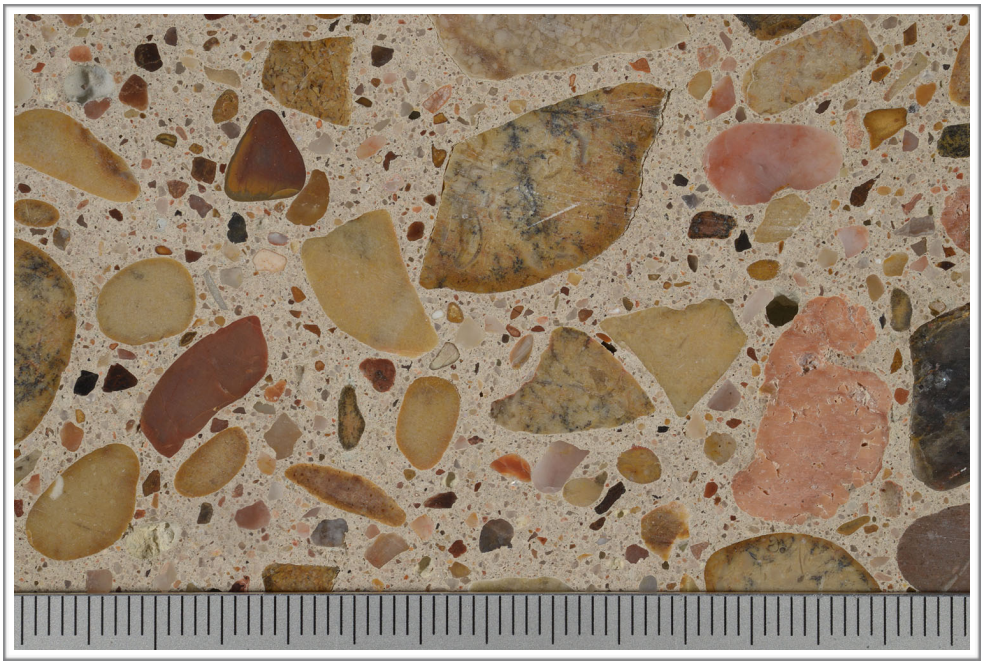

Figure B6. Photograph of the polished surface showing overview of coarse aggregate; scale in millimeters.

Figure B7. Reflected light photomicrograph of the polished surface showing the fine aggregate.

(a)

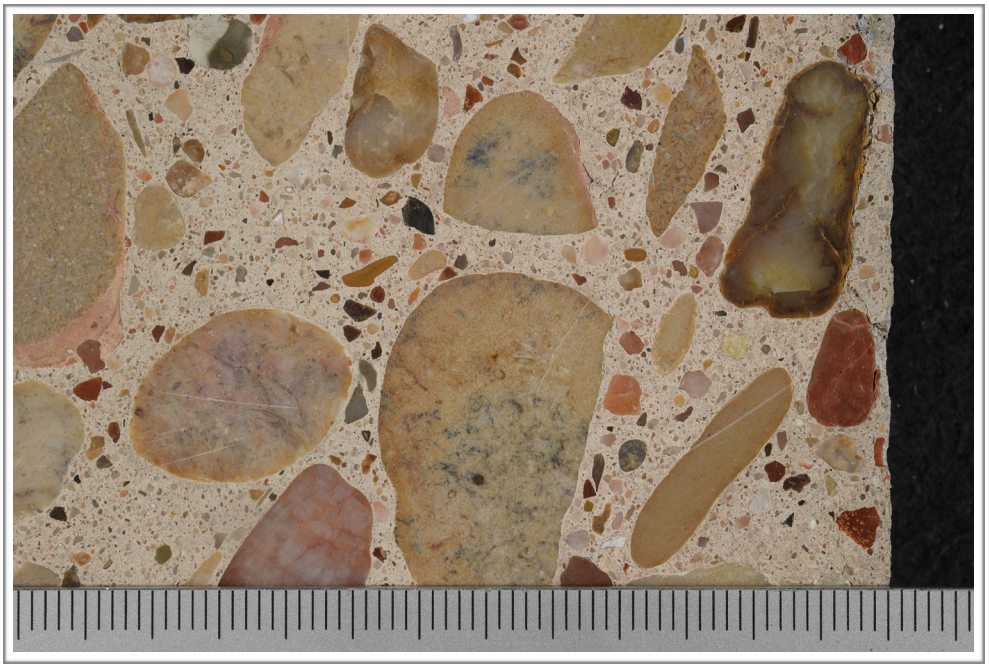

(b)

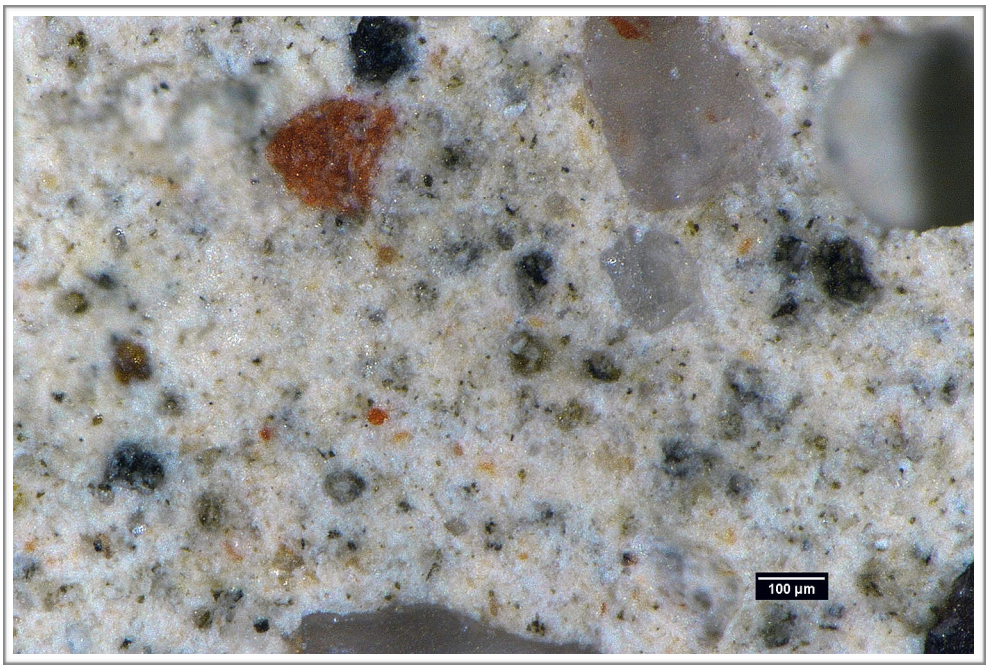

Figure B8. (a) Photograph of the polished surface showing overview of the paste at the outer end of the core. Scale in millimeters. (b) Reflected light photomicrograph of the polished surface showing detail of paste in the middle of the core.

(a)

(b)

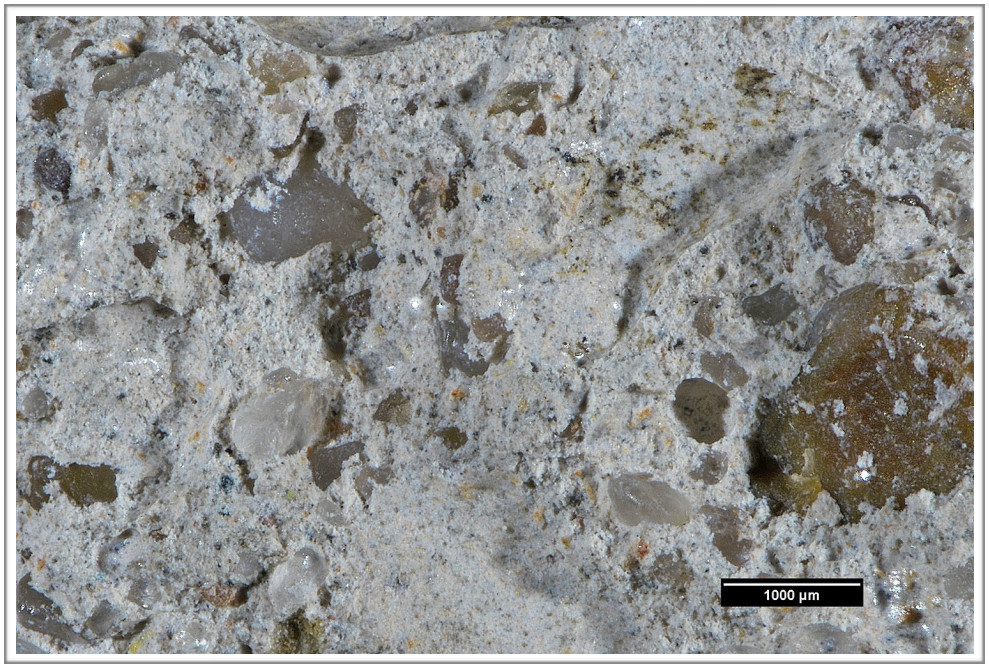

Figure B9. (a) Photograph and (b) reflected light photomicrograph of fresh fracture surface. The scale is in millimeters in (a).

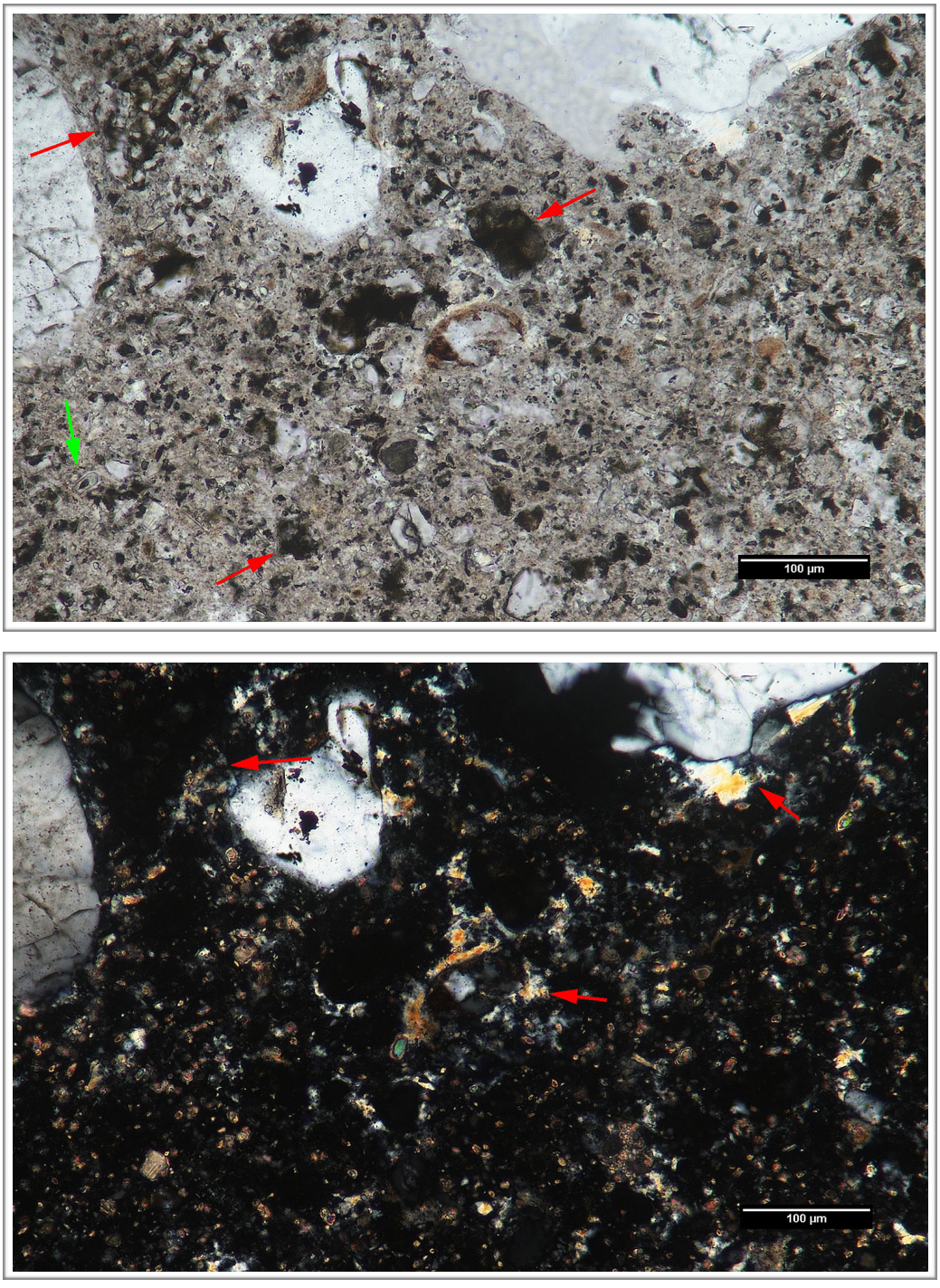

Figure B10. Transmitted light photomicrographs of thin section showing detail of paste in (a) plane-polarized and (b) cross-polarized light. The red arrows in (a) indicate RRCG; in (b) they indicate CH. The green arrow in (a) indicates a fly ash particle.

(a)

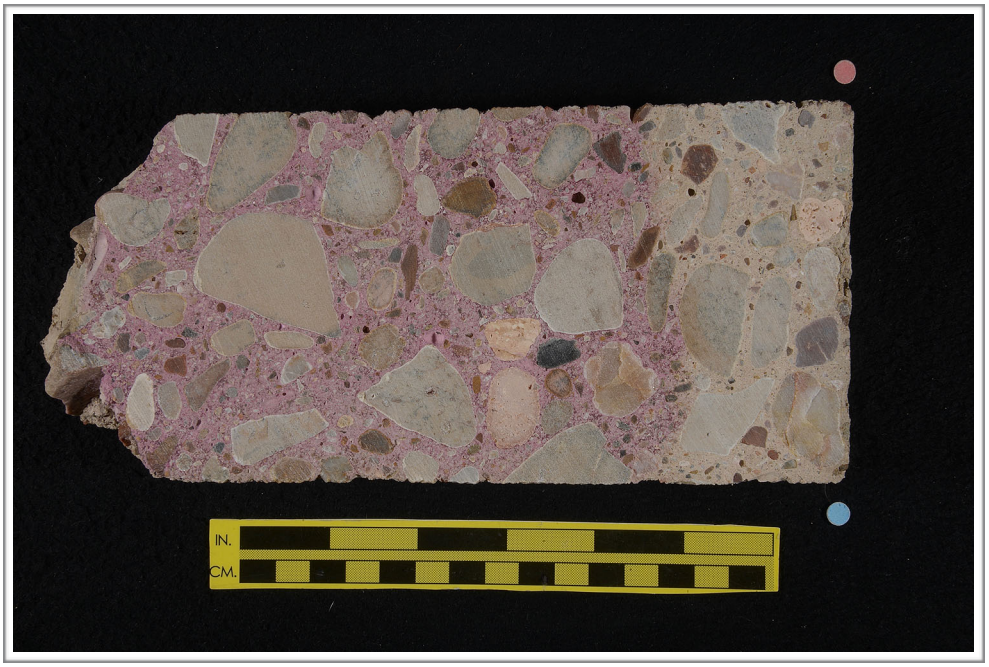

(b)

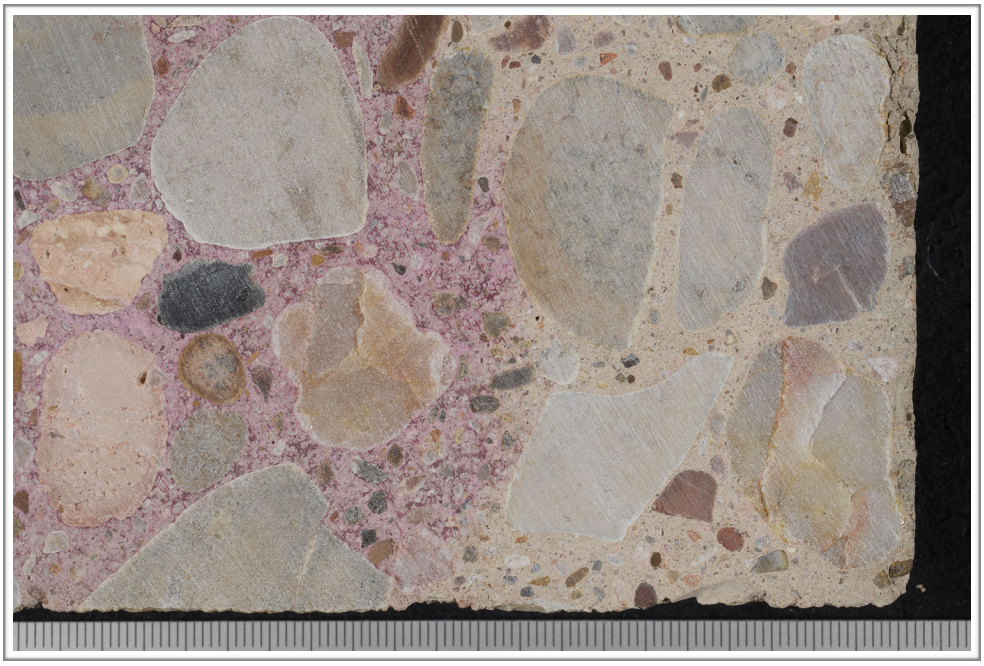

Figure B11. Photographs showing (a) overview of phenolphthalein-stained surface and (b) detail of surface near the outer end of the core. The large and small divisions on the yellow scale in (a) are in inches and centimeters, respectively. The scale in (b) is in millimeters.

PROCEDURES

ASTM C856--Petrographic Analysis The petrographic work was done following ASTM C856 [**1**] with sample preparation done at **DRP** in the following manner. After writing the unique **DRP** sample number on the sample near the received label, the sample was measured and inspected visually and with a hand lens. The orientation of the saw cuts used to prepare the sample was then indicated on each sample with blue and red dots. The sample was then photographed in their as-received condition.

A slab representing a longitudinal cross section was cut using a Diamond Pacific® TR-24, a 24-inch diameter oil-lubricated saw. This produced two (3) longitudinal sections—one main slab with flat surfaces on each side and two hemi-cylindrical sections with a flat surface on one side and a curved surface on the other. These sections were rinsed in an aqueous solution with a detergent to remove the cutting oil and oven dried overnight in a Gilson® Bench Top laboratory oven at ~ 40°C (~ 105°F) to remove remaining traces of the oil. After drying, each piece was labelled with the appropriate **DRP** sample number. One piece was set aside for phenolphthalein staining and the other was set aside for thin section preparation.

The main slab was lapped and polished on a Diamond Pacific® RL-18 Flat Lap machine. This machine employs an 18-inch diameter cast iron plate onto which Diamond Pacific® Magnetic Nova Lap discs with progressively finer grits are fixed. The Nova Lap discs consist of a $^{1}/_{16}$ in. backing of solid rubber containing magnetized iron particles that is coated with a proprietary Nova resin-bond formula embedded with industrial diamonds of specific grit. The slab preparation involved the use of progressively finer wheels to a 3000 grit (~4 μm) final polish following procedures outlined in ASTM C457 [**2**]. An aqueous lubricant is used in the lapping and polishing process. The polished slab from each sample was examined visually and with a Nikon® SMZ-25 stereomicroscope with 3-158x magnification capability following to the standard practice set forth in ASTM C856.

Phenolphthalein was applied to a strip along the freshly saw-cut surface from the remaining section to assess the extent of carbonation, along with thin section analysis. Phenolphthalein is an organic stain that colors materials with pH of greater than or equal to ~ 9.5 purple. Portland cement concrete generally has a pH of ~ 12.5. Carbonation lowers the pH of the paste below 9.5, so areas not stained by phenolphthalein are an indicator of carbonation. The depth of paste not stained by phenolphthalein was measured from each exposed surface.

1 *Standard Practice for Petrographic Examination of Hardened Concrete.* Annual Book of ASTM Standards, V C856-17.

2 *Standard Test Method for Microscopical Determination of Parameters of the Air-Void System in Hardened Concrete* Book of ASTM Standards, Vol. 4.02, ASTM C457-16.

A petrographic thin section was prepared by cutting billets from the remaining portion of the section used for phenolphthalein staining. Outlines marking the area of the billets (as well as sections for SEM analysis) were drawn with a marker on the saw-cut surface after visual and microscopical examination of saw-cut and polished surfaces. The billet was labeled with the unique **DRP** number assigned to the sample and impregnated with epoxy. The impregnated billet was then fixed to glass slides with epoxy. After the epoxy cured, the slide was trimmed and ground on a Buehler® Petro-Thin device to a thickness of ~ 30 µm (1.2 mil). The slide was then ground and polished by hand using glass plates and silicon carbide grits in a non-aqueous environment. The grinding and polishing of the thin sections was done in a non-aqueous environment. The thin section was examined with a Nikon® E-Pol 600 petrographic microscope equipped to provide a 20-1000x magnification range following the standard practice set forth in ASTM C856.

APPENDIX G Tyfo SCH-41 Properties (CFRP)

AEGION®
Stronger. Safer. Infrastructure.®

FYFE®

TYFO® SCH-41 COMPOSITE

using Tyfo® S Epoxy

DESCRIPTION

The Tyfo® SCH-41 Composite is comprised of the Tyfo® S Epoxy and Tyfo® SCH-41 reinforcing fabric. Tyfo® SCH-41 is a custom, uni-directional carbon fabric orientated in the 0° direction. The Tyfo® S Epoxy is a two-component epoxy matrix.

USE

The Tyfo® SCH-41 fabric is combined with Tyfo® S Epoxy to provide an ambient-cure, wet-layup, composite system for strengthening bridges, buildings and other structures.

ADVANTAGES

- ICC-ES ESR-2103 listed product
- UL listed, fire-rated assembly component
- NSF/ANSI Standard 61-G listed product
- Proven long-term performance and durability
- Excellent wet-out and handling properties
- 100% solids, solvent-free epoxy matrix
- Low viscosity, long working time
- Ambient cure application

PACKAGING

Tyfo® SCH-41: 24" x 300 lineal ft. (600 sq.ft.)
Typically ships in 12" x 13" x 27" boxes.

Tyfo® S Epoxy: Pre-measured 5-gallon units with a combined material volume of 4 gallons or in 55-gallon drums.

COVERAGE

Approximately 3 to 4 units of Tyfo® S Epoxy per roll of the Tyfo® SCH-41 fabric.

CONSUMPTION RATE

Fabric-to-epoxy ratio by weight:
For Tyfo® SCH Fabrics: 1 : 1
For Tyfo® SEH Fabrics: 1 : 0.8

SHELF LIFE

Epoxy - two years in original, unopened and properly stored containers
Fabric - 10 years in proper storage conditions

STORAGE CONDITIONS

Store epoxy at 60°F to 100°F (15°C to 38°C). Resin is susceptible to crystallization at temperatures below 50°F. If crystallized, epoxy must be reheated until clear. Store fabric rolls flat, not on ends, and at temperatures below 100°F (38°C). Avoid moisture and water contamination.

TYPICAL DRY FIBER PROPERTIES

Material properties are based on standard laboratory conditons (23°C, 50 percent relative humidity.)

PROPERTY	TYPICAL TEST VALUE
Tensile Strength	620,000 psi (4.3 GPa)
Tensile Modulus	36.0 x 10^6 psi (250 GPa)
Ultimate Elongation	1.7%
Density	0.064 lbs./in.^{3} (1.77g/cm^3)
Minimum weight per sq. yd.	19 oz (644 g/m^2)

COMPOSITE GROSS LAMINATE PROPERTIES

PROPERTY[1]	ASTM METHOD	TYPICAL TEST VALUE	DESIGN VALUE[2]
Ultimate Tensile Strength in Primary Fiber Direction	D3039	143,000 psi (986 MPa) (5.7 kip/in width)	121,000 psi (834 MPa) (4.8 kip/in width)
Elongation at Break		1.0%	0.85%
Tensile Modulus		13.9 x 10^6 psi (95.8 GPa)	11.9 x 10^6 psi (82 GPa)
Flexural Strength	D790	17,900 psi (123.4 MPa)	15,200 psi (104.8 MPa)
Flexural Modulus		452,000 psi (3.12 GPa)	384,200 psi (2.65 GPa)
Longitudinal Compressive Strength	D3410	50,000 psi (344.8 MPa)	42,500 psi (293 MPa)
Longitudinal Compressive Modulus		11.2 x 10^6 psi (77.2 GPa)	9.5 x 10^6 psi (65.5 GPa)
Longitudinal Coefficient of Thermal Expansion	D696	3.6 ppm/°F	
Transverse Coefficient of Thermal Expansion		20.3 ppm/°F	
Nominal Laminate Thickness	D1777	0.04 in. (1.0 mm)	0.04 in. (1.0 mm)

[1] Contact Fyfe Co. LLC for appropriate cure schedule.
[2] Contact Fyfe Co. LLC engineers to confirm project specification values and design methodology (i.e. design values may vary slightly using ACI 440 gross laminate methodology).

INSTALLATION OF THE TYFO® SCH-41 SYSTEM

DESIGN

The Tyfo® SCH-41 system is designed to meet specific project criteria dictated by the engineer of record and any relevant building codes and/or guidelines. The design shall be based on the allowable strain for each type of application and the design modulus of the material. Fyfe Co. LLC engineering staff may provide preliminary design, specification wording and application details based on the project requirements.

INSTALLATION

The Tyfo® system is to be installed by Fyfe Co. trained and certified applicators in accordance with the Fyfe Co. quality control manual, project specifications, and design requirements.

SURFACE PREPARATION

The required surface preparation is dependent on the type of element being strengthened. In general, the surface must be clean, dry and free of protrusions or cavities to prevent voids behind the Tyfo® system. Column surfaces that will receive continuous wraps typically only require a clean, sound substrate. Discontinuous wrapping surfaces (walls, beams, slabs, etc.) require a minimum CSP-2 profile to prepare for bonding, achieved by light sandblast, grinding or other approved methods per ICRI 310.2R-2013. Tyfo® Composite Anchors may be incorporated in the designs. Fyfe Co. LLC engineering staff will provide the proper specifications and details based on project requirements.

MIXING TYFO® S EPOXY

For pre-measured units in 5-gallon containers, pour the contents of component B into the component A container. Mix thoroughly with a low speed mixer at 400 to 600 RPM until uniformly blended. Ensure epoxy is transferred between the A and B buckets. For 55-gallon drums, mix component A and component B per the appropriate weight or volumetric mix ratio. Resin may be heated to achieve desired viscosity (i.e. radiant heating, drum heaters, water bath). Mixed Tyfo® S Epoxy may be thickened by adding up to 7 percent by weight of fumed silica (such as Cab-o-sil TS-720). DO NOT THIN. Solvents will prevent proper cure.

EPOXY MATERIAL PROPERTIES

Cure schedule: 72 hour post-cure at 140°F (60°C)[1]

PROPERTY	ASTM METHOD	TYPICAL TEST VALUE
Glass Transition Temperature, T_g	D4065/E1356	180°F (82°C)
Tensile Strength	D638 Type 1	10,500 psi (72.4 MPa)
Tensile Modulus		461,000 psi (3.18 GPa)
Elongation		5.0%
Compressive Strength	D695	12,500 psi (86.2 MPa)
Compressive Modulus		465,000 psi (3.2 GPa)
Flexural Strength	D790	17,900 psi (123.4 MPa)
Flexural Modulus		452,000 psi (3.12 GPa)
Shore D Hardness	D2240	87±3
Water Absorption (24 hours) Water Absorption (13 weeks)	D570	0.33% 1.98%
Adhesion Strength[2] Concrete (ASTM D7522) Steel Epoxy	D4541	 >400 psi (concrete failure typ.) >1200 psi >1200 psi

[1] Testing temperature: 73°F (23°C).
[2] Adhesion strength dependent on surface preparation and substrate thickness. Cure schedule: 7 days at 73°F (23°C).

PROTECTIVE COATINGS

Apply a final coat of thickened Tyfo® S Epoxy to all fabric edges, including butt splice, termination points and jacket edges. Paint between 24 and 72 hours after final application of epoxy. If more than 72 hours after application, prepare the surface by light sandblast or hand sanding to lightly etch the surface. Please refer to Fyfe Co.'s NSF Listing for the NSF-61G listed application method (www.NSF.org).

LIMITATIONS

Recommended substrate temperature range is 50°F to 100°F (10°C to 38°C). All coating applications to be performed at a minimum of 5.4°F above the dew point. Maintain conditions for the first 48 hours of cure. Temperatures below 50°F will significantly increase the viscosity of the mixed product. Higher viscosity will reduce fabric penetration, introduce additional air into the system, and extend the cure times beyond 48 hours. DO NOT THIN. Solvents will prevent proper cure.

CAUTION!

CLEANUP

Collect with absorbent material. Dispose in accordance with local disposal regulations. Uncured material can be removed with approved solvent. Cured materials must be mechanically removed.

HAZARDS

Consult the Safety Data Sheets (SDS) for associated hazards. SDS will be supplied upon request. Carbon fiber is electro-conductive.

CONSULT SAFETY DATA SHEET (SDS) FOR MORE INFORMATION. FOR INDUSTRIAL USE ONLY.

AEGION® Stronger. Safer. Infrastructure.®

FYFE®

Fyfe Co. LLC
4995 Murphy Canyon Rd., Suite 110,
San Diego, CA 92123
Tel: 858.642.0694 Fax: 858.444.2982
Email: info@aegion.com
Web: www.fyfeco.com

Fyfe Asia Pte Ltd
6 Clementi Loop, #02-20
(Level 4), Singapore 129814
Tel: +65.6898.5248 Fax: +65.6898.5181
Email: fyfeasia@aegion.com
Web: www.fyfeasia.com

Fyfe Europe/Insituform Linings Ltd
4-8 Brunel Close
Park Farm Industrial Estate
Wellingborough, Northamptonshire NN8 6QX
Tel: +44 1933 678266
Web: www.fyfeeurope.com

REFERENCES

AASHO. (1957). *Standard Specifications for Highway Bridges*. Washington, D.C.: AASHO.

AASHTO. (2017). *AASHTO LRFD bridge design specifications* (8th ed.). Washington, D.C.: AASHTO.

CRSI. (2001). *Evaluation of reinforcing bars in old reinforced concrete structures*. Chicago, Ill: CRSI.

fib. (2013). Model code for concrete structures 2010. Berlin, Germany: Ernst & Sohn.

Pham, T. M., M. N. Hadi, and J. Youssef. "Effects of Fabrication Technique on Tensile Properties of Fiber Reinforced Polymer." Journal of Testing and Evaluation. 45.5(2017): 1524-1534